NAVAL RESEARCH REVIEWS

Volume 50, Number 4/1998

Challenges and Issues in Fatigue Damage

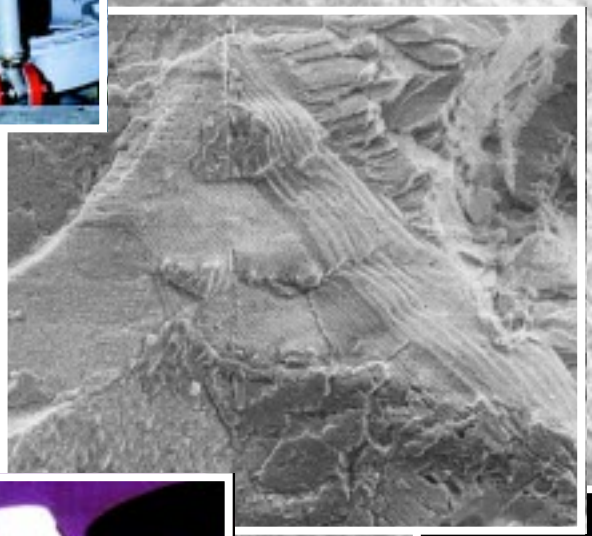

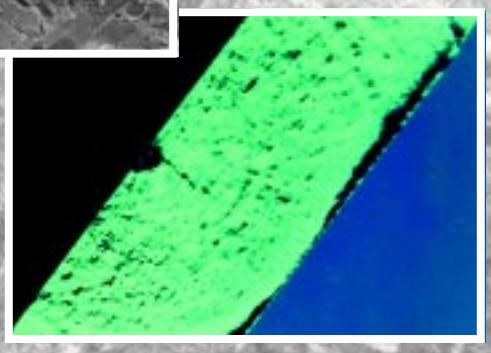

and more . . .

From the Guest Editors . . .

Structures and their components almost invariably acquire defects at some point in their life cycle, either during their manufacture, fabrication, assembly, or maintenance. Under a variety of loading and environmental conditions, these defects initiate cracks that can grow with time and ultimately lead to the failure of the component. Depending on the function of the component, the effects of this accumulating fatigue damage can range from a minor degradation in system performance to a catastrophic failure of the entire structure.

Fatigue damage is one of the major life-limiting factors for most structural components. An analysis of past fatigue failures in aircraft components shows that many cracks initiate at (1) stress concentration sites such as changes in radius, corners, rivet holes, or other design features in the structure, (2) initial manufacturing defects, or (3) defects that were inadvertently introduced during assembly, structural inspections, or repairs. Recognition of these causes has had a profound effect upon aircraft design philosophy, spurred the development of materials with improved defect quality, and led to better inspection and maintenance practices.

Even with better design techniques, better materials, and inspections, however, components still fail prematurely and unpredictably. The inability to make accurate predictions of fatigue life for a particular structure or component stems from many factors. These include — but are not limited to — variations in loads experienced by components during service; exposure to different chemical environments that affect crack growth rates; differing crack growth behavior for short cracks and long cracks; uncertainties in the size, location, and type of material defects; and the unpredictability of how long it takes to initiate a crack.

A better understanding of these factors needs to be supplemented by accurate, more reliable methods of detecting fatigue damage during routine maintenance or scheduled inspections. This combination will give operators and maintainers the tools to make better decisions regarding the inspection, repair, or replacement of structural components.

The application of damage tolerant approaches to controlling fatigue damage in aging aircraft fleets is unquestionably becoming more important. Ideally, these methodologies must comprehensively model the entire realm of damage by describing crack growth behavior from the crack nucleation stage through the stages of short and long crack growth to the point of final component failure.

The field of fracture and fatigue includes many topics, but this issue of *Naval Research Reviews* focuses primarily on two of them: loads and environment. The selected articles give a bird's-eye view of some of the developments of the past several decades in the area of fatigue damage analysis. These articles discuss current practices in fatigue life prediction, the measurement and analysis of loads, new work in the understanding of the physics of material damage, and the effects of the physical environment upon the rates of corrosion and crack growth.

Research into these topics, and others, can ultimately provide a vastly improved baseline of information for current and future life prediction methods. These data, when used with enhanced predictive models, could have a significant impact on life cycle costs by reducing maintenance costs. An increased use of health and usage monitoring systems for aircraft and other systems is leading to more efficient determination of service life for flight-critical components based on the actual severity of their operational usage. Research to advance life prediction methods needs to keep pace.

A.K. Vasudevan
Office of Naval Research

Margery E. Hoffman
Naval Air Systems Command

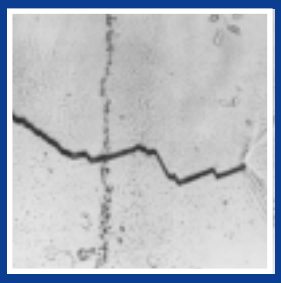

NAVAL RESEARCH REVIEWS

Service Life Analysis:

A Prescription for Fatigue

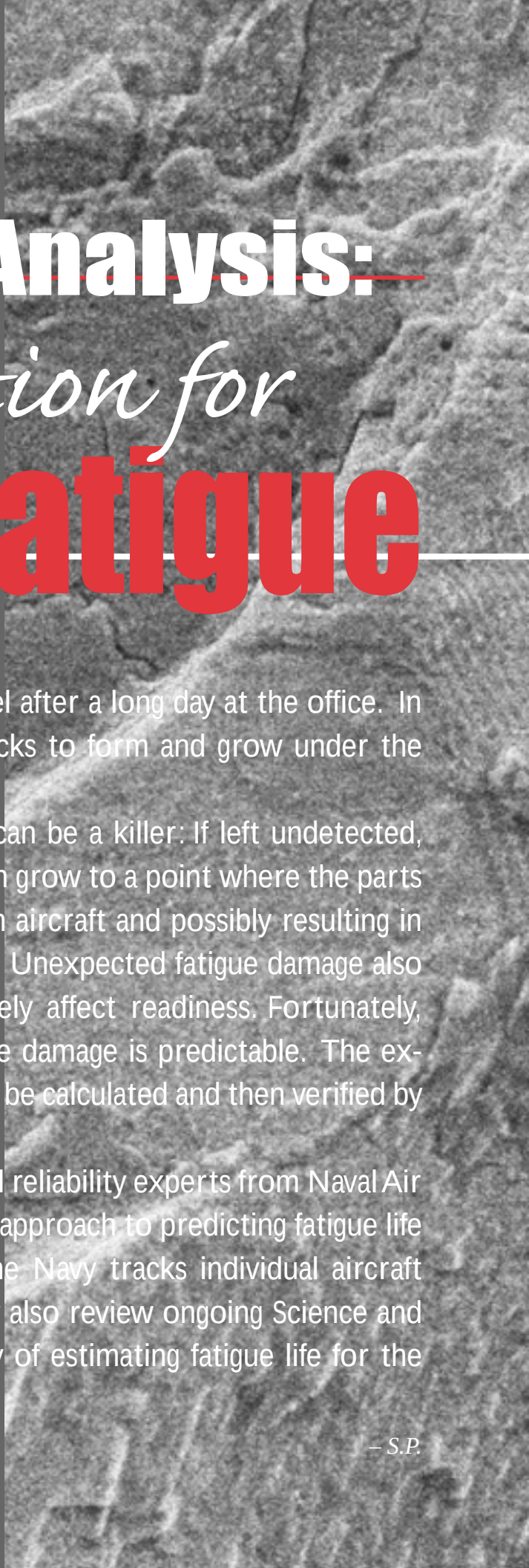

"Fatigue" is more than something you feel after a long day at the office. In metals, fatigue is the tendency for cracks to form and grow under the repeated application of stress.

In aircraft, just as in people, fatigue can be a killer: If left undetected, fatigue cracks in flight-critical components can grow to a point where the parts can catastrophically fail, causing the loss of an aircraft and possibly resulting in the death or injury of its aircrew and others. Unexpected fatigue damage also can require costly maintenance and adversely affect readiness. Fortunately, however, the formation and growth of fatigue damage is predictable. The expected service life of aircraft components can be calculated and then verified by full-scale tests.

In the following article, two structural reliability experts from Naval Air Systems Command explain the naval aviation approach to predicting fatigue life for aircraft components and discuss how the Navy tracks individual aircraft according to the severity of their usage. They also review ongoing Science and Technology work to extend the current way of estimating fatigue life for the Navy's older aircraft.

– S.P.

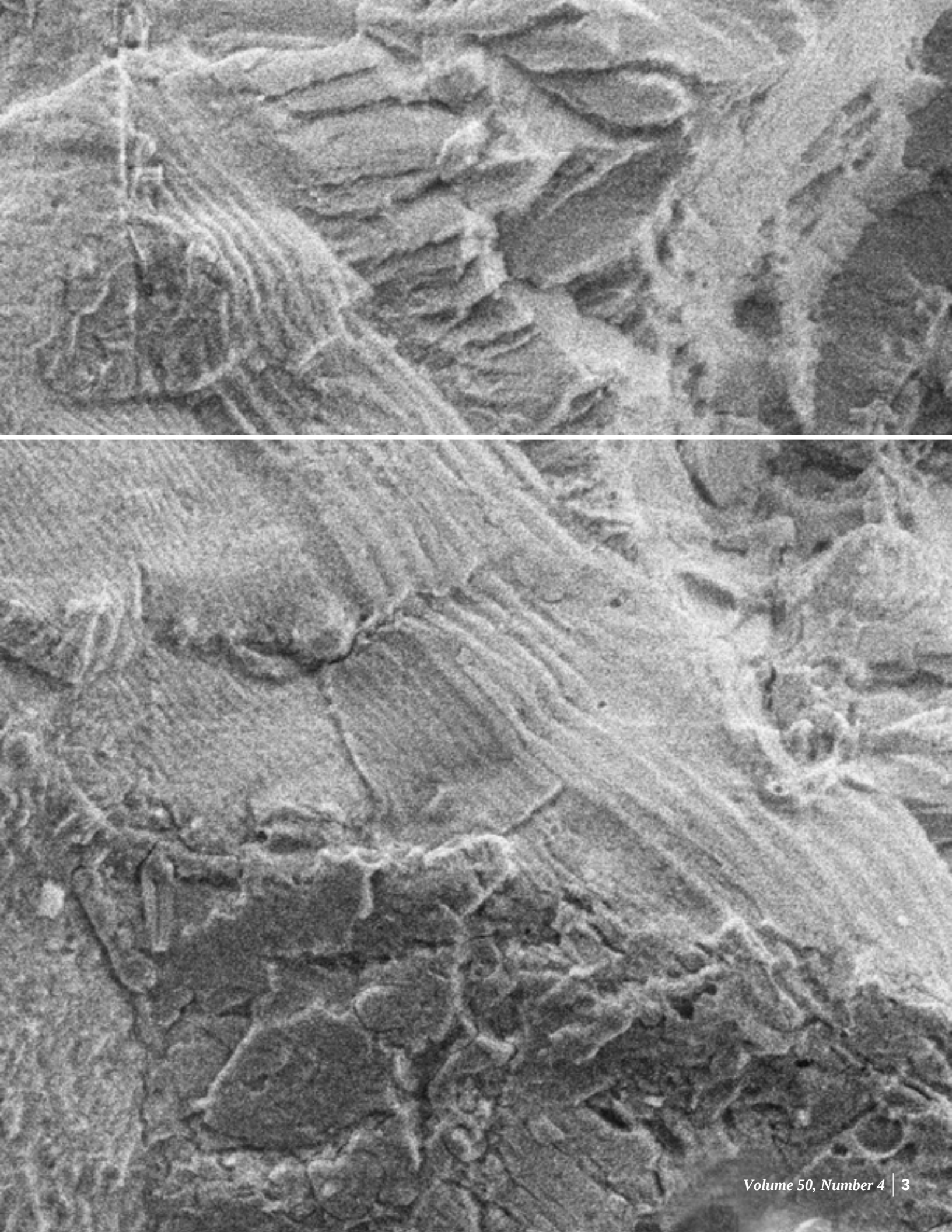

About the photo on the preceding page:

A full-scale fatigue test of a Grumman EA-6B "Prowler" wing, which was conducted in the late 1960s and early 1970s, determined that the wing fatigue life limited the aircraft's service life. That test was terminated due to fatigue failure of the lower wing skin in the center wing panels after flight spectrum loading equivalent to 9,000 flight hours. The EA-6B is currently projected to stay in the inventory until the year 2013, which will result in usage that is well beyond the service life determined by the full-scale fatigue test.

To enable the EA-6B to continue flying until 2013, the EA-6B's center wing panels will be replaced. However, this raises questions about the structural integrity of the outer wing panels, which did not fail during the full-scale fatigue test but also have not been subjected to fatigue testing that would verify and validate an extended service life.

Will the outer wing panels make it to 2013, too, or will they have to be replaced as well? To answer this question, metallurgists at the Naval Research Laboratory are analyzing samples from the outer wing panels of the EA-6B to help determine the aircraft's remaining fatigue life.

The photograph on the preceding page shows a fatigue crack that is growing from an imperfection in the inside of a fastener hole in one of those EA-6B outer wing panels, which was tested more than 25 years ago. Each of the diagonal bands that can be clearly seen at the center of page 3 is fatigue crack growth that resulted from one cycle of stress.

The narrow bands at left center are approximately 320 nanometers wide. In other words, it would take nearly 80,000 cycles of stress to grow the crack an inch. The wide bands at the center of the page resulted from cycles of higher stress and are 740 nanometers wide (about 35,000 per inch).

– S.P.

Photograph courtesy of the Naval Research Laboratory.

Current and Future Fatigue Life Prediction Methods for Aircraft Structures

Margery E. Hoffman and Paul C. Hoffman

Structures Division – Naval Air Systems Command
Patuxent River, Maryland

Introduction

The austere operational realities of the Navy's mission require Navy aircraft to withstand random fatigue loading during their design service life without cracking. Carrier-based aircraft operate from "floating air bases" that have runways only one-tenth the length of land-based runways, they often perform missions at altitudes barely clearing the waves, and they are on deployment away from maintenance hangars for months on end. The fundamental constraint for Navy aircraft, with respect to service life management, is that the broad theater of operations of aircraft carriers and the limited space onboard for aircraft maintenance facilities restrict routine inspections for fatigue cracks.

Readiness is the priority of the Navy airborne fleet. The need for readiness demands that structural integrity be incorporated into the design of an aircraft: Cracking should not be an issue when it's time for the aircraft to perform its mission. With a crack-resistant design, aircraft maintenance demands are minimized and safety does not rely upon routine inspections of the aircraft structure. The challenge is to design airframes that will last a lifetime, to predict fatigue damage before it happens, and to recognize it when it does.

Designers of Navy aircraft use a "Safe-Life" approach to structural design that allows the aircraft to withstand fatigue loading. Furthermore, Navy personnel use structural data recorded onboard the aircraft to predict the occurrence of crack initiation on every airframe individually.

In this paper, we will:

- Define and discuss the Safe-Life approach to aircraft structural design from the Navy perspective

- Show the mathematical basis for using the number "2" as a factor of uncertainty
- Describe the Navy's aircraft structural life surveillance program
- Discuss the future of aircraft life predictions (with respect to metal fatigue in fixed-wing air vehicles)

Background

There are two basic approaches to fatigue design. The first approach, known as "safe-life," predicts the amount of time until crack initiation. The second approach, known as "damage tolerance," predicts crack growth.

The Navy has adopted a safe-life approach for a number of reasons, but especially because carrier-based aircraft can spend months at sea, away from the hangars and other facilities where routine maintenance and repairs take place. In contrast, the US Air Force uses a damage tolerance approach to manage its aircraft. Unless the aircraft are deployed to the field for extended periods of time, the US Air Force has ready access to their fleet; therefore, they can more safely rely on structural inspections to attain and extend the life of their aircraft.

Both the safe-life and the damage tolerance methods have served their respective services well.

The Naval Aviation Approach to Fatigue Life Prediction

There are two major activities associated with fatigue life predictions. The first is analytically determining the service life of an aircraft structure and then validating that life through a full-scale fatigue test. The second is setting up an individual fatigue-tracking program that collects aircraft usage data and performs fatigue predictions quarterly for every fatigue critical component of over 3,500 airframes in the Navy and Marine Corps inventory.

Service Life

Service life limits are established for an aircraft based on operational requirements, design criteria, technical analysis and fatigue test results. In the safe-life approach used by the Navy, a piece of primary aircraft structure is considered to have reached the end of its fatigue life (i.e., it has failed) when a crack reaches 0.01″ in length.

Engineers can use detailed computer models to predict the service life of an aircraft's structure if they know the details of its design (such as the materials from which the aircraft is made) and the types of missions that the aircraft will fly.

The analytically predicted service life is then validated in the laboratory by subjecting a full-scale aircraft (usually one of the first to roll off the production line) to loading that mimics the severe load conditions that the aircraft might experience during flight. Large sets of computer-controlled hydraulic rams push and pull on the aircraft either until part of the structure fails or until cracks proliferate to the point where further testing is not warranted.

Critical parts of the aircraft structure are monitored during the test for evidence of cracking. After the test has been completed, components that have cracked are removed from the test article for further study. The surfaces of the cracks are inspected under a microscope, and the number of flight hours needed for the crack to grow to a length of 0.01″ (i.e., the fatigue life of that component) is noted. Incidentally, cracks always form in the full-scale fatigue test article; no aircraft was ever so well designed that no cracking occurred during the rigorous full-scale test.

The Test Spectrum

The most influential factor in determining service life from test data is the test spectrum, which is constructed from aircraft usage curves. The test spectrum is designed to simulate the full set of flight loads that an aircraft will experience during its entire service life. In the test spectrum, engineers try to account for every type of maneuver and mission that the aircraft will be expected to perform: takeoffs, landings, rapid climbs to high altitude, in-flight refuelings, high speed turns, etc.

One way to measure aircraft usage is to look at the profile of N_z exceedances per thousand hours of flight. "N_z" is measured in g's and is the acceleration in the *z* direction (i.e., downward through the floor of the

aircraft). An exceedance curve is a cumulative sum of occurrences reported at several acceleration levels. In other words, the exceedance curves tell the engineers how often the aircraft exceeds 2 g's, 3 g's, 4 g's, etc., during a certain period of time.

During the aircraft design phase, exceedance curves are constructed from historical data, including data that were obtained from accelerometer readings of past and current aircraft that are flying in the same role planned for the new aircraft. The design requirements for the new aircraft include the roles, missions, and approximate flight time per month, among other factors.

Military specifications provide guidance for formulating conservative flight-by-flight spectra from N_z data [1-5]. The current guidance, which is relevant for the Joint Strike Fighter (JSF) aircraft, is simply that the test spectrum shall represent the service life and usage adjusted for historical data, potential weight growth and future aircraft performance. For aircraft now being designed, specifications call for 90 percent of the aircraft in the fleet to meet the service life if they fly according to the test spectrum. Aircraft designers meet this guidance by developing a spectrum that represents at least 90% of the expected fleet usage during the operational service life.

The ninetieth percentile of a normal distribution is the mean + 1.32 times the standard deviation. Figure 1 shows the exceedance curves for two operational aircraft; it also shows the exceedance curve that matches a test spectrum designed from the fleet average usage. Aircraft that are now operational, such as the F/A-18C/D, were tested to a more rigorous spectrum that represented the mean + 3.0 times the standard deviation of the usage distribution. The current joint performance specification is less restrictive due to better notions of aircraft usage.

As mentioned previously, engineers try to include in the test spectrum loads that represent all of the maneuvers that an aircraft will be expected to make during its service life. In all full-scale tests, however, the test spectrum is modified for several practical reasons:

- Infrequent high loads are omitted from the test spectrum, because extremely high loads can introduce residual stresses in metals that can actually retard damage formation and crack growth. Removal of these high loads from the test spectrum causes damage to accumulate in the test article more quickly, resulting in a conservative value for service life for the aircraft in the fleet.
- Low loads are omitted from the test spectrum if they do not contribute to crack growth or other damage. Removal of these loads, which are often extremely frequent, saves a great deal of time in testing.
- Loads are introduced to provide "marker bands" on the surfaces of any cracks present in the test article. Because these marker cycles are introduced at known times in the test spectrum (which correlate to specific numbers of flight hours), the resulting marker bands help metallurgists analyze the crack growth rate and determine when cracks reached 0.01″ in length.

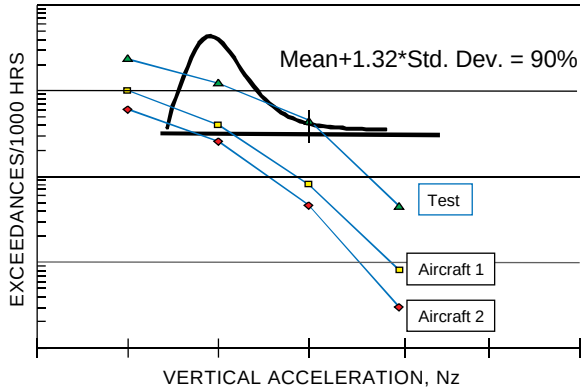

Fig. 1 - Exceedance curves for two operational aircraft, and an exceedance curve that matches a test spectrum derived from the fleet average usage

The marker cycles are made by rearranging the sequence of simulated flights, regrouping sequences of loads, or substituting cycles into the test spectrum. Marker cycles are designed so that they neither add nor retard damage in the test article.

The actual test spectrum is negotiated when the contract is written to buy the aircraft. For aircraft that were designed and tested before the F/A-18E/F, the criteria for test spectra were more severe. This severity was necessary because there were many unknowns

about the use and performance of the aircraft design. The Navy's newest acquisitions, the F/A-18E/F and JSF, are incrementally less different in performance and anticipated usage than the aircraft that they replace, relative to the differences between F-14 and F/A-18 A/B/C/D aircraft and the planes that they replaced.

The Factor of 2

For each critical cracking location in the test article, the time to crack initiation (i.e., the equivalent flight time needed for cracks to reach 0.01″ in length) is divided by two to obtain the component service life. For critical locations that have not cracked, the number of equivalent flight hours at the end of the test is divided by two. This factor of two is an engineering factor of uncertainty [1] and is used to calculate the desired service life by:

$$\text{Desired Service Life} = \frac{\text{time to failure}}{\text{factor of uncertainty}} \qquad (1)$$

where service life is a unit of time such as equivalent flight hours. Factors of uncertainty are used to provide some degree of assurance that variations in materials, fabrication, and aircraft usage do not result in the failure of a structural component. You may ask, however, "Why the number '2'?"

Full-scale fatigue tests take a lot of time to complete (from two to five years), and therefore they are very expensive. For this reason, only one test is completed and the results are assumed to be the median of a lognormal distribution of fatigue lives, such as the curve shown in Fig. 2. Next, the acceptable probability of crack initiation (P_f) for an aircraft over its lifetime is required by Navy management to be 0.0013 or less. This level of lifetime P_f is consistent with a P_f of 1×10^{-7} per flight for an aircraft with average flight duration of one hour and 10,000 flight hours at retirement. Finally, we assume that the standard normal deviate, σ, is 0.1, based on multiple tests reported in References 6 and 7. With these four assumptions in place, the factor of uncertainty — which has been reported to be a function of sample size [6] — can be evaluated according to the following equation:

$$\text{Factor of Uncertainty} = 10^{(z_{spec})\sigma\sqrt{(1/n+1)}}, \qquad (2)$$

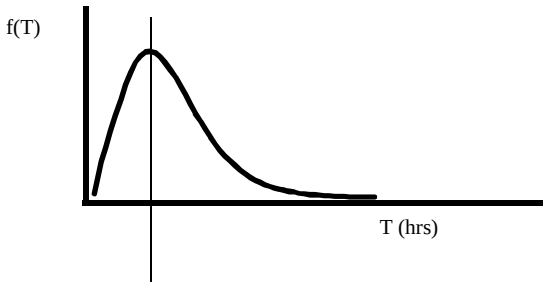

Figure 2 - A representative lognormal distribution of fatigue lives for a fleet of aircraft. (The median value represents the average fatigue life: Half of the fatigue lives will be longer, and the other half will be shorter.)

where σ is 0.1, n is the number of samples, and z_{spec} is the value from the standard normal table corresponding to the specified P_f. (For a $P_f = 0.0013$, $z_{spec} = 3.02$.)

Figure 3 shows this relationship for several different combinations of σ and P_f. The middle curve represents a $P_f = 0.001$ and $\sigma = 0.10$, which are the values directed by current Navy policy. Notice that the factor of uncertainty varies from 2.7 for a sample size of 1 (at the left side of the curve) and that it approaches 2.0 for a sample size of 10 or greater. The number 2 is selected as the factor of uncertainty, based on the presumption that engineering experience allows us to assume an infinite sample size.

The top curve in Fig. 3 shows the relationship of factor of uncertainty and sample size for a slightly larger standard deviation of $\sigma = 0.12$. Note that this slight increase in standard deviation increases the factor of uncertainty to 3.2 for a sample size of 1 (and to 2.5 for

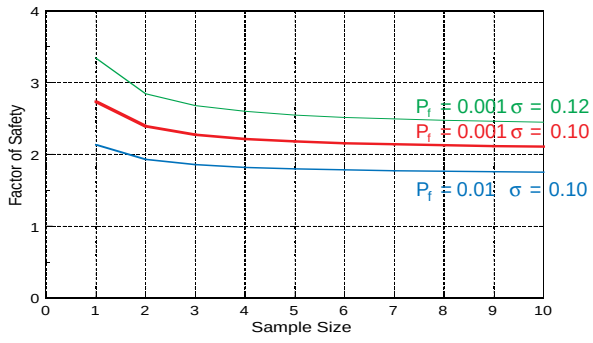

Figure 3 - Factor of safety as a function of sample size

larger sample sizes) to maintain a probability of failure of 0.001.

The bottom curve in Fig. 3 shows the relationship with $P_f = 0.01$ and $\sigma = 0.10$. This curve illustrates that reducing the current factor of uncertainty from 2.0 to 1.8 increases the probability of failure by an order of magnitude, from 0.001 to 0.01.

The Fatigue Algorithm: Tracking Individual Aircraft

Very few aircraft will fly missions according to the service life simulated in the test spectrum. Some aircraft will fly sets of missions that are more severe than the test spectrum, while most aircraft will accumulate exceedances at a slower rate. Therefore, the Navy uses techniques — known as fatigue algorithms — that can help predict the fatigue damage and crack formation that may occur in a particular aircraft based upon the manner in which the aircraft is actually flown.

Most Navy and Marine Corps fixed-wing aircraft have equipment that record flight data that indicate aircraft usage, which is used to calculate crack formation. Fatigue damage is reported as fatigue life expended (FLE), which is an index relative to the test flight hours it took to form 0.01″ cracks. FLEs are calculated at 5 to 9 locations for fighter/attack aircraft and at 20 to 30 locations for patrol and support aircraft. FLEs are used to schedule routine maintenance and structural inspections, life assessment programs, service life extension programs, and retirements of aircraft from the active fleet.

The strain-life approach was first used to predict crack initiation on the F/A-18 aircraft in the 1980s, and it is now the standard of all FLE calculations. The strain-life method models the response of a material near notches or other portions of a component where stress and strain are elevated. When loads applied to a structure are low, stresses in the material are elastic (i.e., stresses and strains are linearly related, or proportional to one another). As load levels rise, however, stresses near a notch or hole in the structure can easily exceed the stress that a material can withstand; in such a case, the material responds plastically to relieve the local stress field. The strain-life method uses the fluctuating local plastic deformation in a material to predict fatigue damage.

Every material has a particular strain-life curve, which is determined by subjecting smooth, unnotched, hourglass-shaped specimens of the material to full-reversed constant amplitude loading until they fail. (Full-reversed, constant amplitude loading means that the loading cycles between a peak tensile stress and a peak compressive stress of the same value.) The time needed to fail the smooth specimens is highly correlated with the time to form a 0.01″ crack at a fastener hole under identical loading [8]. The assumption of equivalency in damage accumulation between the two cases (i.e., the test article and actual aircraft components) is considered to be slightly conservative and is therefore useful for calculating fatigue damage and service life.

Figure 4 shows a typical strain-life curve, which exhibits two distinct portions: low-cycle fatigue, where strains are high and fatigue life is relatively short, and high-cycle fatigue, where strains are low and fatigue life is relatively long. For most materials, the transition in behavior between high-cycle and low-cycle fatigue occurs in the region of the curve between 1,000 and 10,000 cycles to failure. The strain-life curve is defined by adding the effects of two mechanisms together. Total strain amplitude, $\Delta\varepsilon/2$, is the sum of the elastic and plastic strains:

$$\frac{\Delta\varepsilon}{2} = \frac{\sigma'_f}{E}(2N_f)^b + \varepsilon'_f(2N_f)^c \qquad (3)$$

where N_f is the number of cycles to failure. The terms b and σ'_f are the slope and intercept respectively of the elastic strain-life relationship, and the terms c and ε'_f are the slope and intercept respectively of the plastic strain-life relationship, which are obtained when strain amplitude vs number of cycles to failure are plotted on a log-log scale, as shown in Fig. 4. Service life is determined by using the strain-life curve to make calculations of total strain amplitude. Additional terms are added to account for cycles of variable amplitude loading that have mean stresses greater than zero.

The advantage of using the strain-life method over stress-life methods is the relative simplicity of the testing required to establish the materials database.

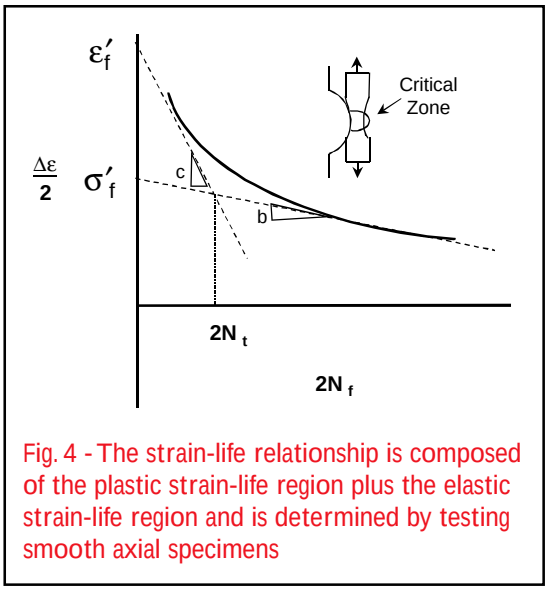

Fig. 4 - The strain-life relationship is composed of the plastic strain-life region plus the elastic strain-life region and is determined by testing smooth axial specimens

The strain-life method employs a single strain-life curve that is used along with the stress-strain curve to generate predictions for any geometry in the structure. In contrast, stress-life methods need several stress-life curves representing a range of stress concentrations (geometries) present in the structure along with the stress-strain curve to generate predictions.

But the prime advantage of the strain-life method is that it can account for localized plastic behavior of materials near stress concentrations, whereas the stress-life method cannot. For these reasons, the strain-life approach is attractive to the Navy and manufacturers of aircraft alike.

The major limitation of the strain-life method is that it is valid only while a crack is forming in a material. After a crack has formed, stresses are relieved in the material through crack-tip plasticity and crack propagation. At that stage, crack growth models are needed to predict service life.

The Structural Appraisal of Fatigue Effects Program

The Structural Appraisal of Fatigue Effects (SAFE) program is the Navy's tool for individually tracking critical locations on airframes so that service life is maximized. Calculating fatigue damage by tracking aircraft usage rather than using a representative or conservative stress history assures more efficient use of service life for individual aircraft. Individual stress histories are determined from data collected from the aircraft as they perform their missions. Summary data are used to schedule structural inspections and/or modifications, to modify operational usage to extend service life, and to retire aircraft. Additionally, aircraft usage data collected now will be used to design new aircraft in the future.

Fatigue damage accumulation on an airframe (as measured by Fatigue Life Expended, or FLE) is reported in a monthly or quarterly SAFE report. The FLE data is used to project aircraft service life in terms of flight hours. Type Commanders use the SAFE report to project aircraft readiness and schedule maintenance.

Figure 5 summarizes the first two of the four elements of the FLE tracking process. The four main elements of tracking are data collection, data reduction, damage calculation, and information dissemination, which will be described next.

Fig. 5 - The Fatigue Tracking Process: Data are downloaded from the aircraft and reduced to sequences of stresses at critical locations

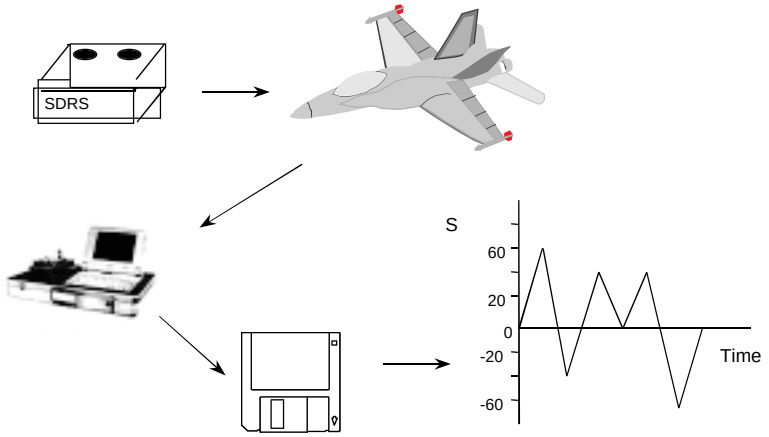

Data Collection: Data recorders and sensors such as accelerometers help construct exceedance curves for the aircraft as it conducts its flight operations. New aircraft are delivered with manufacturer-supplied multi-channel data recorders. Older aircraft are being retrofitted with the Structural Data Recording Set, SDRS, a generic multi-channel recorder. These

recorders allow sequences of aircraft loading cycles to be saved in chronological order for input into the strain-life algorithm. At regular intervals, maintenance crews perform data recovery from individual aircraft. Depending on the type of aircraft and recording set, data storage units fill up weekly. Data are sent monthly to Naval Air Systems Command, Patuxent River, Maryland, for processing.

Data Reduction: After the data are subjected to strict quality control measures, a stress history (such as the one shown in Fig. 6a) is developed for each monitored location of aircraft structure. These stress histories are then used to construct hysteresis loops such as the one shown in Fig. 6b. Hysteresis loops, which are created by plotting local stress versus strain, identify damaging events. The area within a closed hysteresis loop is the energy per unit volume that is dissipated during a loading cycle, and it represents a measure of the plastic deformation work done on the material [6]. After the ranges and means of the closed hysteresis loops are determined, equivalent strain amplitude is calculated and then the strain-life relationship (Figure 6c) is used to calculate the Fatigue Life Expended.

Damage Calculation: As mentioned earlier, each single cycle of loading causes a certain amount of fatigue damage; repeated cycling at that level of loading will eventually cause the material to fail. N_f, the number of cycles needed to cause a material to fail at a particular level of loading, can be obtained from the strain-life curve for the material. Correspondingly, the damage fraction for a single cycle of loading is defined as $1/N_f$.

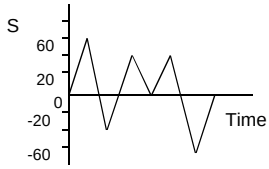

Fig. 6a - Typical stress history for a critical structural location

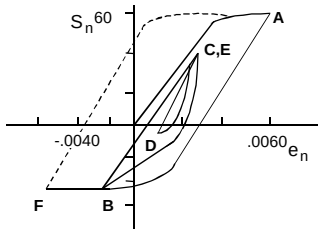

Fig. 6b - A typical hysteresis loop, which identifies load cycles that cause fatigue damage

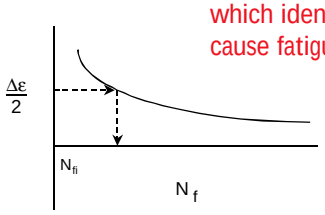

Fig. 6c - The equivalent strain amplitude (obtained from Equation 3) is used to calculate the Fatigue Life Expended (FLE)

The incremental damage is calculated by multiplying each of the damage fractions ($1/N_f$'s) by the number of loading cycles that have the same equivalent strain amplitude and summing them, as represented by the following equation (known as Miner's Rule):

$$\text{Cumulative Damage} = \sum_{i=1}^{nt} \frac{n_i}{N_{fi}}, \qquad (4)$$

where *nt* is the total number of discrete strain amplitude levels (which correspond to different levels of loading), n_i represents the number of cycles that have occurred at the *i*th strain amplitude level, and N_{fi} represents the number of cycles needed to cause failure of the material at the *i*th strain amplitude level. According to Miner's Rule, when the cumulative damage equals 1, failure is predicted to have occurred.

In applying Miner's Rule to naval aviation, failure is defined as the formation of a 0.01″ crack, based on data obtained from the full-scale test article. This linear damage summation method is widely used in fatigue algorithms, independent of the sophistication of their damage equations. Open loops are typically included in the monthly incremental damage as half the damage of a closed loop, and are also saved for closing with future data. The level of residual stress to carryover from month to month of data receipt is often a topic of discussion among the engineers responsible for tracking aircraft usage, especially as lapses occur in data receipt and usage must be assumed.

FLE is calculated by multiplying the cumulative damage suffered by the aircraft since it began flight operations by 200%, which is consistent with applying a factor of uncertainty of 2. (In other words, when an aircraft component has accumulated fatigue damage equivalent to the full-scale test article at half of its life, the FLE has reached 100% and the end of its service life. As mentioned earlier, the service life of a component is determined by dividing the time to failure — the time needed to grow a 0.01″ crack — by 2.) Figure 7

shows FLE, which represents the percentage of life used toward failure, plotted versus flight hours. Aircraft are nominally retired when FLE = 100%.

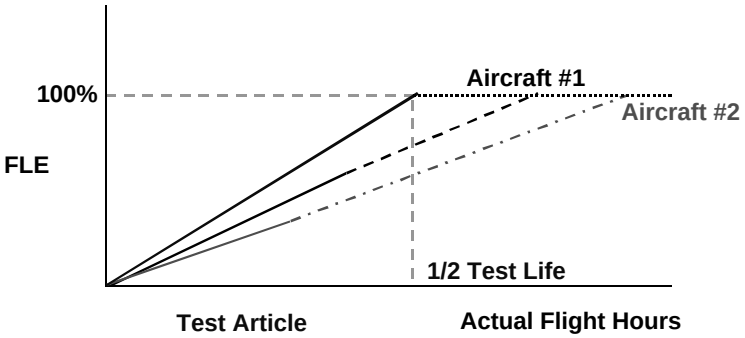

Fig. 7 - FLE is an index that represents the portion of fatigue life expended, as compared to the fatigue life obtained for the test article. (When FLE reaches 100%, an aircraft is nominally retired.)

Information Dissemination: FLE, FLE rates, total flight hours and the number of aircraft landings are reported by individual aircraft bureau number and published monthly on a floppy disk, or quarterly on paper by aircraft model. Scatter plots of FLE by type, model, and series of aircraft are used to project maintenance and retirement. These SAFE reports are provided to the relevant squadron and organizational level personnel for their planning and fleet management. FLE rates are also used by OPNAV to plan readiness levels and procurement needs.

Each month's flight data statistics are available at the end of the next month. Near-term plans include using secured websites to obtain and disseminate data so that this turn-around time is reduced.

The Future of Life Prediction for Aircraft Structural Components

What are the implications of our current approach to fatigue life estimation? You could say that we are testing and validating our design every time an aircraft flies. We've had good experiences with our aircraft. Class A mishaps due to structural failures are extremely rare: A reasonable estimate of occurrence is 1 incident for every 15 million flight hours. The chances of an aircraft falling out of the sky for structural reasons is one-tenth the chance that the pilot will be struck by lightning.

These statistics are related to past events, however. What do they imply about the safety of future flights?

In the current socioeconomic climate, replacement planes are not guaranteed. Legacy airframes must last 30, 50, or even more years beyond their FLE limits. As long as an aircraft is flying within its FLE limits, we know from the full-scale test experience where to expect cracking. Inspections are designed for these specific locations. The probability of crack initiation is small.

As aircraft fly beyond their limits, however, we expect that cracks will form at other sites that were not detected during testing. Consequently, the fidelity of the inspections degrades. To put it simply, it's infinitely harder to find cracks if you don't know where to look. An inspection technique can be perfect but it will not have much value if we're looking in the wrong place. Service life predictions are complicated by mission changes for the fleet and by modifications to the power plant or structure. We need to account for the random aspects of structural loads in addition to exceeding the original design life. We need a new tracking approach to handle intense operational demands in an environment of reduced budgets.

Flying more than the flight hours associated with 100% FLE is venturing into a sky of uncertainty. We are only beginning to fly aircraft beyond our previous experiences. The current life prediction approach is not extensible to FLEs greater than 100%. A current Science and Technology Initiatives Program (STIP) that is funded by the Naval Air Systems Command Science and Technology Office (NAVSTO) is focused on providing reliabilities resulting from various actions and allowing the decision maker (operations commander) to heuristically weigh the costs. These reliabilities go beyond crack initiation; they will be based on *total life*. This research and development is a natural progression in answer to the changing socioeconomic realities.

Normally cracks are modeled as having three distinct behaviors at three stages of life: nucleation, growth as a small crack, and growth as a large crack. Of course, the

crack doesn't know what stage of life it's in, it simply responds to the driving forces that are thrust upon it! Therefore, the Navy's working definition of total life will encompass a two-stage model, consisting of crack initiation and crack growth. Figure 8 compares these two models of total life.

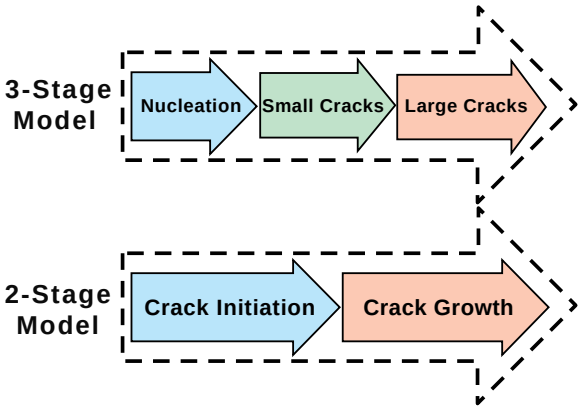

Fig. 8 - Two different models of "Total Life"

From our perspective, the Navy has a need to consider the life of small cracks in the calculation of fatigue life, because small cracks will develop when aircraft are required to fly beyond an FLE of 100%. Consequently, this is an area where the greatest payoff in modeling can come. Ironically, the Air Force also has a need to consider the life of small cracks, because that is the regime that will provide their aircraft with longer service lives. Both services are working the same modeling problem but coming at it from the opposite ends of the life model.

Figure 9 depicts the total life concept. The life of an aircraft is a random variable: We can not say with certainty how long an aircraft will fly without suffering a catastrophic failure due to cracking. Using a probabilistic approach to modeling, we can say with what reliability life can be obtained. Life is composed of two stages, as described by our model: crack initiation and crack growth. The total life probability density function is a joint probability of times to crack initiation and the times to reach critical crack size at a critical location.

Concluding Remarks

In this article we have presented an overview of aircraft fatigue life prediction. We have described our new

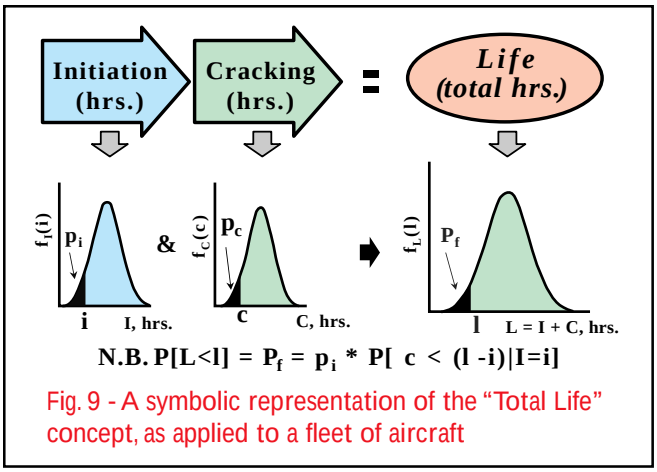

Fig. 9 - A symbolic representation of the "Total Life" concept, as applied to a fleet of aircraft

focus on a total life approach to predicting life with a calculated probability of failure. In order to improve Naval aviation readiness and ensure safety, the following areas of research need to be addressed with funded programs: small crack modeling, probabilistic methods and decision theory. Failure to address these areas will adversely affect readiness and the cost of maintaining the aircraft in the current inventory. Furthermore, initiating studies in these areas can possibly lead to new ways to decrease weight - and therefore decrease operational costs - in future aircraft.

We hope this article has educated our readers on the complexity, randomness and uniqueness of naval aviation and the ways that we currently account for these uncertainties. Additionally, we hope this article highlights the need to fund new research that is directed at formulating a total life approach that will have the flexibility to quantify safety and readiness for life extension programs and reduce the cost and weight of future aircraft.

Acknowledgments

The authors would like to gratefully acknowledge Mr. Don Polokovics, of the Tactical Strength and Airframe Technology Branch, for his many valuable discussions with us; and Mr. Kalmen Leikach, Structures Division Head, and Mr. Barry Sturgis, of the Aircraft Structural Life Surveillance Branch, for their continuing support of our work. Finally, we acknowledge Mr. David Eby for his thorough historical archive searches and publication procurement.

References

1. Joint Service Guide Specification, *Aircraft Structures, General Specifications for, (Draft)*, ASC/ENFS, Wright-Patterson AFB OH 45433-6503 or Naval Air Systems Command/4.3.3, Patuxent River MD 20670-1906, DRAFT 1997.

2. NAVAIR 01-1A-13, *Fatigue of Aircraft Structures*, Naval Air Systems Command, Department of the Navy, 1966.

3. MIL-A-8861B, *Airplane Strength and Rigidity Flight Loads*, 5 Dec 1994.

4. MIL-A-8866C, *Airplane Strength and Rigidity, Reliability Requirements, Repeated Loads, Fatigue, and Damage Tolerance*, 3 Oct 1994.

5. MIL-A-8867C (AS), *Airplane Strength and Rigidity Ground Tests*, 3 Oct 1994.

6. A.O. Payne, "Determination of the Fatigue Resistance of Aircraft Wings by Full-scale Testing," in *Full-scale Testing of Aircraft Structures*, 5-11 June 1959, Amsterdam, Netherlands, (Pergamon Press, New York NY, 1961), pp. 76-132.

7. E.D. Bouchard, "Evaluation of Fatigue Capabilities on High Performance Military Aircraft," (paper No. 24 presented at the 5th Pacific area national meeting of the American Society for Testing and Materials, Seattle WA, 31 Oct.-5 Nov. 1965).

8. J.A. Bannantine, J.J. Comer, and J.L. Handrock, *Fundamen-*

The Authors

Dr. Margery E. Hoffman is a Senior Technical Investigator in the Aircraft Structural Life Surveillance Branch of the Structures Division, Naval Air Systems Command, Patuxent River, MD. She holds B.S. and M.S. degrees in Structural Engineering from Purdue University, and a Sc.D. in Structures and Dynamics from George Washington University. She also has held engineering research positions at the USAF Wright Laboratories and the USDA Forest Products Laboratory. Her research interests are metal fatigue and crack growth, probabilistic methods, and computational neural networks as approximators.

Dr. Paul C. Hoffman is a Senior Technical Investigator in the Tactical Aircraft Strength Branch. He is the Structures S&T team lead and the Structures/Materials Aging Aircraft team lead for the Air Vehicle Department, Naval Air Systems Command, Patuxent River, MD. He previously held a faculty position at Villanova University. He holds a B.S. degree in Mathematics, University of Scranton; a B.C.E. degree and M.C.E. degree, Villanova University; and a Ph.D. in Structural Engineering from The Pennsylvania State University. His research interests include structural reliability, uncertainty factors, structural repair, corrosion fatigue, and aging aircraft.

What's Eating Us?

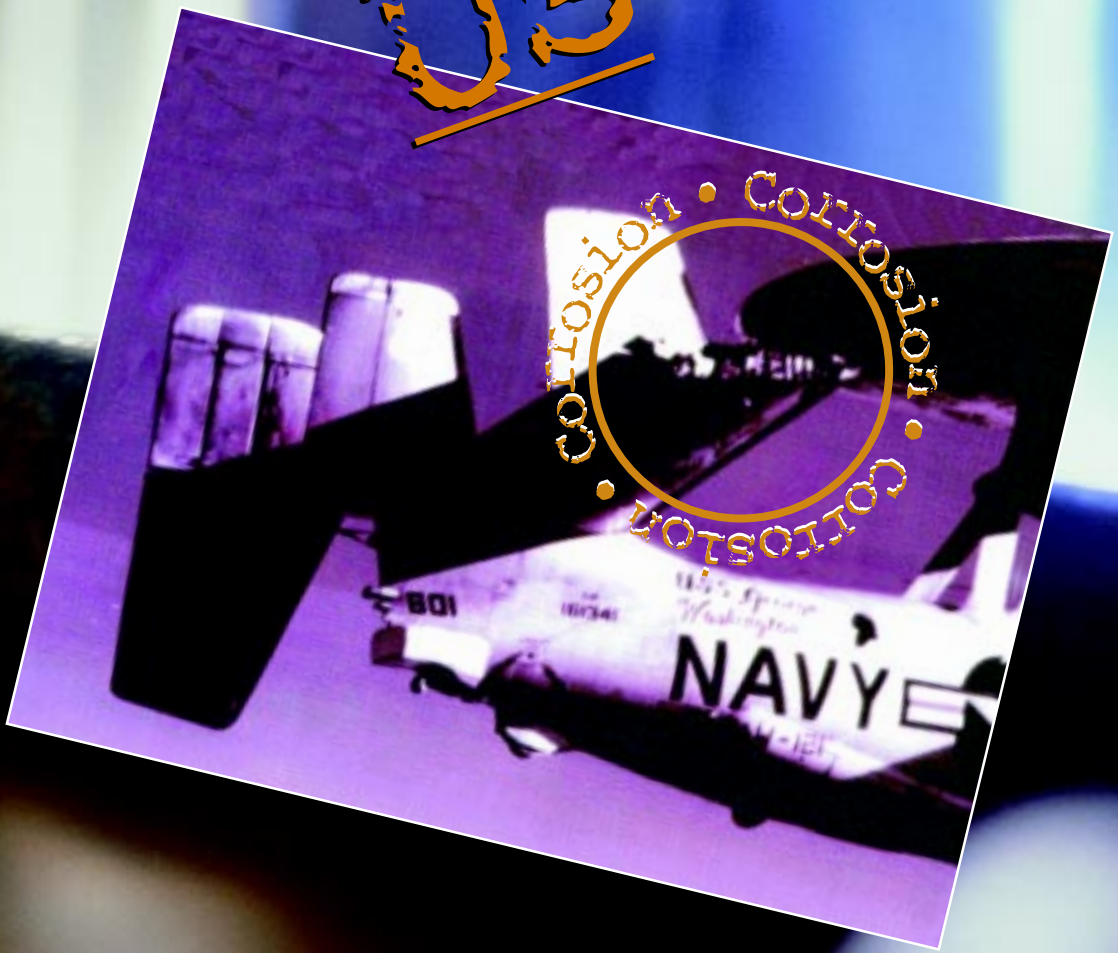

Corrosion!

Automobile mufflers and old tin cans aren't the only things that get rusty. Even high-strength steels, titanium alloys, and other advanced aerospace materials succumb to the gradual degradation that results from exposure to the elements.

In the weakened state brought on by corrosion, materials become even more susceptible to the fatigue damage caused by the repeated cycling of high stresses. And even though the degradation can be substantial, it often isn't easily detectable. As a result, unexpected failures in aircraft components (such as the in-flight loss of a tail surface from an E-2 aircraft shown in the photograph at left) can occur.

Most of the damage that comes from corrosion, however, isn't as dramatic as pieces falling off of an aircraft. Usually, it's merely similar to the rust on your porch swing and your lawn mower. But that doesn't mean it's not a problem: DoD spends nearly $3 billion each year for corrosion repairs and other maintenance costs for its fleet of aircraft.

In the following article, a scientist in the Aircraft Division at the Naval Air Warfare Center at Patuxent River, Maryland, discusses some of the corrosion-related factors that affect the rate of crack growth in aerospace materials.

– S.P.

Fatigue and Corrosion: Aircraft Concerns

Vinod S. Agarwala

Naval Air Warfare Center – Aircraft Division
Patuxent River, Maryland

Introduction

Unfortunately, many of the high-strength materials used in load-bearing aircraft structures are also susceptible to the effects of corrosion. Although materials like 7075-T6 aluminum alloy have higher toughness, they also have poor resistance to corrosion fatigue and stress corrosion cracking. Similarly, steels like AISI 4340 or 300M, in their highest strength temper, are well suited for landing gear, but these materials exhibit problems in an environment where the effects of corrosion play a dominant role.

Corrosion and corrosion-related factors undermine the fatigue and toughness properties of these materials to such a significant extent that service failures become a serious concern. For example, corrosion in aging aircraft can aggravate other problems such as metal fatigue to the point where service life is reduced. In fact, catastrophic failures of aircraft structure due to corrosion have occurred. To help prevent such failures, the effects of corrosion on the fatigue properties of existing aircraft materials are being reviewed with a renewed perspective. At the same time, the search is on for new materials that are both strong and tough *and* resistant to corrosion fatigue and stress corrosion cracking.

Research into the mechanical, metallurgical, and electrochemical aspects of corrosion fatigue may lead to an in-depth understanding that will allow structural analysts to better assess the remaining life of an aging component. Sensors that can detect and monitor the initiation and growth of cracks from sites of corrosion pitting or crevice corrosion are being developed; if reliable, these new tools may allow maintenance crews to apply preventive measures and possibly extend the service life of affected components.

This paper discusses how various chemical environments interact with *in situ* properties of a material, as well as the electrochemical properties of the surface and tip of a crack, to affect the crack growth rate in the material [1]. Other topics include the interaction of corrosion and stress, and how crevices in structures play a critical role in initiating and accelerating cracking under low and high amplitude stresses in the presence of a corrosive environment.

The Concern

The Department of Defense spends nearly $3 billion each year for corrosion repairs and other maintenance costs for its fleet of approximately 15,000 aircraft. The Navy's share of this annual amount for its fleet of more than 4,600 aircraft is about $1 billion. Not all of these maintenance costs are directly associated with corrosion fatigue, but this phenomenon most certainly causes a significant portion.

Avoiding corrosion fatigue for any aircraft is a formidable task, but it is especially difficult for those involved in naval aviation because they operate in one of the world's most severe environments. Aircraft components are exposed to a multitude of corrosive agents (including sea water and exhaust gases like sulfur dioxide [SO_2], nitrogen oxides [NO_X], and others) under extremely high flight loads and vibrational stresses that often approach and sometimes exceed the limits that the aircraft's materials can handle.

These high-performance naval jets not only experience damaging stresses when they perform flight maneuvers. Because they operate from aircraft carriers, the planes also must endure enormous loads and stresses

when they are catapulted from the flight deck or when they land at high speeds and high sink rates to make sure that their tailhooks engage the carrier's arresting cable. In such an operational environment, it is virtually impossible to keep water from intruding into the aircraft joints, places where hinges overlap, or other gaps in the structure even when sealant is present. The most common result of this exposure is a phenomenon called crevice corrosion and pitting.

Engineers can use detailed analytical techniques (such as fracture mechanics and finite element analysis) to design an aircraft component that can operate safely even though it contains a crack or other defect of a certain size. However, these analytical techniques become much less accurate when the effects of corrosion are considered, because the precise effect of corrosion on the material's strength and other properties are neither easily quantifiable nor fully understood. Therefore, the analytical model that predicts the rate of fatigue damage in aircraft components fresh off of the factory floor (i.e., those made of pristine, uncorroded material) is no longer valid for materials that have been degraded by corrosion.

FRACTURE MECHANICS. The concepts and equations used to determine how cracks grow and how cracks affect the strength of a structure.

FINITE ELEMENT ANALYSIS. An analysis technique (usually computerized) that divides a complicated structure or component into smaller, discrete, more manageable units called *finite elements*.

As discussed below, each of these methodologies used to design aerospace structures — the "fail-safe" approach and the "safe crack growth" approach — are intrinsically inadequate to consider the effects of corrosion.

"Fail-safe" design: The fail-safe design approach assumes that multiple, redundant load paths through a component will reduce the stresses produced by the applied loads to safe levels (i.e., levels that produce stress intensities below a threshold stress intensity [ΔK_{th}] or a certain value of fracture toughness [K_{IC}]). This approach to aircraft design also assumes that the multiple load paths in a component will provide design features that arrest a crack before it grows to a length that will cause the part to catastrophically fail.

THRESHOLD STRESS INTENSITY (ΔK_{TH}). The value for change in stress intensity below which, theoretically, there is no crack growth.

FRACTURE TOUGHNESS. The parameter that measures a material's resistance to fracture (usually symbolized by "K_{IC}"). When the stress intensity factor for a component is equal to the fracture toughness for the material, the component breaks.

The question, then, is whether the ΔK_{th} and K_{IC} values assumed for a material are realistic if the effect of corrosion is included. The K_{IC} value for most materials depends upon the test conditions under which it was measured, including factors such as the magnitude of the stresses, the rate at which the stress cycles occur, and the environment in which the test was conducted (temperature, humidity, the presence of corrosive agents, etc.).

In most cases, a component's built-in safety margin allows engineers to develop a conservative estimate of fatigue life. But as the aircraft ages, the cumulative damage due to corrosion and plastic deformation (caused by vibrational stresses and wide spectrum fatigue) change the material properties, which become difficult to estimate.

Obviously, analytical models that predict service life can only be as good as their input data. Therefore, developing a fair understanding of the effects of corrosion so that we can obtain reasonably good data that can be applied to an aging aircraft is an important element in more accurately estimating an aircraft's fatigue life.

The Aloha Airlines Boeing 737 disaster, where widespread fatigue damage around the fastener holes was determined to be the cause for failure, is a clear example that fail-safe design criteria do not always offer protection from catastrophic failure of components.

"Slow Crack Growth" design: The U.S. Air Force uses the slow crack growth design approach for their aircraft. This analytical approach presumes that undetectable manufacturing flaws exist in structural components when the aircraft rolls off of the production line. However, these flaws are not a matter of great concern because the aircraft is designed to ensure that even the largest undetectable flaw in the worst possible location will not grow to critical size during two lifetimes of service life. For this reason, the "slow crack growth"

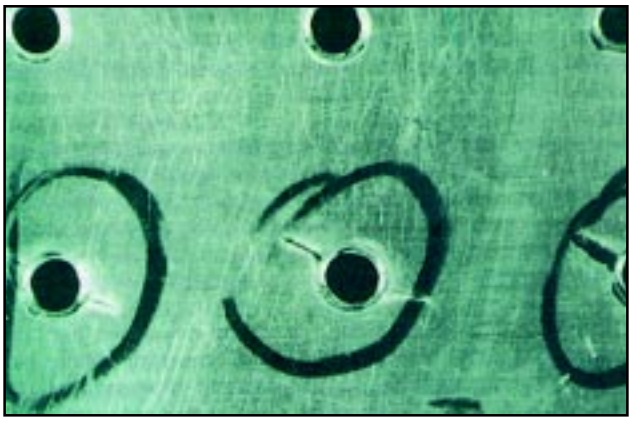

Fig. 1 - Multiple fatigue cracks found at countersunk fastener holes during a teardown inspection of a US Air Force KC-135 tanker aircraft. (The cracks can be seen extending from each of the circled holes at the 10 o'clock and 4 o'clock positions.)

design approach is also known as the "damage tolerance" approach.

The approach depends on the presumption that the flaws in a structure are smaller than the detectable size and are therefore not of great concern. What is frequently overlooked is that no inspection can be absolute and deterministic in value, especially for damage in hidden areas of structure (such as those beneath the heads of rivets or screws, areas for which there is no precise minimum detectable flaw size). Therefore, new and innovative tools and techniques that can rapidly and effectively detect small cracks that exist in large areas of structure are needed.

The Navy Approach: The US Navy has adopted the safe-life design approach for its aircraft. This approach differs from the damage tolerance approach in that the aircraft structure is designed to have a low probability of cracking during the design service life, the so-called "safe" life. This approach generally accounts for changes in loads and usage, but makes no acknowledgement of actual material condition, which may degrade with time. Large structures will always have some defects or small flaws that either are introduced during manufacture or develop during operational service. Even if these flaws are not detected due to limitations in the inspection technique, it is dangerous to conclude that they do not exist.

Another assumption about flaws that should be reconsidered is that small, supposedly subcritical cracks will not grow. The effects of corrosion can cause even small cracks under dynamic stress (and even small cracks under static, or constant, stress) to grow. Therefore, the relevance of a threshold for cracking under the fail-safe design approach does not exist. In some instances, cracks have been observed to grow at stress intensity factors even below the so-called design K_{IC} values. In other cases, tests conducted in corrosive environments under static conditions have found K_{ISCC} values that are lower than those determined for the same material in non-corrosive environments.

The Role of Corrosion

A simplistic way to understand the effects of corrosion on the low-cycle fatigue behavior of a high strength alloy [2] is to look at Fig. 2, which shows a plot of crack growth rate in AISI 300M steel as a function of the change in stress intensity factor (ΔK). In the plot, the rate of crack growth is displayed along the vertical axis and is expressed in units of change in crack length per cycle of stress (da/dN).

STRESS INTENSITY FACTOR. A parameter that mathematically describes the stresses at a crack tip in terms of both the magnitude of the stress applied to a component and the shape of the component. Stress intensity factors are usually symbolized by the letter "K"; subscripts help distinguish between different types of stress intensity factors.

K_{ISSC}. The threshold stress intensity for stress corrosion cracking. If the stress intensity for a component is kept below K_{ISSC}, then no stress corrosion cracking should occur.

The crack growth rate data shown in Fig. 2 were obtained in tests where the stresses varied between their maximum and minimum values at a frequency of 0.1Hz (or 1 cycle every 10 seconds), a typical rate for low-cycle fatigue. Test results show that the crack growth rates are about an order of magnitude higher for a wide range of ΔK values when test conditions are changed from very dry (less than 15% relative humidity, depicted by the open circles) to very moist (MA, depicted by the open triangles).

As chlorides are added to the moist air (MA + Cl^-, depicted by the X's in Fig. 2), the crack growth rate accelerates to a rate several times faster than the crack growth rate in dry air. Mechanical or stress intensity aspects of fatigue seem to play a smaller role in this behavior. In fact, the crack growth rate becomes almost independent of the stress intensity factor, which is a clear indication that the effects of corrosion are beginning to dominate the damage process [2].

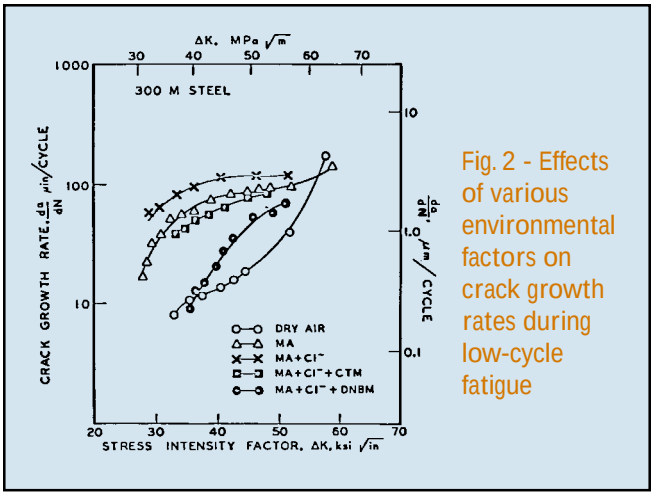

Fig. 2 - Effects of various environmental factors on crack growth rates during low-cycle fatigue

Even for values of stress intensity factor below 30 ksi√in, if moisture is present the fracture mechanics under pure fatigue behavior seems to be less important. Researchers at Lehigh University have shown that even at very low vapor pressures of moisture, the crack growth behavior of aluminum under low-cycle fatigue is still governed by the fast kinetics of corrosion and not by pure fatigue [3]. As long as there is some moisture present, the predominant reaction kinetics at the bottom of a crack, pit, or other defect is due to corrosion mechanisms. Other studies of the growth of short cracks have also indicated that crack velocities under corrosive conditions are significantly high [4].

Mechanistic studies on fatigue and corrosion have been very difficult to relate to one other, because most crack growth rate measurements have been made in a quasi-transient state condition (i.e., on a time scale that has extended well beyond the state where transient phenomena occur, and after an initial stress has been applied) [5]. Therefore, most analytical prediction models previously available in the scientific literature were primarily based on defining the physico-chemical processes occurring either after the cracking or in a quasi-steady state condition. These types of models provide an inaccurate prediction of the remaining fatigue life of a material.

Studies of Agarwala [6], Turnbull [7], Chung and Macdonald [8], and Pickering [9] were some early efforts to characterize the crack tip processes during a transient state; they were also the first studies that attempted to measure the electrochemical potential of the crack tip.

Electrochemical Factors: Under cyclic stresses and in the presence of an ion-conducting liquid, the bottom of a corrosion pit becomes an anode (i.e., it acquires a positive charge) and its adjacent side the cathode (i.e., it acquires a negative charge). Measurements of the changing potential for a crack growing through a 300M steel compact tension (CT) specimen in a moist saline environment show that the electrochemical potential of the surface of the crack tip can be quite high (nearly –1.1 volt relative to a Saturated Calomel Electrode (SCE)). The crack tip can also develop a voltage difference of up to 300 mV with respect to its adjacent side.

Figure 3 shows measurements of electrochemical or electrode potential that were taken with a microprobe (electrode) located at the bottom of the notch in a CT specimen. Voltages were measured relative to an SCE, which served as a reference electrode. As seen in the figure, the notch-tip (electrochemical) potential drops very rapidly from approximately –0.1 V (the potential associated with a passive surface of alloy steel) to –1.1 V when the tip of the crack reaches the microprobe. This 1.0-V drop in electric potential acts as a driving force that will further accelerate corrosion in the material at the crack tip. If described in terms of galvanic action, this difference in electrochemical potential is similar to a battery and can produce a current as high as 10 amperes per square centimeter (A/cm^2) over the exceedingly small area of the crack tip. Under the influence of such high currents, the material at the bottom of a notch or the tip of a crack could dissolve at rates that are orders of magnitude higher than the rate that a crack would grow under pure fatigue.

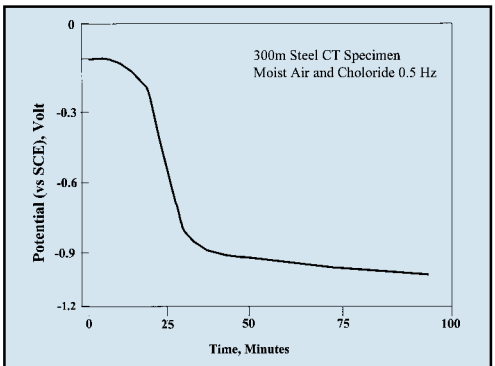

Fig. 3 - Changes in electric potential as an advancing fatigue crack passes a microprobe

In 7075-T6 aluminum alloy compact tension specimens undergoing corrosion fatigue in a 3.5% sodium chloride (NaCl) solution, Kendig and Mansfeld [10] measured a potential that was at least 200 mV more active than the bulk potential for the material. However, when the crack tip was passivated by an inhibitor (i.e., when corrosion was reduced to very low rates), the potential became more positive (called "passive" or "noble") as measured with alternating current impedance spectroscopy.

To better understand the effect of corrosion on crack growth rates for short cracks and for very low values of stress intensity, crack-tip potentials were monitored during corrosion fatigue experiments [6,11]. Figure 4 shows a plot of crack growth rate vs. the change in stress intensity for 300M steel exposed to moist (relative humidity above 90%), salt water conditions.

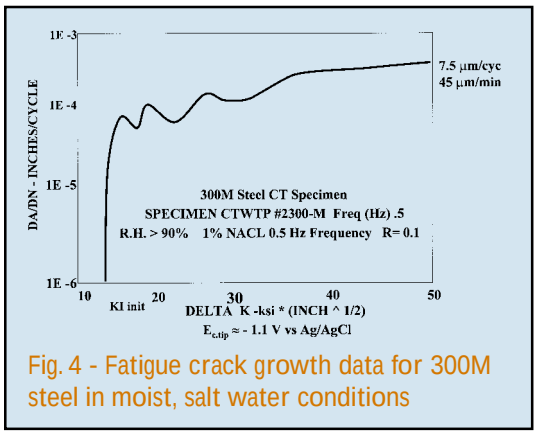

Fig. 4 - Fatigue crack growth data for 300M steel in moist, salt water conditions

Monitoring crack growth rates below 10^{-6} mm/cycle is very tedious and time consuming. Nevertheless, the data show that the rate of crack growth rose very sharply even for changes in stress intensity below 12 ksi√in, a threshold that is markedly below the critical flaw size where cracks are not supposed to grow under pure fatigue. The electric potential measured at the crack tip was approximately –1.1 V vs. an SCE reference electrode, a value that indicates corrosion is occurring [6]. This data suggests that even short cracks have a very active crack tip in the presence of a corrosive environment.

The data in Fig. 4 were obtained in an experiment where the stress varied at a rate of 1 cycle every 2 seconds. As seen in the upper right portion of the figure, for large changes in stress intensity in a moist salty environment, the crack would grow through 300M steel at approximately 45 mm per minute. At that rate, a crack would take less than 10 hours to grow about 1 mm. If the conditions were dry, the predicted time to grow the same distance would have been an order of magnitude greater under similar fatigue loading.

The Effect of Chemical Modification on Crack Growth Rate

Table 1 summarizes the results of experiments of chemical modification on crack growth rates in 10-in. three-point loading bend bar specimens made of high-strength 4340 steel. In these studies, the notch area of the specimen was chemically modified to reflect the test environment by introducing vapors of various additives through atomization in a closed chamber [1,2,12]. The test results show dramatic effects of chemicals in the specimen's environment on the rate of crack growth. In wet conditions, the crack growth rate increased by nearly a factor of 10 over the rate observed for dry conditions (from 12 to 110 µin/cycle, respectively). Correspondingly, the fatigue life (i.e., the number of cycles need to cause the specimen to fail) dropped from 17,500 cycles for dry conditions to 1,800 cycles for wet conditions. The presence of chloride ions further accelerated the rate of crack growth and reduced the fatigue life of a 1-inch-thick bend bar to 1,200 cycles.

Table 1 indicates that chemical formulations such as DNBM (which contains ions of dichromate [D], nitrite [N], borate [B], and molybdate [M]) can be used to effectively retard crack growth. When you compare the data in Rows 3 and 8 of the table, you see that the presence of DNBM slowed the crack growth rate in a wet air and chloride ion environment by a factor of 8.

Rows 4 through 7 of Table 1 show the effects of some of the individual chemicals in the DNBM formulation on crack growth rate and fatigue life. The dichromate is excellent corrosion inhibitor ("passivator") and performs exceedingly well in the absence of chloride (see Row 4). However, dichromate's passivating property is compromised when the chloride ion is present in the environment; the chloride ion breaks down the passive film as soon as it forms.

Table 1 – Effect of crack-tip chemistry on low-cycle fatigue behavior of 4340 steel [13]

Crack-tip Environment	Corrosion Mechanism/Observations	Crack Growth Rate (μin/cycle)	Stress Intensity Factor (ks√in)	Fatigue Life (cycles)
1. Dry air (15% RH)	Almost no corrosion	10	70	17,500
2. Wet air (100% RH)	Severe corrosion	110	35	1,800
3. Wet air + chloride	Extremely severe corrosion	200	30	1,100
4. Wet air + dichromate (D)	Passive film formed at the crack tip	40	50	6,800
5. Wet air + borate (B)	Adjustment in pH	65	35	3,300
6. Wet air + chloride + molybdate (M)	Some passivation and chloride counteraction	60	45	4,500
7. Wet air + chloride + (D) + (B) + nitrite (N)	Breakdown of passivity due to chloride	180	34	1,200
8. Wet air + chloride + DNBM	Passivation, pH modification, chloride counteraction	25	48	6,700

The test results show high crack growth rates and poor fatigue lives even when chemicals like borate (a pH modifier) and nitrite (an oxygen scavenger) were added (see Row 7). However, when molybdate is added to the mixture of DNB, the other inhibitors (N and B) retain their functional properties and the passive film is reinforced. Therefore, the corrosion fatigue data for DNBM in the presence of chloride showed the lowest crack growth rate and the best fatigue life (see Row 8) for tests conducted in potentially corrosive environments. It must be noted, however, that the fatigue life obtained by using DNBM in the wet air and chloride environment does not even approach that obtained during tests in dry conditions; indeed, it is less than 40% of the fatigue life in dry-air conditions. This confirms the hypothesis that as long as there is some moisture present, the low frequency fatigue behavior will not show a crack growth rate equivalent to that obtained for pure fatigue in dry-air environment, even when stress intensities are very low or the cracks are short.

Role of Pitting

It is believed that most cracks that lead to corrosion fatigue failure initiate from portions of the material where there is pitting or localized corrosion. Figure 5 is the photo of a crack surface in 7075-T6 aluminum alloy in which the fatigue crack began growing into the material from the corrosion pit (located at the left center of the picture), grew through the material, and then continued growing until the component failed.

Therefore, understanding the complex relationship between corrosion and pitting behavior and fatigue life is critical. Research that studies the depth, size, and density of pits that nucleate and grow is relevant to the fatigue life of materials, because these characteristics have a significant effect upon the amount of service life that can be expected from a structure. The frequency with which pitting occurs is also relevant, because up to 10% of pits can become passive or dormant and then reactivate. Furthermore, the deepest corrosion pit is not necessarily the weakest spot in the structure; under the proper conditions of stress and chemical environment, any non-critical pit can become activated, link up with others and grow. Also, it is well known that the growth rate for corrosion pits can be several times faster than general corrosion. Therefore, any prediction of remaining structural life that is based on the current size and depth of corrosion pits will be inaccurate and will likely be non-conservative (i.e., an overestimate). A corrosion pit or short crack that is now subcritical may not remain so indefinitely; indeed, it may grow very fast even under little or no stress. For aging aircraft, one can not simply use the existing condition of a component (pit size, pit depth, etc.) and predict its remaining fatigue life. As discussed earlier,

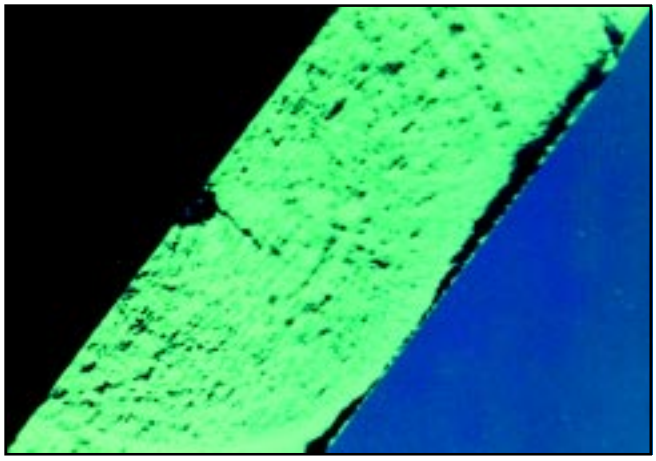

Fig. 5 - The fatigue crack that led to the failure of this component initiated at the active corrosion pit shown at the left center of the photograph

a corrosion pit that is passive or dormant today may become active tomorrow; if certain chemical ingredients are present, only moisture is needed to activate the corrosion and further degradation of the material.

To be accurate and deterministic, any analytical model to predict the remaining life of a material under fatigue must account for the effects of localized corrosion. The damage should be characterized in terms of pit nucleation and growth, regardless of whether the damage initiated from existing cracks or flaws in the material, stress corrosion cracks or crevices, or galvanic corrosion and/or microstructural corrosion. The research of Macdonald [13] confirms this, and it also suggests that no crack growth model can be considered deterministic if it does not conform to the laws of physics and chemistry, including the laws of equilibrium, Faraday's Law, the laws of conservation of mass, charge and momentum, and others. Therefore, accurately determining corrosion behavior (such as the susceptibility of materials to localized corrosion; the rates of corrosion and pit nucleation; and damage growth parameters (size, density, etc.)) is just as important as an accurate understanding of fatigue behavior in general.

For aluminum alloys, the rates of pit nucleation and growth are directly related to electrochemical potential of the crack or pit surface, the concentration of chloride ion in the environment, and the length of exposure to the environment [13]. This research also showed that the pit density grows by a factor of 4 within 5 years, and up to 2% of corrosion pits can be up to 8.5 mm in depth. The research further demonstrated that if the electrochemical potential at the bottom of the pit increases, the pit growth rate increases and deeper pits are formed. This phenomenon happens even at lower stress intensities, where analyses that consider only pure fatigue may overestimate the remaining life for a component or material.

For example, a number of F/A-18s deployed on the USS *Midway* in the mid-1980s developed corrosion pits up to 40 mils (750 mm) deep in a 7075-T6 aluminum longeron after less than 6 months of exposure. In another example, researchers have produced corrosion pits up to 80 mm in depth on a bare sheet of aluminum (0.08″ thick, with no crevices or joints) in the laboratory environment by placing the material in a salt spray chamber [14].

LONGERON. A major load-bearing structural component that runs along the length of an aircraft's fuselage.

A Possible Solution

The interaction of corrosion and fatigue must be addressed if we hope to find a solution for widespread fatigue damage and catastrophic failures in aircraft structures. We must understand the mechanisms of crevice corrosion and pitting — as well as the role of the chemicals in the environment — when the material is subjected to stress, fretting, and fatigue.

The rates of crack growth through corroded or uncorroded areas of a structure must be determined under realistic conditions. Furthermore, no pit of corrosion should be assumed to be passive or dormant. Under certain conditions, any defect can become active and grow faster than the predicted rate.

Systematic data on the fatigue life and fracture toughness of materials must be determined in an environment that is representative of expected operational conditions, not in dry or unspecified conditions. Fatigue data obtained in a vacuum or in an inert atmosphere can help provide estimates of the maximum effects that one can expect due to environment. Even under modest design engineering limits, a component's margin of safety can have limitations, because corrosion can reduce the actual fatigue life to one-fifth of that reported in the literature or in handbooks.

Materials that have a high resistance to localized corrosion and a greater threshold for corrosion fatigue and stress corrosion cracking must be used for structural applications. The avoidance of galvanic coupling (i.e., placing dissimilar metals in contact with each other) and the use of corrosion-preventive compounds and sealants in joints and other structural areas susceptible to corrosion will provide greater structural reliability and will enhance fatigue life. This is especially important for naval applications, because corrosion-resistant coating systems serve as a barrier that blocks the entry of moisture and harmful chemicals into hidden areas of aircraft structure. These measures do not protect an aircraft indefinitely, however, because coating systems gradually break down with exposure to vibration, ultraviolet light, and extremes in temperature. Once developed, intelligent sensors that can be placed between the metal and its protective coating will help maintenance crews detect early signs of corrosion and greatly enhance the practice of condition-based maintenance.

Concerns about the gradual structural degradation brought about by corrosion and fatigue require that aircraft structures be inspected periodically for damage. The wide variety of sizes, shapes, materials, and levels of access for structural components means that many different types of non-destructive inspection (NDI) techniques must be used to locate and characterize damage. When more than one NDI technique is used to inspect the same area of structure, the probability of detecting damage increases, and the results provide substantial benefit by increasing the overall reliability of each set of inspections. NDI techniques now used with some degree of success include visual inspections, eddy current, X-ray, ultrasound, neutron radiography, and thermal imaging.

Although these inspection techniques can be precise, finding a crack, corrosion, or other defect under two or three layers of paint or protective coating is a very time-consuming process. New NDI technologies such as broad scan visual enhancement, early stage corrosivity monitoring, guided wave ultrasonic, auto signal processing, fluorescence imaging spectroscopy, and superconducting quantum interference devices (SQUIDs) are making their way into the field. The best option to increase aircraft and component service life is to develop a system with intelligent sensors that can monitor its own “corrosion health” for hidden corrosion damage. The ability to detect damage early will be the key to reducing aircraft maintenance and enhancing the service life of their components.

Concluding Remarks

Even though corrosion can significantly aggravate fatigue damage — resulting in increased crack growth rates and reduced fatigue life — interest in the effects of corrosion and the development of corrosion-preventive technology lags behind the general research into fatigue, crack growth, and analyses of residual strength. The influence of corrosion on fatigue life is complex and is not well understood, because the rates and the effects of corrosion can vary greatly depending upon operational and environmental conditions. For example, the current standard for the allowance of thickness loss due to corrosion alone used in analytical models — a value of 10% — is based on tests that were conducted under static conditions (i.e., unvarying stress), not under conditions of fatigue (where stresses vary).

In addition to the mechanical aspects of stress and fatigue, one must also look at the effects of a material’s microstructure on corrosion. The corrosion susceptibilities of individual grains and inclusions in a metal, their compositions, and the active nature of the grain boundaries have a strong effect on the rate of corrosion; therefore, these properties have a great influence upon the crack growth rate and the remaining fatigue life of aircraft components.

The large number of factors that affect the rate of corrosion — including the characteristics of the corrosive environment, changes in the rate of cycling of stresses, the role of corrosion inhibitors on the crack-tip chemistry, and the influence of electrochemical parameters on pit nucleation and growth — suggest that no analytical model will be sufficient to accurately predict fatigue life and address all of the Navy’s concerns about the structural integrity of the aircraft in its fleet. Where corrosion is concerned, the present analytical models will, at best, be non-conservative and overestimate the fatigue life of aircraft and their components.

It seems that no crack length is a safe crack length when it comes to estimating the remaining fatigue life

of an aircraft component, unless corrosion is controlled. Research into the growth rates for short cracks (even those of microstructural defect size) in the presence of a chemical environment that simulates actual operational conditions must be pursued. Because very little research of this type has been done, it is recommended that additional studies that investigate the effect of corrosion on low-cycle fatigue be conducted.

References

1. V.S. Agarwala and J.J. DeLuccia, *Corrosion*, **36**, 208-212, 1980.
2. V.S. Agarwala, "Multipurpose Corrosion Inhibitors for Aerospace Alloys in Naval Environments", in *New Materials and New Processes*, Vol. 3 (JEC (Japan) Press Inc., Cleveland, 1985), 178-189.
3. A. Alavi, C.D. Miller, and R.P. Wei, "Electrochemical Reactions with Bare Metal Surfaces and Corrosion Fatigue Crack Growth," Lehigh University Technical Report 19, IFSM 86-143, 1986.
4. R.O. Ritchie and J. Lankford, *Small Fatigue Cracks*, (The Metallurgical Society of AIME, Warrendale, PA, 1986).
5. P.S. Pao and R.P. Wei, *In Environment Sensitive Fracture of Engineering Materials*, (The Mineral, Metals and Materials Society, Warrendale, PA, 1979), 566-580.
6. V.S. Agarwala, "An In-Situ Experimental Study of the Mechanisms of Catastrophic Damage Phenomena, in Hydrogen Effects on Materials Behavior", Eds. N.R. Moody and A.W. Thompson (The Mineral, Metals and Materials Society, Warrendale, PA, 1990), 1033- 1045.
7. A. Turnbull, *Corrosion Science*, **23**, 833, 1983.
8. H. Chung and D.D. Macdonald, *Corrosion*, **41**, 150, 1985.
9. H.W. Pickering, *Corrosion*, **42**, 125, 1986.
10. M.W. Kendig, F. Mansfeld, and V.S. Agarwala, *Evaluation of Electrochemical Kinetics of the Fatigue Crack Tip of Aluminum Alloy* (The Electrochemical Society, San Diego, CA, 1986).
11. V.S. Agarwala, "Catastrophic Damage Phenomena: An In-Situ Crack-Tip Study", in *Proceedings of 6th International Conference on Mechanical Behavior of Materials, Kyoto, Japan*, Vol.2 (Pergamon Press, 1991), 711-718.
12. V.S. Agarwala, "Modification of Crack-tip Chemistry to Inhibit Corrosion and Stress Corrosion Cracking in High Strength Alloys", *in Embrittlement by the Localized Crack Environment*, ed. R.P. Gangloff (The Metallurgical Society of AIME, Warrendale, PA, 1984), 405-419.
13. D. Macdonald, "The Deterministic Prediction of Corrosion Damage in Aircraft", paper given at the Third International Aircraft Corrosion Workshop, Solomons, MD, August 1998.
14. K.K. Shankaran, R. Perez, R.J. Lederich, et al., "The Effect of Pitting on the Mechanical Behavior of 7075-T6 Aluminum," paper given at the AEROMAT 98 Conference, Abstract AALE1.2.ASM International, June 1998.

The Author

Dr. Vinod S. Agarwala is a Senior Staff Scientist in the Aerospace Materials Division of Naval Air Systems Command, Patuxent River, MD. He was educated at Massachusetts Institute of Technology and at Banaras Hindu University in India. He holds a B.Sc. in Physics; an M.Sc. in Physical and Electrochemistry; an M.S. in Metallurgy; and a Ph.D. in Metallurgy (Corrosion Science). He is a Fellow of ASM International and National Association of Corrosion Engineers (NACE) International, a registered Professional Engineer, and a NACE-certified Corrosion Specialist. He has published more than 120 research papers, edited two books, and has been awarded 10 patents. Dr. Agarwala's research interests include sensors for corrosion detection and monitoring, "smart" coatings and materials, mechanisms of corrosion fatigue and inhibition, hydrogen embrittlement and environment-assisted cracking, alloy development, electroplating and finishing, and tribology (wear and lubrication).

You Can Count on RAIN

Rain makes some things grow and others shrink. In the figurative sense, one of the things that rain can shrink is the amount of data needed to represent the sequence of stresses that a component experiences during operation.

In the following article, a scientist from Fairfax Materials Research in Springfield, Virginia, explains a technique known as the "rainflow" method of counting stress cycles, which can be used to reduce extremely large stress histories to a relatively small set of data that can be easily stored and analyzed. These abbreviated stress sequences also more closely match the type of stress histories used in crack growth testing in the laboratory.

The article also discusses the development of mathematical techniques for modeling crack growth that use the basic physics of material behavior to more closely link the analytical world of cycle counting methods and the real world of fatigue damage.

– S.P.

Cycle Counting and Beyond in Variable Amplitude Fatigue

Michael S. Duesbery

Fairfax Materials Research, Inc., Springfield, Virginia 22153

Introduction

In the early 1980s, the American Helicopter Society conducted a bold experiment in which hypothetical load sequences for a pitch link — a flight-critical component in a helicopter's rotor system — were provided to seven major helicopter manufacturers. The manufacturers were expected to use their preferred in-house methods to analytically determine the amount of the pitch link's fatigue life that was expended during the load sequence. The manufacturer's estimates varied by more than three orders of magnitude, from 9 hours to 28,000 hours. A statistical analysis of these results [1] showed that 85% of the variance in the estimates was attributable to just two sources: the amount of safety factor used in the analysis, and the method used to count the cycles of stress in the load sequence.

The various methods used to count cycles in load or stress histories have evolved from two basic imperatives.

1. First of all, a variable amplitude, cyclic loading sequence must be converted into a form that can be analytically compared to data obtained from constant amplitude fatigue tests, which is the only form in which laboratory results are widely available.

2. The second need — which, by the way, is becoming increasingly unimportant as the cost of storing computer data drops — is to distill a general load sequence into a form that permits the compact storage of information without the loss of its relevant physical characteristics.

An unprocessed stress history includes a large number of data points that provide a comprehensive record of stress at some location of interest in an aircraft or other structure. If stress data is sampled every few seconds (as it often is in flight test programs that investigate fatigue crack growth in components that experience a rapidly changing stress environment), the resulting stress histories can quickly become very large. For example, a mere 100 hours of flight data would yield a stress history that contained 36,000 data points if measurements were taken once every 10 seconds — a rate that is not uncommon.

Many cycle counting techniques have been developed over the years and are thoroughly discussed in several excellent reviews [2-4]. The technique that has come to be accepted as the modern standard — in large part because it implicitly includes the effects of many of the competing methods of cycle counting — is known as the "rainflow" method.

Background

A simplified visual depiction of the rainflow method of counting and reducing the number of cycles in a stress history is presented in the sidebar at right. This technique also can be described in procedural and mathematical terms as follows [5]:

1) A sequential set of maximum and minimum stresses are extracted from the full stress history by discarding all data points that lie within monotonically increasing or decreasing ramps. The remaining "peaks" and "valleys" of stress are then digitized to form an abbreviated stress history.

2) Data points in the abbreviated stress history are then considered sequentially, in sets of four.

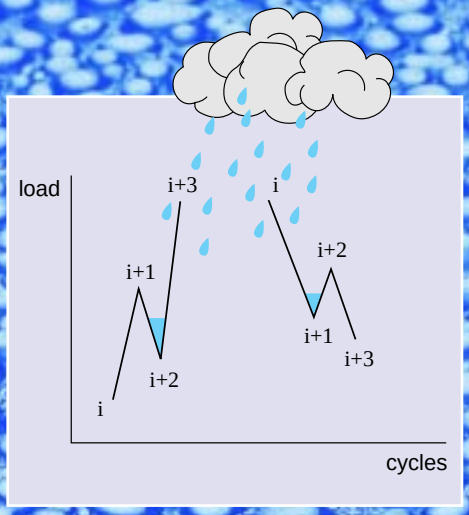

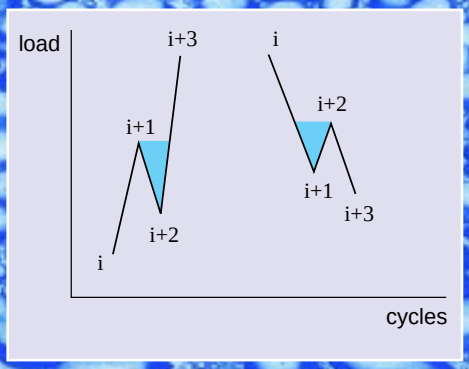

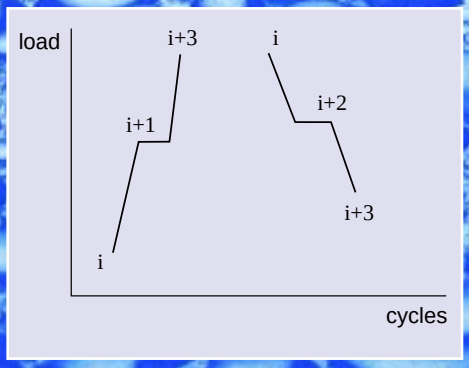

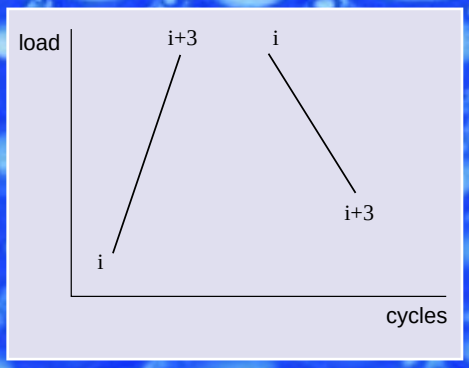

The Rainflow Method of Counting Stress Cycles

The "rainflow" method of counting and reducing stress cycles takes its name from a visual representation of the process, which is shown at left.

The top diagram (which also appears as Fig. 1 in the main article) depicts two sets of four stress cycles. The set shown on the left represents a trend of generally increasing stress, with a small intermediate drop in stress; the one on the right represents a trend of generally decreasing stress, with a small intermediate rise in stress.

If you imagine these diagrams to be the cross-sectional, side view of a roof, you can see that the intermediate peaks in the roof form "gutters" that will collect rain. When the gutters become completely full of rainwater, the roof will appear as shown in the second diagram. Any additional rainfall that strikes the upper portion of the roof will spill into the full gutter and then immediately continue to flow downward as if the gutter weren't there.

Now, let's move from the "roof" analogy back to our sequence of loads and stresses. If we neglect the gutter shown in the second diagram, the sequence of four stresses then becomes a single-direction change in stress level that is interrupted by a short pause at some intermediate level of stress, as shown in the third diagram.

Because short pauses in stress should have little if any effect on the rate of fatigue crack growth, these pauses can be neglected. Therefore, the sequences of four stresses shown in the top diagram can be replaced by the simple changes in stress shown in the bottom diagram.

– S.P.

(Figure 1 shows two examples of variations in stress for load points *i*, *i+1*, *i+2*, and *i+3*. Note that for any particular component, the stress in the component is directly proportional to the applied load.)

If conditions on the stress values for the sets of four load points shown in Fig. 1 satisfy the criteria:

$$\begin{aligned} |\sigma_{i+2} - \sigma_{i+1}| &\le |\sigma_{i+1} - \sigma_i| \\ |\sigma_{i+2} - \sigma_{i+1}| &\le |\sigma_{i+3} - \sigma_{i+2}| \end{aligned} \qquad (1)$$

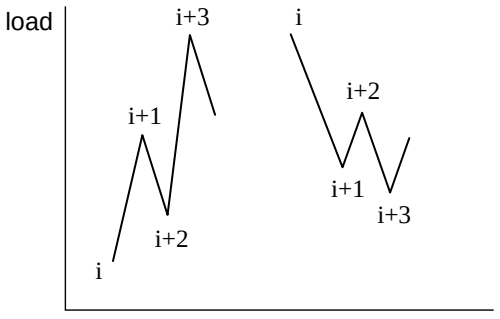

Fig. 1 - Four-point subsections of an abbreviated stress history. (Generally increasing stress [at left] and generally decreasing stress [at right].)

(in other words, if the subcycles defined by the load points *i+1* and *i+2* [which also can be represented as subcycles A and B in the load-strain diagram shown in Fig. 2] are completely contained within the stress cycles defined by the extrema load points *i* and *i+3*), as is true for both sequences of four load points shown in Fig. 1, then the range of stress for the intermediate load points (i.e., $\Delta\sigma = \sigma_{i+2} - \sigma_{i+1}$) and the mean stress (i.e., $\sigma_{mean} = 0.5(\sigma_{i+2} + \sigma_{i+1})$) are recorded in a density matrix **n.** Information is stored in the density matrix (where each element takes the form of n_{jk}) according to the following pattern:

$$\begin{aligned} \sigma_j &= 0.5 * (\sigma_{i+2} + \sigma_{i+1}) \\ \Delta\sigma_k &= |\sigma_{i+2} - \sigma_{i+1}| \end{aligned} \qquad (2)$$

After all of the load points in the stress history have been processed using this technique, the result can be expressed as the density matrix **n** of counted subcycles with recorded mean stress and stress range and a

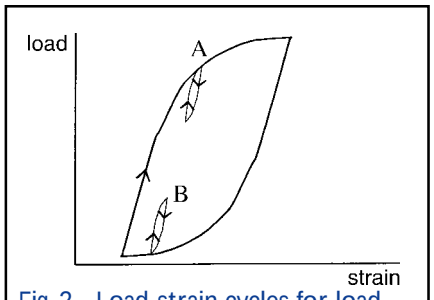

Fig. 2 - Load-strain cycles for load histories shown in Fig. 1. (Generally increasing stress is shown by the upper curve; Subcycle A represents intermediate charges in stress from load point *i+1* to load point *i+2*.)

residual load sequence with few features. To complete the cycle counting exercise, the residual sequence is duplicated, joined to itself and reprocessed as above [6].

The accumulation of fatigue damage

By the Palmgren-Miner rule [7], the fatigue damage D_{ij} that is caused by the matrix element $\boldsymbol{n_{ij}}$ is

$$D_{ij} = \frac{n_{ij}}{N_{ij}} \qquad (3)$$

where N_{ij} is the total number of fatigue cycles to failure for a mean stress of σ_i and stress range $\Delta\sigma_j$. The parameter N_{ij} can be estimated from N_{0j}, the number of cycles to failure at zero mean stress for the stress range $\Delta\sigma_j$, by means of the relation

$$N_{ij} = N_{0j}\left(1 - \frac{\sigma_i}{\sigma_a}\right)^b \qquad (4)$$

in which σ_a and *b* are constants that are determined from the stress-strain curve for the material. Finally, the fraction of lifetime expended by the load sequence (also known as Fatigue Life Expended, or FLE) is given by

$$f = \sum_{i-1}^{m} \sum_{j-1}^{m} D_{ij} \qquad (5)$$

where the damage D_{ij} is found using Eq. (3).

The power of the rainflow method is that the original load sequence can be reproduced in terms of the

number and magnitude of subcycles by inversion of the reduction procedure. The rainflow method of counting stress cycles is complete, because the decomposition matrix of the reconstructed load sequence is the same as that of the original load sequence. However, the sequential order of the subcycles removed from the original load sequence cannot be recovered; therefore, any time correlation in the loading history is lost.

In effect, fatigue life analyses that use such a reconstructed stress history ignore load-load interactions. Lifetime predictions that use stress histories reduced by the rainflow method tend to be conservative [7]. In other words, these calculations overestimate the accumulation of fatigue damage in a component and therefore underestimate its fatigue life.

A Different Way to Calculate Fatigue Damage

There are several drawbacks with using the Palmgren-Miner rule, discussed in the previous section, to predict the accumulation of fatigue damage. Equation 3 assumes that damage increases linearly as the number of cycles increases, and Eq. 5 assumes that this damage combines linearly to predict the Fatigue Lifetime Expended. This is clearly not true; for any particular change in stress (and with all other factors being equal), the rate of growth of a long crack is faster than that for a short crack. Perhaps most importantly, however, the Palmgren-Miner rule includes no tangible damage parameter. Therefore, the accuracy of any predictions using this technique can only be verified when the component ultimately fails.

Any method of counting cycles — whether it be the rainflow method or a competing technique — is completely empirical, and both its performance and its justification can be improved by considering the basic physics of fatigue crack propagation. There are two obvious changes that can reinforce the connection between the analytical world of cycle counting methods and the real world of fatigue damage accumulation. First, the length of a fatigue crack can be adopted as the damage parameter that is missing from the fatigue life calculations that are based on the Palmgren-Miner rule. Second, changes in load or stress that serve as the driving force for crack propagation in the Palmgren-Miner rule can be replaced by the change in stress intensity, which is more closely related to the rate of crack growth. Incorporating these two fundamental changes of philosophy into the techniques for calculating fatigue crack growth require us to modify both our cycle counting procedure (Eq. (2)) and our method for calculating the accumulation of fatigue damage (Eqs. 3 through 5).

Changes in the cycle counting technique will be addressed first. Figure 3 illustrates the conventional definition of the driving factors for crack growth according to the Palmgren-Miner rule — the average stress and the change in stress — as they were defined in Eq. (2). [Note, however, that the stress values in those equations has been replaced by the stress intensity at the crack tip (K).] For subcycles in both increasing and decreasing loading ramps (labeled A and B, respectively, in Fig. 3), the change in stress intensity (ΔK) is defined by the amplitude of the subcycle, and the magnitude of the stress intensity K is determined from the average stress value for the subcycle.

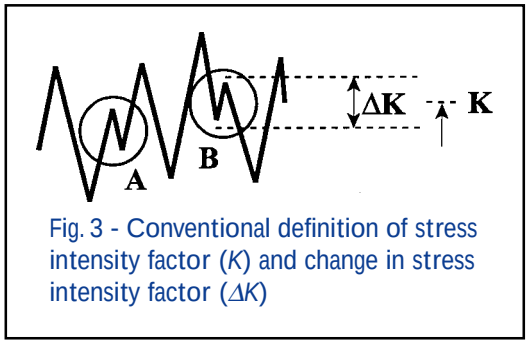

Fig. 3 - Conventional definition of stress intensity factor (K) and change in stress intensity factor (ΔK)

From the physics of fracture, however, it is known that K_{max} and ΔK play well-defined roles in fatigue crack propagation. K_{max} is a parameter that governs the ease of emission of dislocations from the crack tip; it is therefore related to the strength of the interatomic bonds at the crack tip and is sensitive to corrosion. Because it is localized to the crack tip, K_{max} is unaffected by details of the microstructure of the material. The parameter ΔK, on the other hand, governs the behavior of the plastic zone — a region of stress-deformed material that surrounds the crack tip and extends some distance from it. The plastic zone usually contains paired dislocation dipoles, which tend to harden the material without shielding the crack. However, when the applied K_{max} exceeds a certain

threshold value for the material, unpaired positive dislocations are emitted from the crack tip into the plastic zone. Conversely, a reduction in stress intensity of ΔK permits the plastic zone to restore its paired condition, either by emission of negative dislocations from the crack tip or the absorption of positive dislocations into the crack. The degree of restoration possible depends on the magnitude of the drop in ΔK and also on the microstructure of the material (e.g. the hardening, grain size, second phase content).

This clarification of the physical roles of K_{max} and ΔK enables a more logically intuitive decomposition of the variable load spectrum. Figure 4 shows the same stress history and subcycle (B) that were shown in Fig. 3, but the new definitions of stress intensity parameters are depicted. In this case, K_{max} is defined naturally as the value of stress intensity that is associated with the peak stress, rather than the value associated with the mean stress for the cycle. The parameter ΔK is shown as the range of stress intensity values associated with the unloading stroke after the peak of the cycle. The effect of these changes in definitions for a simple rainflow decomposition will be to leave ΔK unchanged for subcycles on a loading ramp (such as subcycle A in Figs. 3 and 4). For subcycles on an unloading ramp (such as subcycle B in Figs. 3 and 4), the value of ΔK will be increased. For both the loading and unloading types of subcycle, K_{max} will be increased slightly, from the mean to the peak value.

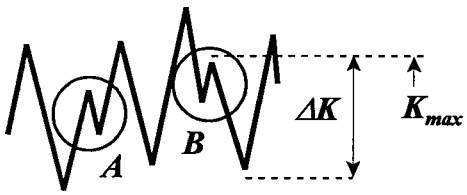

Fig. 4 - New definition of maximum stress intensity factor (K_{max}) and change in stress intensity factor (ΔK)

As previously mentioned, the prediction of accumulated fatigue damage according to the Palmgren-Miner rule involves both the linear scaling of damage (Eq. (3)) and the linear combination of damage (Eqs. 4,5). Both of these dubious assumptions can be avoided if we adopt the fatigue crack length a as the damage parameter and then use fracture mechanics to form the link between cyclic stress and the resulting damage due to fatigue crack growth.

The rate at which the fatigue crack extends for each load cycle (da/dn) is usually expressed in the form

$$\frac{da}{dn} = F\left[\Delta K, K_{\max}, \beta_p, \beta_E\right] \qquad (6)$$

where F is a mathematical function that depends upon the parameters enclosed by the brackets. For Eq. (6), β_P and β_E are parameters that describe the effect of the plastic zone and the chemical environment of the crack tip, respectively. If the detailed dependence of crack growth on these parameters is known, then the calculation of accumulated fatigue damage is a matter of numerical integration rather than simply counting the cycles in the load spectrum.

Because this type of damage calculation does not necessarily condense stress histories into an abbreviated form (as is done for many classical techniques of counting cycles of stress), time correlations are preserved and load-load interactions can be retained in the damage estimate. The first attempt to quantify fatigue damage using an equation of the form shown in Eq. (6) was made by Paris and Erdogan [8], who suggested a form dependent on ΔK only

$$\frac{da}{dn} = const.(\Delta K)^p \qquad (7)$$

where the exponent p is empirically determined from experimental data. It is now known that the rate of crack extension depends on K_{max} as well as ΔK; this dependence is usually introduced into the crack growth calculations either explicitly or by a dependence on R, the stress ratio ($R = K_{min}/K_{max}$).

To account for load-load interactions, it would normally be necessary for crack growth to be dependent upon both K_{max} and ΔK. This can be avoided, however, by including a dependence on the plastic zone (via which the loads are time-correlated) by way of the parameter β_P, although it is by no means clear how this should be done. Lastly, the effect of the environment on crack growth rate is acknowledged by including a parameter β_E; the detailed nature of this dependence is similarly unknown but is expected primarily to take the form of a modification to the K_{max} dependence.

When all these dependences are accounted for, the right-hand side of Eq. (6) becomes a state function. In other words, if the values and relative influences of the parameters enclosed in the brackets on the right side of the equation remain the same, then the resulting crack propagation rate will always be predictable. Therefore, it is not necessary to know the full load history of a component or test specimen in order to predict its fatigue life, provided that all the parameters included on the right side of Eq. (6) are known or can be measured.

The effects of most or all of the parameters in Eq. (6) are included in the crack growth calculations performed by several advanced computer programs [9]. Figure 5 shows crack growth data collected from a test specimen made of 7075-T651 aluminum alloy that was subjected to a loading spectrum from a fighter aircraft in laboratory air conditions. The solid line, which closely follows the more conservative of the two sets of data, is the prediction of the US Air Force AFGROW computer program [10]. While AFGROW does not show the same high performance in every case, this example shows that in some cases the combination of cycle counting and fracture mechanics can provide an excellent capability for predicting fatigue life.

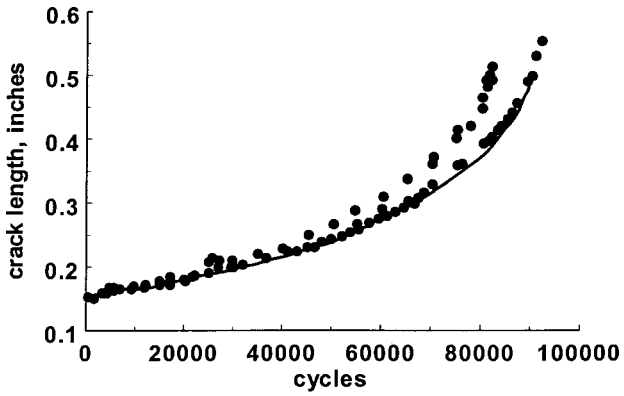

Fig. 5 - Plots of actual crack growth data in test specimens (dots) and the prediction of the AFGROW computer program (solid line)

References

1. C.T. Gunsallus, E. Nagy, P.G. Stennett, and W.G. Flannelly, "Investigation of Variation in Fatigue Life Calculated using Damage Fraction," *J. Amer. Helicopter Soc.*, May, 35 (1990).
2. C. Amzallag, J.P. Gerey, J.L. Robert, and J. Bahuaud, "Standardization of the Rainflow Counting Method for Fatigue Analysis," *Fatigue*, **16**, 287 (1994).
3. R.K. Holman and P.K. Liaw, 1997, "Methodologies for Predicting Fatigue Life," *J. of Metals*, **49**, 46 (1997).
4. S. Suresh, *Fatigue of Materials* (The University Press, Cambridge, 1998), pp. 264-267.
5. A.K. Khosrovaneh and N.E. Dowling, "Fatigue Loading History Reconstruction based on the Rainflow Technique," *Int. J. Fatigue*, **12**, 99 (1990).
6. K. Sobczyk and B.F. Spencer, Jr., *Random Fatigue - from Data to Theory* (Academic Press, New York, 1992), pp. 104-107
7. N.E. Dowling, *Mechanical Behavior of Materials: Engineering Methods for Deformation, Fracture and Fatigue* (Prentice-Hall, Englewood Cliffs, NJ, 1993).
8. P.C. Paris and F. Erdogan, "A Critical Analysis of Crack Propagation Laws," *J. of Basic Engrg.*, **85**, 528 (1963).
9. K. Walker, " An Evaluation of Empirical and Analytical Models for Predicting Fatigue Crack Propagation Load Interaction Effects" (Paper presented at *USAF Structural Integrity Program Conference*, San Antonio, Texas, 2-4 Dec. 1997).
10. J. Harter, (1998). AFGROW, http://fibec.flight.wpafb.af.mil/fibec/afgrow.html.

The Author

Dr. Michael S. Duesbery is Research Director at Fairfax Materials Research in Springfield, Virginia. He was educated at Cambridge University and holds M.A., Ph.D., and Sc.D. degrees in Physics. Before joining Fairfax Materials Research in 1990, he was employed at Oxford University, the National Research Council of Canada, and the Naval Research Laboratory in Washington, DC. Dr. Duesbery has published more than 80 papers on the physical properties of materials and was awarded the annual medal of the Canadian Metal Physics Conference in 1986. In addition to his work at Fairfax Materials Research, he co-edits the Elsevier series of monographs "Dislocations in Solids" with F.R.N. Nabarro. His current research interests center on computer modeling of the deformation, fatigue and fracture of metals.

a helicopter with

extra sensory perception

Modern aircraft are literally bristling with antennas, sensors, and instruments. Some of these sensors provide the aircrew with airspeed, altitude, and other vital real-time information. Other sensors, such as accelerometers and strain gauges, enable post-flight analysis and tracking of the strains and stresses that the aircraft experiences during flight maneuvers.

Some parts of the aircraft, however, are difficult — if not impossible — to instrument. This is especially true for components that are embedded in engines or other rotating systems. Nevertheless, the stresses and strains in such components are of immense interest because these moving parts can be a significant source of maintenance costs for the aircraft.

Researchers at the Carderock Division of the Naval Surface Warfare Center in Bethesda, Maryland, have designed a system for the SH-60 helicopter that uses easily measured flight parameters to predict the loads in critical life-limited components in the helicopter's rotor system. In the following article the scientists describe the system, which acts as a "virtual" strain gauge that, in essence, gives the helicopter a sensor where none actually exists.

This extra "sense" isn't a crystal ball, but it could be almost as good as one. These load predictions could help SH-60 maintenance personnel more effectively schedule their aircraft inspections and component replacements, thereby avoiding costs associated with the retirement of a component before it actually reaches the end of its service life. The technology can also be used as a real-time warning system that tells pilots when damaging loads occur in the rotor, thereby helping to conserve the useful life of critical components.

– S.P.

Neural Network Based Virtual Strain Gauges for Monitoring Fatigue Critical Loads

David J. Haas, Kelly M. McCool, and Lance A. Flitter

Carderock Division – Naval Surface Warfare Center
Bethesda, Maryland

Abstract

A neural network approach is utilized to develop "virtual" strain gauges to monitor rotor system vibratory loads on a Navy SH-60 helicopter. The neural network model is based on input parameters that can be readily measured and recorded in the fuselage using a flight data recorder. The neural network was developed using flight test data from a highly instrumented SH-60B aircraft which included a slipring assembly and strain gauges mounted in the rotating system. The strain gauge measurements provide a reference vibratory load for training and validation of the neural network. Two types of neural network algorithms are used, a self organizing feature map algorithm for selection of training data and a modular neural network algorithm for load predictions. The virtual strain gauges were demonstrated in a flight test evaluation on a second SH-60 aircraft where the algorithms were embedded in an onboard processor for real-time load predictions. Assessment of the flight test results show that the predicted loads compare quite well with strain gauge measurements on the two separate flight test aircraft. The results also demonstrate the potential to use the algorithms for real-time pilot cueing to minimize operation in fatigue damaging flight conditions.

STRAIN GAUGE. An instrument used to measure the small deformations of components or test specimens that are caused by tension, compression, bending, or twisting. Strain gauges are usually adhesively bonded to the specimen at or near a location of interest to structural analysts.

ALGORITHM. A step-by-step, often computerized procedure for solving a mathematical problem.

Introduction

In an effort to improve the reliability and reduce operating costs of helicopters, an increasing emphasis is being placed on developing systems that can monitor the severity of aircraft usage and the health of various subsystems [1,2]. The rotor system, in particular, is a significant source of helicopter maintenance and operational costs. During flight, the rotor blades encounter complex and variable aerodynamic loads that subject flight-critical components to severe vibratory loads. These loads cause fatigue damage that can accumulate and ultimately result in the catastrophic failure of a structural component if the damage remains undetected.

The rate of accumulation of fatigue damage in the structure varies according to the magnitude of the stresses and the frequency of the cycling, which ultimately depends upon the types of maneuvers flown. Accurate knowledge of the component loads is the key to making valid predictions of component service life. Due to the challenges of instrumenting the components of a rotating system, however, there is currently no practical way to measure in-flight rotor system loads on fielded aircraft. Therefore, calculations of accumulated fatigue damage are typically based on data that is more easily obtained, such as the number of flight hours logged and an assumed severity of flight usage. This assumed usage spectrum must be quite conservative in order to represent (and therefore protect) the most severely flown helicopter in the fleet. As a result, some aircraft

components on helicopters with less severe flight usage are needlessly retired before they reach the end of their useful life.

The objective of this work is to develop and demonstrate a method of using an artificial neural network to monitor dynamic loads in fatigue-critical rotor system components. Such an approach would use only parameters that are readily measured in the helicopter fuselage, and therefore the need to directly instrument components of the rotor system would be eliminated.

Approach

Background: An artificial neural network (ANN) is a method of computing that is inspired by the structure and function of the brain and nervous system, which is made up of large numbers of individual neurons (processing elements) that, in concert, can evaluate inputs and make decisions. ANNs use sets of complex equations with nonlinear transfer functions to solve difficult and seemingly intractable problems. (In engineering terms, they can "map" a given set of inputs to a set of outputs.)

An ANN consists of a set of processing elements ("nodes") that are connected by links. Each processing element is linked to at least one other processing element and is usually linked to several others in the network. Each of these links has an associated "weight," which represents the importance of that link in computing the output of the network. The outputs of one set of processing elements may become the inputs to the processing elements in the next "layer" of the network. In addition to a set of inputs, processing elements frequently have a special input called a "bias" that is set to a constant value (which is usually a value of 1). A processing element's contribution to the final output of the network is usually calculated by summing the bias and inputs to the processing element, modified by their associated weights, and then sending the sum through a transfer function to obtain the output for the processing element [3].

Neural networks vary in physical design, training model, and functionality [4]. A feed forward neural network consists of an input layer, one or more hidden layers, and an output layer. Figure 1 shows a schematic of a simple three-input, two-output feed forward neural network. The hidden layer is composed of individual processing elements, which are represented as circles.

For each set of inputs, the ANN uses the connection weights, node biases, and the transfer functions for each node in the network to calculate a set of outputs. At the same time, the ANN calculates a "prediction error," which represents a measure of the difference between the predicted outputs (from the model that is built into the network) and the desired outputs (as they are observed in the real world).

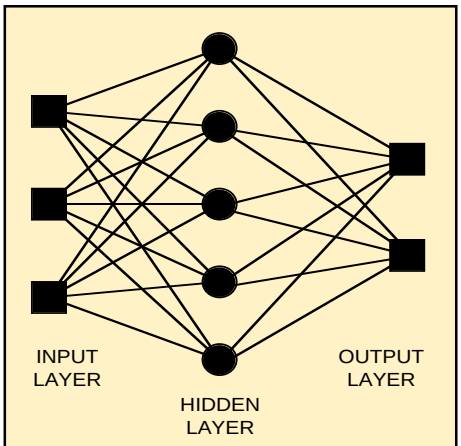

Fig. 1 - Schematic of a feed forward neural network

The most distinguishing feature of a neural network is its ability to "learn." As an ANN is exposed to more and more data, it adjusts the connection weights between the nodes in the network. When the changes in these connection weights stabilize, the ANN is considered to be "trained"; at that point, the values for the connection weights are fixed (i.e., they are no longer allowed to fluctuate). Once a network has been successfully trained, it is capable of analyzing sets of data that are somewhat different from those it was originally exposed to during its training sessions. In other words, the ANN is capable of generalization. Furthermore, neural networks are often capable of producing desired responses even if they are presented with "noisy" or confusing data.

There are two basic methods for training ANNs: supervised and unsupervised.

- In supervised training, the neural network is presented with paired sets of stimuli and

responses (inputs and outputs). The network then attempts to determine the relationship between the inputs and outputs so that it can reproduce the appropriate response (output) when it is presented with a specific stimulus (input). During the learning phase, the prediction error is communicated through the network in some manner and is used to adjust the network weights such that the prediction error is minimized.

- In unsupervised training, the neural network is exposed only to stimuli, and it organizes itself based on characteristics of the input data. The output of such networks is usually some categorization of the input space.

A key advantage of ANNs over traditional statistical methods is that they provide a straightforward means to include nonlinear effects without having to determine the specific relationships between inputs and outputs.

Neural Network Development: For this research, the neural network-based load prediction algorithms were developed using data collected from an SH-60B helicopter during a flight loads survey test program. The helicopter was instrumented with strain gauges and a slipring assembly to measure loads in the rotor system. During the flight test program, which included 56 test flights, the helicopter was flown through a wide variety of maneuvers at several different combinations of altitude, gross weight, and weight distribution. Flight data were recorded throughout these 56 flights and sampled at 8 times each second. The nearly 9 hours of data obtained during this flight loads survey yielded 255,401 data points, which were then used to train and validate the neural network.

One of the keys to successfully training a neural network is the proper selection of a training data set. The data set used to train the ANN must include data that are representative of the problem domain. In other words, the ANN must be trained through exposure to a wide range of inputs that will be similar to those that the network will actually encounter while in service.

Great care must be used to select a set of training data because, in the entire population of data points, some sets of inputs may occur much less often than others. In such a case, a random selection of training data points may result in the inadvertent exclusion of data that occur infrequently. To ensure that a training data set fully represents the entire population of possible inputs (i.e., to ensure that it also includes data that occur infrequently), a neural network called a Self-Organizing Feature Map (SOFM) is utilized.

The SOFM is a neural network algorithm that uses unsupervised learning to develop a map of the input space. In general, a SOFM merely changes the format of the sets of inputs. For this research, the SOFM transformed a 12-dimensional input space (see Table 1 for the 12 inputs measured during the flight loads survey) into a more manageable 2-dimensional grid that measured 50 nodes by 50 nodes. Each of the 2,500 nodes in this grid served as a “bin” into which data could be placed. Each set of inputs collected from the flight loads survey (more than 255,000 data points total) was then placed in one of the 2,500 bins, which were characterized by the 12 measured parameters. Several data points from each bin were then selected as training data for the neural network.

Another example of how a SOFM’s “binning” of data can be useful, which may be easier to understand, is related to the US postal system. Suppose we wanted to do a survey of representative letters and packages that flow through the mail system, and we want to make sure that a sample of mail is included from all parts of

Table 1 - Neural Network Inputs

	INPUT PARAMETER
1	Airspeed (kn)
2	Main rotor speed (%)
3	Engine torque (%)
4	Load factor (g’s)
5	Pitch attitude (deg)
6	Roll attitude (deg)
7	Lateral stick position (%)
8	Longitudinal stick position (%)
9	Collective stick position (%)
10	Pitch rate (deg/sec)
11	Rate of climb (ft/min)
12	Gross weight (lb)

the country. We know that a lot of mail goes to and from New York City (because a lot of people live there), and quite a bit less goes to relatively rural parts of the country such as northern Maine and western Wyoming. In fact, a random survey of 10,000 pieces of mail may not find many (if any) letters or packages that are destined for northern Maine. However, if we sort a very large amount of mail by ZIP code groups and then take an equal number from each group, we can ensure that we include examples of mail from ZIP codes that begin with "047" (northern Maine), as well as other portions of the country that typically have a much lower volume of mail.

For the SH-60 helicopter used in our research — and for helicopters in general — the population of loads data primarily consists of low loads, because a significant amount of a helicopter's flight time is spent in relatively steady flight maneuvers, such as straight-and-level flight or hovering. A random selection of data points from this population would therefore be skewed toward sets of inputs that contained low loads. However, data sets that contained high loads were of the most interest, because high loads result in more fatigue damage in the components of the rotor system. To increase the importance of high loads during the training of the ANN, the training data that contained high loads were weighted. Using this approach, only 7,500 data points — less than 3% of the baseline flight data collected in the flight loads survey — were required to train the neural network.

This research evaluated several different neural network designs for load prediction, including simple feed forward networks and modular networks. Results showed that a modular neural network (MNN) was the best predictor of rotor system loads because it produced a lower average root mean square error and a higher average correlation. A modular neural network is a "collection-of-experts" style network that uses supervised learning. In a collection-of-experts network, several neural networks function in concert with each other. Each individual network is an "expert" in solving some portion of the problem, and the collective network is designed so that input data are "directed" to the appropriate expert. The MNN design used for this study is the "Adaptive Mixtures of Local Experts" [5], which consists of several experts and a gating network (Fig. 2). During training, the expert networks learn how to predict the proper response to inputs, and the gating layer learns how to partition the data among the experts.

The MNN used in this research has 3 expert networks (each with 65 hidden nodes) and a gating network with 9 hidden nodes. The network uses 12 input parameters (previously listed in Table 1) that were measured by a flight data recorder unit to predict rotor system component loads.

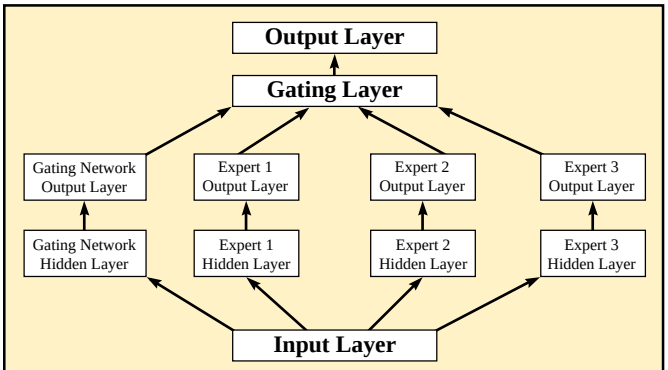

Fig. 2 - Modular neural network architecture

Network Validation on Baseline Data: After the neural network was sufficiently trained using the baseline data, the connection weights were fixed and the performance of the network was assessed with validation data. Validation data are distinct from training data and include data to which the network has not previously been exposed. As previously discussed, only 7,500 of the 255,401 baseline data points were used to train the network used for this research. After training was complete, the network's load monitoring algorithms were validated using the remaining 247,901 data points obtained during the first phase of flight testing. Because the training data makes up such a small portion of the overall data (less than 3%), results are presented for the entire baseline data set.

Table 2 shows the overall statistical performance of the MNN for load predictions in two components of the helicopter system: the main rotor pushrod (which controls the pitch of each rotor blade), and the main rotor lead-lag damper (which stabilizes and damps the in-plane motion of the rotor blade). Linear correlation, *R*, is displayed in the center column of Table 2. The value of *R* indicates the degree of linearity in the

relationship between the actual and predicted loads. A number close to 1.0 indicates that a linear relationship exists and that the neural network does a good job of predicting the loads in the components of the rotor system.

Root mean squared (RMS) error, which is shown in the right column of Table 2, is normalized as a percentage of the maximum vibratory load. This maximum load corresponds to the largest anticipated load and is determined from an inspection of the baseline data set. The maximum vibratory load was found to be 5,000 lb for the pushrod and 7,000 lb for the lead-lag damper. Because the baseline data consists of a variety of high load maneuvers that were performed to determine the boundaries of the flight envelope, these values are considered to be reasonable estimates for the largest load that could be anticipated during actual service. For assessment of this study's load predictions, the normalized RMS error is the primary measure of network accuracy.

Table 2 - Statistical summary of load prediction results for the baseline data

LOAD	R	NORMALIZED RMS ERROR
Pushrod load	0.94	3.65
Damper load	0.78	7.62
Damper > 60 kn	0.88	4.14
Damper < 60 kn	0.61	13.51

Analysis of the load prediction results shows that, for a given load value, between 94% and 96% of the data point errors fall within a range equal to twice the RMS error. For this reason, there is a 95% confidence that the MNN's load predictions will be accurate to within twice the RMS error value. Using this approach and the results shown in Table 2, there is a 95% confidence that the pushrod load predictions are accurate to within ±7.3% of the load range for the baseline data.

Results for load prediction in the lead-lag damper were found to be significantly different when the baseline data was separated into prediction above and below 60 kn of forward airspeed. For flight test data collected at airspeeds above 60 kn, the normalized RMS error is 4.1% of the load range. However, for flight test data collected at airspeeds below 60 kn, the RMS error is 13.5% of the load range. This significant change in prediction accuracy may be due to the damping characteristics of the SH-60 lead-lag damper, which operates in two separate modes depending on blade lead-lag velocity. At small lead-lag velocities, the slope of the force/velocity curve is rather high; at higher lead-lag velocities, the damper enters a "bypass mode" and the slope of the force/velocity curve is much lower. This transition into bypass mode occurs at helicopter airspeeds between 60 and 70 kn. Also, at airspeeds below 60 kn, the damper load is quite sensitive to the blade lead-lag velocity, which is not a neural network input. This characteristic is likely to be one reason for decreased prediction accuracy for data obtained at airspeeds below 60 kn. Another factor that may contribute to inaccurate predictions for lead-lag damper loads in the low-speed flight regime is that blade lead-lag velocity is a function of aircraft airspeed, which cannot be reliably measured when the helicopter is traveling at airspeeds below 40 kn.

Figure 3 is a scatter plot of the ANN's load predictions for the pushrod load; Figures 4a and 4b are scatter plots of the load predictions for damper loads at airspeeds above and below 60 kn, respectively. A scatter plot is useful for identifying specific data points where the load predictions were particularly inaccurate, but it does not allow for a complete view of how dense the data points are around the 45° line (where the predicted load matches the actual load). A comparison of Figs. 4a and 4b clearly shows that load predictions for helicopter airspeeds greater than 60 kn have much less scatter.

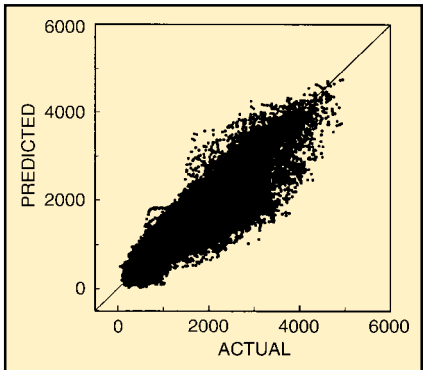

Fig. 3 - Scatter plot of main rotor pushrod predictions for the baseline data

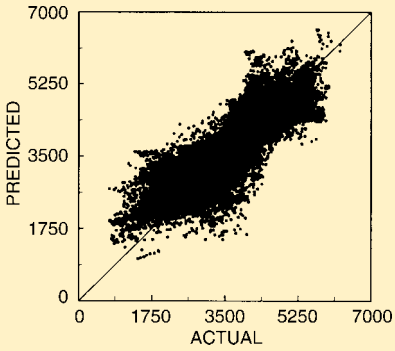

Fig. 4a - Scatter plot of damper predictions for airspeeds greater than 60 kn for the baseline data

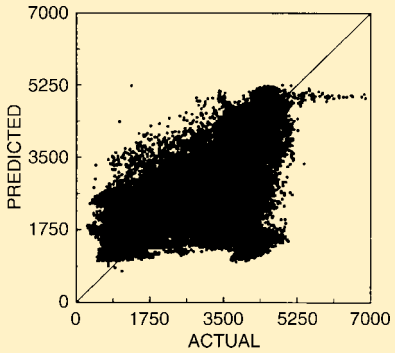

Fig. 4b - Scatter plot of damper predictions for airspeeds less than 60 kn for the baseline data

While scatter plots, correlation, and RMS error provide good measures for statistically analyzing load predictions, these measures do not fully highlight the extent to which the load predictions of the neural network follow the trends of the actual measurements obtained from the strain gauges. Figures 5 and 6 show time history traces of the predicted vs. actual pushrod and damper loads encountered during a right turn with a 60° angle of bank. Even though the RMS error for the pushrod load prediction was found to be the highest during this particular maneuver, Fig. 5 indicates that the predictions of the neural network accurately capture the significant changes in pushrod load level during this highly dynamic maneuver.

Flight Test Evaluation and Results

System Description: During a second phase of validation and flight testing, a flight test evaluation of the neural network's load prediction algorithms (which could also be referred to as "virtual strain gauges") was conducted on an SH-60F helicopter that was instrumented with strain gauges on the main rotor pushrod (see Fig. 7) and the lead-lag damper. (These strain gauges were located in the same position that was used on the SH-60B helicopter during the first phase of flight testing.) Power was supplied to these rotor system strain gauges through an existing aircraft slipring assembly that is typically used for power during blade folding procedures. (In the test helicopter, the blade fold capability was disabled during the flight test evaluation.)

Analog strain gauge measurements were recorded on a flight data recorder, digitized, and then post-processed into steady and vibratory components. These strain gauges provided a reference strain measurement that could later be compared with the neural network load predictions.

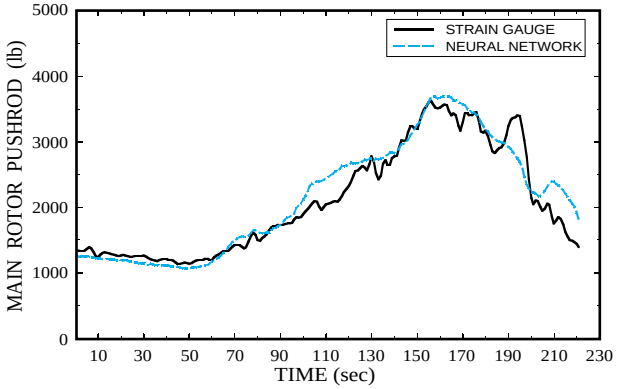

Fig. 5 - Pushrod load predictions for a 60º angle of bank right turn in the baseline data

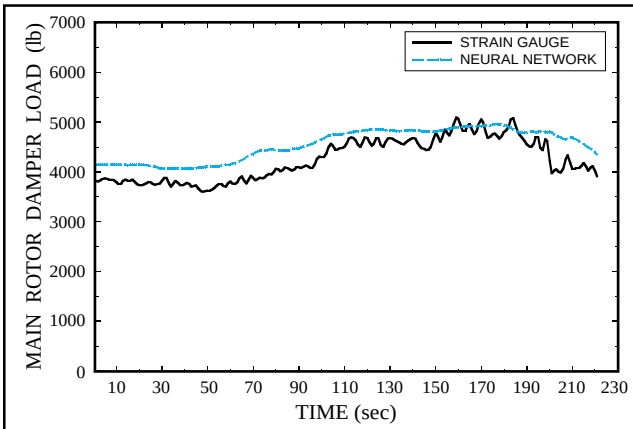

Fig. 6 - Damper load predictions for a 60º angle of bank right turn in the baseline data

Fig. 7 - Instrumented main rotor pushrod

The load prediction algorithms that had been developed in the first phase of flight testing were programmed in the C computer language and compiled, and then the executable program was embedded in a 486-based central processing unit (CPU) in an upgraded Structural Data Recording Set.

During this phase of flight testing, the neural network load predictions were performed in real time, using 12 parameters of flight data (see Table 1) that were collected 8 times each second. Each data sample was time-tagged so that the neural network's load predictions could be synchronized with actual load measurements during post-flight data analysis.

Flight Test Demonstration Data: The second phase of flight testing consisted of 20 flights and gathered almost 8 hours of flight data, which yielded 228,704 data points. There are two significant differences between the baseline data collected from the SH-60B and the flight evaluation data collected from the SH-60F in this phase of the test:

- The baseline data was obtained during a flight loads survey that was designed to explore the boundaries of the helicopter's flight envelope. In other words, some of the flight conditions encountered during that phase of testing were not representative of normal flight operations. For example, the baseline data contain some data points that were collected when the helicopter's gross weight exceeded 22,000 lb and when engine torque levels were nominally 120% of the basic operating torque. Flight operations at high gross weight and high torque levels can result in abnormally high vibratory loads.

  However, during the flight test demonstration of the virtual strain gauges (the second phase of flight testing), the helicopter was limited to a nominal torque value of 100% of basic operating torque, which is consistent with fleet operations. Helicopter gross weights during this phase of testing were also consistent with fleet operations, with values ranging from 18,500 lb to 20,600 lb.

  These differences in gross weight and torque levels are among the reasons that the rotor system loads in the flight test demonstration are generally lower than the loads in the baseline data.

- The pullout maneuvers performed during the second phase of flight testing were not flown as aggressively as they were in the baseline data. Peak load factors of 2.7 g's were achieved during the flight test, as compared to 3.3 g's that occurred in the baseline data collected during the flight loads survey.

  While high gross weight and engine torque levels and severe high-g flight maneuvers are very useful for neural network training purposes, the data obtained during the flight test demonstration of the neural network algorithms are more representative of the way the aircraft is actually operated in the fleet.

Results: Neural network predictions for loads in components of the helicopter's rotor system were performed on-board the flight test helicopter in real time. Table 3 shows the overall statistical performance of the MNN for load predictions during the second phase of flight testing. Normalized RMS error for the pushrod load predictions is quite good, at ±2.1% of the load range. Again, the effect of helicopter airspeed on loads prediction for the main rotor lead-lag damper was found to be very significant: Flight test data collected at airspeeds above 60 kn yielded an RMS error of ±3.2%, while data collected at airspeeds below 60 kn yielded an RMS error of ±16%. Scatter plots for

Table 3 - Statistical summary of load prediction results on the flight test data

LOAD	R	NORMALIZED RMS ERROR
Pushrod load	0.91	2.11
Damper load	0.84	7.24
Damper > 60 kn	0.83	3.22
Damper < 60 kn	0.49	16.06

this set of flight test data are shown in Figs. 8 and 9; as was seen in the scatter plots for the baseline data, there is clearly less scatter in the damper predictions when airspeed is greater than 60 kn (Fig. 9a).

The results provided in Table 3 show that the RMS error for load predictions in this phase of flight testing compares favorably with the results for the baseline data, which were shown in Table 2. Furthermore, this indicates that the results obtained from one aircraft can be applied to a second similar aircraft without loss in prediction accuracy.

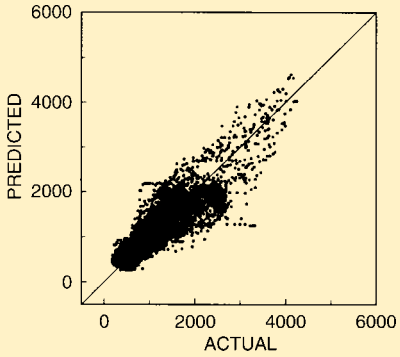

Fig. 8 - Scatter plot of main rotor pushrod load predictions for the flight test demonstration

Figs. 10 and 11 depict time history traces of predicted vs. actual loads (as measured during a high-g symmetric pullout maneuver) for the pushrod and the lead-lag damper, respectively. These figures show that the neural network load predictions compare quite well with those obtained from the actual strain gauge measurements. The overall trend, as well as the increase in load level, is captured in both cases.

Summary and Conclusions

Using an artificial neural network approach, virtual strain gauge algorithms that monitor vibratory loads on

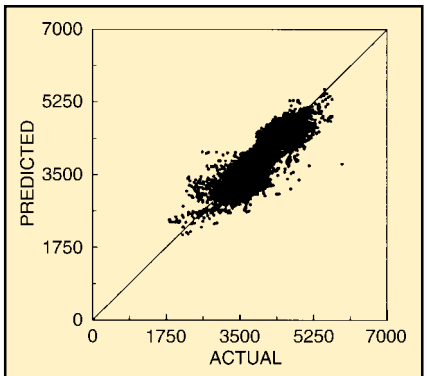

Fig. 9a - Scatter plot of damper load predictions for airspeeds greater than 60 kn for the flight test demonstration

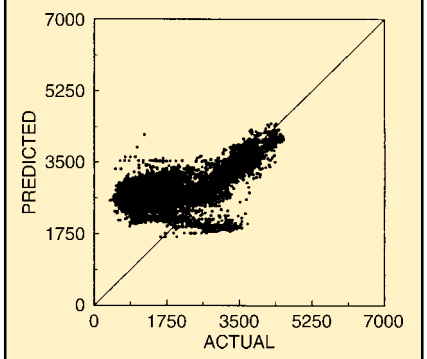

Fig. 9b - Scatter plot of damper load predictions for airspeeds less than 60 kn for the flight test demonstration

fatigue-critical helicopter rotor system components have been successfully developed and demonstrated in flight tests of an instrumented SH-60 helicopter. The neural network uses easily measured aircraft parameters (such as pilot control positions, engine torque, rate of climb, etc.) to predict loads on components in the helicopter's rotor system. The load prediction algorithms were developed using data collected during 56 test flights that included a wide range of helicopter weights, configurations and flight maneuvers. The ANN-generated load prediction algorithms were then embedded in an on-board processor and successfully used to make real-time load predictions during 20 test flights of a second flight test helicopter.

As a result of this research, the following conclusions can be drawn:

- The flight test results show that the neural network load monitoring algorithms that were

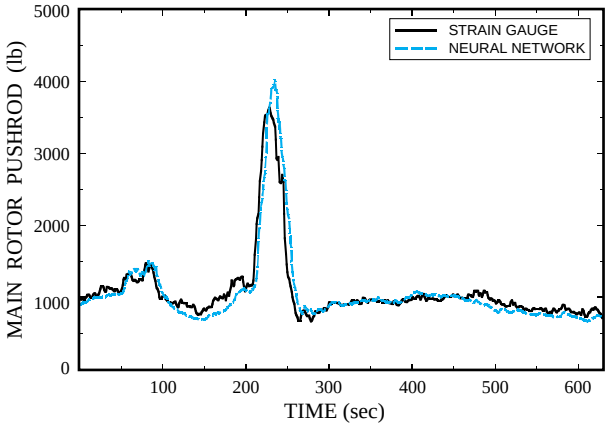

Fig. 10 - Pushrod load predictions for a high-g symmetric pullout maneuver from the flight test demonstration

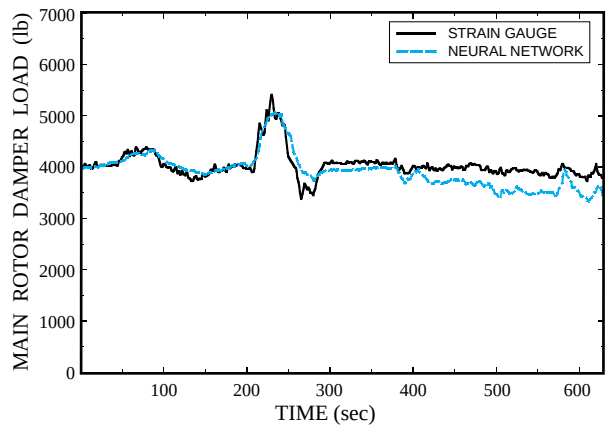

Fig. 11 - Damper load predictions for a high-g symmetric pullout maneuver from the flight test demonstration

developed using flight data from one aircraft are general enough to successfully predict vibratory loads on a second aircraft.

- Artificial neural networks, when properly trained, can be used to consistently predict loads in helicopter rotor system components.
- For pushrod load, the neural network normalized RMS error was 3.6% of the load range for the baseline data (obtained from the first flight test helicopter) and 2.1% for the flight test data (obtained from the second flight test helicopter).
- The neural network's accuracy of predictions for damper loads was highly dependent upon helicopter airspeed. At airspeeds greater than 60 kn, the neural network normalized RMS error is 3.2% of the load range for the flight test data. At airspeeds below 60 kn, the RMS error increases to 16%. Therefore, while damper load predictions are quite good for airspeeds greater than 60 kn, the neural network cannot accurately predict damper loads in low speed flight.
- Artificial neural networks can accurately monitor the significant changes in load levels during highly dynamic maneuvers.
- Demonstration of a real-time load prediction capability illustrates the potential to use virtual strain gauges as part of a warning system that indicates to helicopter pilots that they are flying under conditions that can cause excessive fatigue damage accumulation in flight-critical components.

Acknowledgments

This work was supported by the Office of Naval Research, Dr. P. Abraham and Mr. W. King. The authors also acknowledge the support and guidance of Mr. A. Ragghianti and Mr. G. Barndt of the Naval Air Systems Command and the flight test team at NAWCAD, headed by Mr. M. Hollins.

References

1. M.J. Augustin, "Specifying HUMS to Meet Safety and Reduced Operating Cost Requirements," in *Proceedings of the American Helicopter Society 54th Annual Forum*, 20-22 May 1998, Washington DC, pp. 1201-1210.
2. J.D. Cronkhite, "Practical Applications of Health and Usage Monitoring (HUMS) to Helicopter Rotor, Engine, and Drive Systems," in *Proceedings of the American Helicopter Society 49th Annual Forum*, 19-21 May 1993, St. Louis, MO, pp. 1445-1455.
3. B. Muller and J. Reinhardt, *Neural Networks, An Introduction* (Springer-Verlag, Berlin, 1990).
4. M. Zeidenberg, *Neural Network Models In Artificial Intelligence* (Ellis Horwood Limited, Chichester, West Sussex, England, 1990).
5. R.A. Jacobs, M.I. Jordan, S.J. Nowlan, and G.E. Hinton, "Adaptive mixtures of local experts," *Neural Computation* **3**, 79-87 (1991).

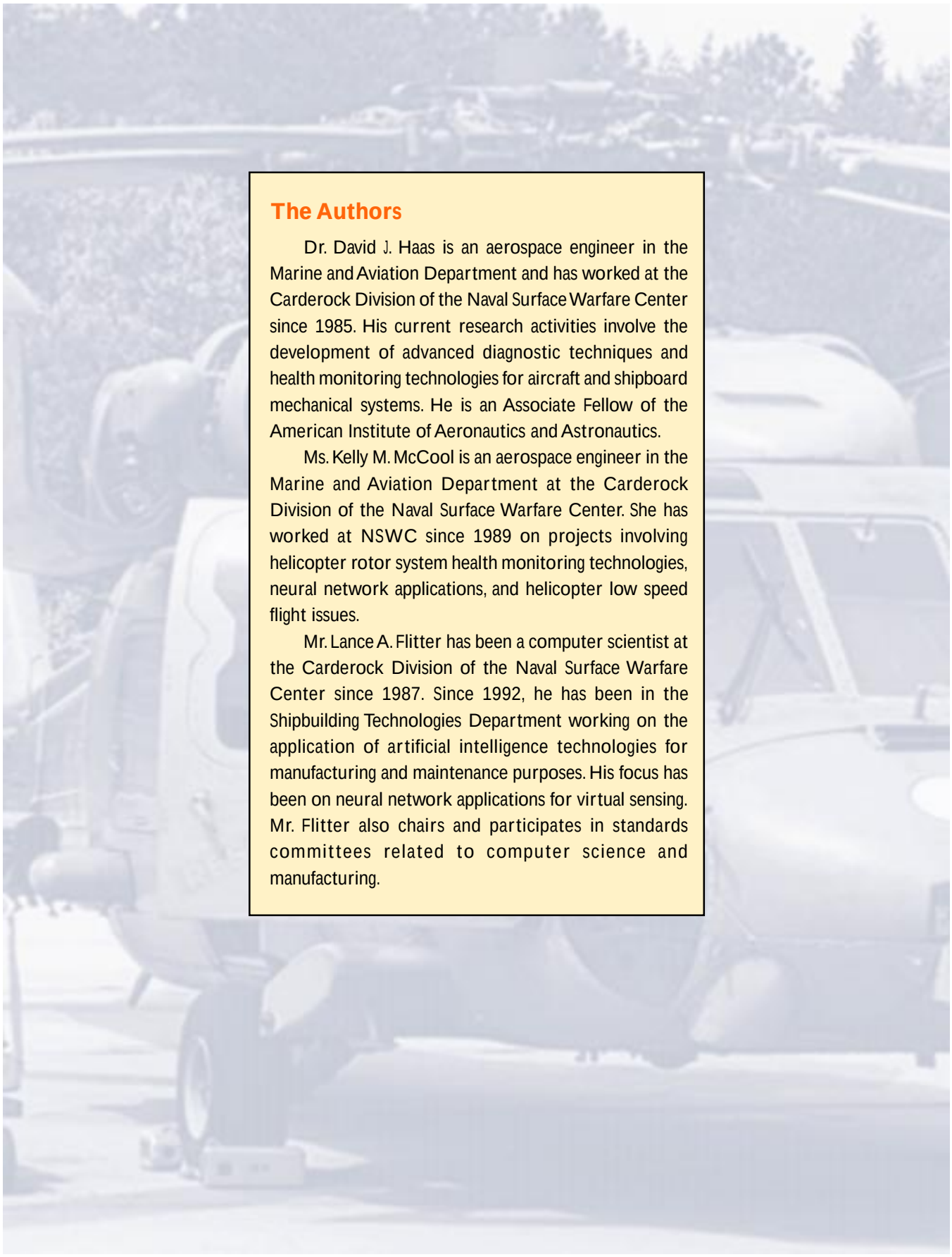

The Authors

Dr. David J. Haas is an aerospace engineer in the Marine and Aviation Department and has worked at the Carderock Division of the Naval Surface Warfare Center since 1985. His current research activities involve the development of advanced diagnostic techniques and health monitoring technologies for aircraft and shipboard mechanical systems. He is an Associate Fellow of the American Institute of Aeronautics and Astronautics.

Ms. Kelly M. McCool is an aerospace engineer in the Marine and Aviation Department at the Carderock Division of the Naval Surface Warfare Center. She has worked at NSWC since 1989 on projects involving helicopter rotor system health monitoring technologies, neural network applications, and helicopter low speed flight issues.

Mr. Lance A. Flitter has been a computer scientist at the Carderock Division of the Naval Surface Warfare Center since 1987. Since 1992, he has been in the Shipbuilding Technologies Department working on the application of artificial intelligence technologies for manufacturing and maintenance purposes. His focus has been on neural network applications for virtual sensing. Mr. Flitter also chairs and participates in standards committees related to computer science and manufacturing.

Clamping down on crack growth

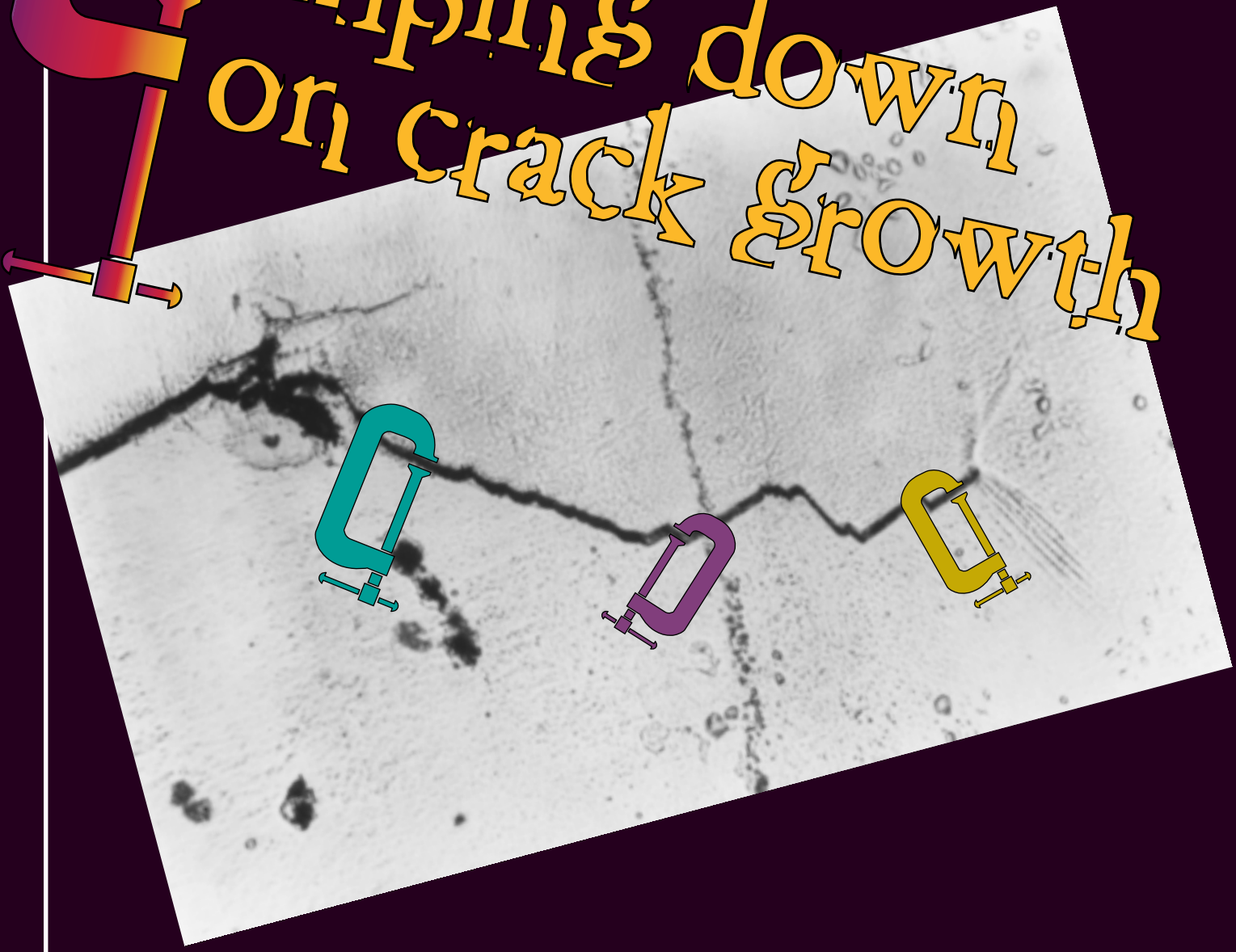

Almost 30 years ago, researchers discovered the phenomenon of crack closure. Simply put, closure occurs when the surfaces of a crack come into contact with each other before the stress in the material falls to zero.

This premature contact of the crack surfaces can result from a number of sources, including the permanent deformation of material as a crack passes through, which tends to act as a clamp on the material just behind the crack tip. Whatever the cause, however, closure prevents the tip of the crack from being exposed to the full range of stresses that it might otherwise experience.

Theoretically, closure should cause crack growth to slow down, or even to stop in some cases. Experiments, however, reveal that closure is a complex phenomenon: some results even show that crack growth can occur in situations where the surfaces of the crack never fully lose contact with each other.

In the following article, the director of Fracture Technology Associates in Bethlehem, Pennsylvania, discusses the phenomenon of crack closure and compares several of the many analytical models to predict crack growth that have attempted to incorporate the effects of crack closure.

– S.P.

The Role of Crack Closure and K_{max} on Fatigue Crack Growth Rate Thresholds

J. Keith Donald

Fracture Technology Associates
Bethlehem, Pennsylvania

Introduction

Fatigue crack growth rate (FCGR) data, when combined with stress analysis of cracks, provides a means of predicting the useful life of a structure or a component that is subjected to cyclic stress in the presence of a crack or defect. However, fatigue life prediction methodology is complicated by a large number of variables, including — but not limited to — the frequency of the cyclic stresses, the cyclic stress intensity range at the crack tip (ΔK), the stress ratio R (the ratio of minimum to maximum stress intensity), the behavior of small cracks, the effects of load interactions, and the physical environment of the component (temperature, humidity, presence of chemicals, etc.).

In theory, a detailed analysis of laboratory tests should allow us to determine the material properties that govern the rate of fatigue crack growth, regardless of the size and shape of the sample of material being tested. In practice, however, this is often not the case.

One of the key variables related to fatigue crack growth is the threshold value of the cyclic stress intensity (ΔK_{th}), below which fatigue cracks will not propagate. In general, the cyclic stress intensity (ΔK) is given by:

$$\Delta K = Y \cdot \Delta\sigma \cdot \sqrt{\pi a}, \qquad (1)$$

where a is the length of the crack, $\Delta\sigma$ is the difference between the maximum and the minimum values of stress in the cycle, and Y is a stress concentration factor that is related to the geometry of the component of interest (such as the presence of holes, notches, corners, or other changes in shape that tend to increase stress).

A commonly used laboratory test to determine ΔK_{th} subjects a sample of material to cyclic stresses and gradually decreases the value of ΔK as the crack length increases. When the fatigue crack either stops growing or grows at a rate less than 10^{-7} mm per cycle of stress, researchers stop the experiment and use Eq. (1) to calculate ΔK_{th}. In this type of test, however, ΔK_{th} is determined at a crack length that is longer than is typical of small cracks at similar stress intensities.

Interference in the crack wake, also known as crack closure, can reduce the range of ΔK and is considered one reason why the value of ΔK_{th} determined from a long crack may be non-conservative for small cracks. A better understanding of this effect, as well as the factors causing stress ratio effects on the rates of fatigue crack growth, should lead to improvements in fatigue life prediction methodology.

Background

Cyclic stresses cause fatigue cracks to grow in metals and other ductile materials. As a general rule, when the stress in a cracked material increases, the surfaces of the crack pull away from each another and the crack has the opportunity to grow. As the stress decreases, the surfaces of the crack should move back toward each other. In theory, you'd expect that the crack surfaces should not touch each other until the stress falls to zero or becomes compressive.

In 1970, however, Elber discovered the phenomenon of crack closure [1,2]. In simple terms, closure occurs when the two surfaces of a crack come into contact with each other before stress in the material falls to zero. Crack closure can result from several sources, including permanent deformation of the material that occurs when the crack tip passes through, irregularities in the crack surface that do not align precisely as the surfaces come back together, and the buildup of corrosion products on the crack surfaces.

The Crack Closure Dilemma

The traditional concept of closure has led to the assumption that the driving force for crack propagation — the effective stress intensity, ΔK_{eff} — exists only when the crack is fully open. In other words, this concept implies that the material just in advance of the tip of a crack will not experience the full value of stress intensity if the surfaces of the crack are touching each other, because this contact will in effect prop open the crack and relieve some of the stress in the material surrounding the crack tip.

However, it will be shown that totally excluding the driving force that exists below the level of load needed to fully open the crack can yield misleading values of ΔK_{eff}. This is particularly true in the near-threshold regime, where the loads needed to open a crack are typically high. In the past, experiments that have attempted to consider the effects of crack closure have been hampered by non-repeatable measurements of closure and by contradictory results [3-10].

The opening load method: A common interpretation of the closure mechanism visualizes the surfaces of a crack as "peeling apart" or "unzipping" as stress is applied. Such an interpretation can lead to the assumption that contributions to ΔK_{eff} are only applied when the last point of contact is lifted off and the crack is fully open. This places tremendous significance on the value of the stress intensity at which the crack is fully open (K_{op}), a parameter that is very difficult to measure with any accuracy.

Attempting to measure K_{op} by comparing the load placed on a test specimen (which is proportional to stress in the material) and the displacement (or movement) of the specimen is difficult due to the gradual change in compliance — the inverse of the slope of the load/displacement curve — as the stress intensity increases and the crack approaches the fully open state. Also, measurement of the load needed to fully open the crack is subject to experimental scatter from a number of sources: signal conditioning noise, sources of non-linearity from test fixtures or instrumentation, etc.

American Society for Testing and Materials (ASTM) standard E647 recommends defining K_{op} as the stress intensity associated with the load needed to cause a 2% deviation in the slope of the linear section of a test specimen's load-displacement curve [11]. The effective stress intensity factor, ΔK_{eff}, for the "opening load" method is then calculated as follows:

(ΔK_{op} method) $$\Delta K_{eff} = K_{max} - K_{op}, \quad (2)$$

where K_{max} is the stress intensity calculated for the maximum stress, and K_{op} is the stress intensity value calculated for the crack opening load (when measured as defined above). The 2% offset value used to establish K_{op} in this method results in an opening load that is somewhat lower than the "true" opening load. Also, measurements of displacement at locations remote from the crack tip generally yield lower apparent opening loads (and, therefore, higher values of ΔK_{eff}) than do measurements of displacement taken near the crack tip.

Despite these limitations, however, this method is able to correlate stress ratio effects very nicely for fatigue crack growth rates above 10^{-5} mm per cycle of stress. Surprisingly, there is a lack of correlation at near-threshold crack growth rates, where opening levels are typically much higher. This lack of correlation is not related to the use of a remote measurement location.

Based on opening load, the ΔK_{eff} at threshold for a low stress ratio (R = 0.1) is often lower than the change in applied stress intensity (ΔK_{app}) for cycles of stress with a high stress ratio (R = 0.98, for example) for which crack growth can be observed. This seemingly contradictory result can only be explained if crack closure only partially shields the crack tip from damaging cyclic strain. Alternative methods of estimating ΔK_{eff} — ones that account for partial closure or that evaluate the closure contribution at the minimum load instead

of at the opening load — will be discussed in a later section.

Sources contributing to crack closure: The most common types of crack closure are plasticity-induced closure (which is caused by the permanent deformation of material in the wake of the crack tip), roughness-induced closure (which is caused by asperities, or irregularities, on the surfaces of the crack), and oxide-induced closure. Experimental evidence shows that plasticity-induced closure can be a very significant source of closure under plane stress conditions, which are most commonly associated with relatively thin specimens of material. However, the effects of plasticity-induced closure are less obvious under conditions of plane strain (which are usually associated with relatively thick specimens of material or with values of stress intensity near threshold) and may be overshadowed by the effects of roughness- and oxide-induced closure.

Three factors are related to the diminishing impact of plasticity-induced closure in plane stress conditions. First, the proximity of the free surfaces of a specimen under plane stress provides a source for the flow of material that ends up in the crack wake. Under plane strain, however, any flow of material that contributes to residual plastic deformation and interference in the crack wake must also contribute to voids or areas of non-contact (due to constant volume plastic flow assumptions).

A second issue related to plasticity-induced closure is scaling. If we assume that residual plastic wake effects are proportional to the size of the plastic zone at the crack tip, the magnitude of this wake effect is proportional to the square of the stress intensity, whereas the elastic profile of the crack is simply proportional to the stress intensity. In other words, as the value of the stress intensity is reduced, the ability for significant plasticity-induced closure to occur beyond the immediate vicinity of the crack tip is proportionally reduced. Therefore, whether plasticity-induced closure even occurs under conditions of plane strain is probably unimportant. The results of opening load measurements on 2024-T3 aluminum alloy show that K_{op} is fairly constant at low K_{max} levels (as can seen in the lower curve in Fig. 1), presumably due to a fairly constant roughness and/or oxide contribution to crack closure.

A third issue related to plasticity-induced closure is the effect of the initial level of K_{max} in decreasing K tests for determining threshold. If a decreasing K test is initiated at a level of K_{max} that is sufficiently high to be partially or predominantly plane stress, the resulting ΔK_{th} is elevated above the "true" long crack threshold and is sensitive to the magnitude of the decreasing K-gradient. The K-gradient refers to the rate of change of K or ΔK with respect to change in crack length. For a high starting K_{max} level of 22.0 MPa√m, the measured K_{op} remains high as ΔK is decreased, although the interference is clearly not near the crack tip (as can be seen in the upper curve in Fig. 1).

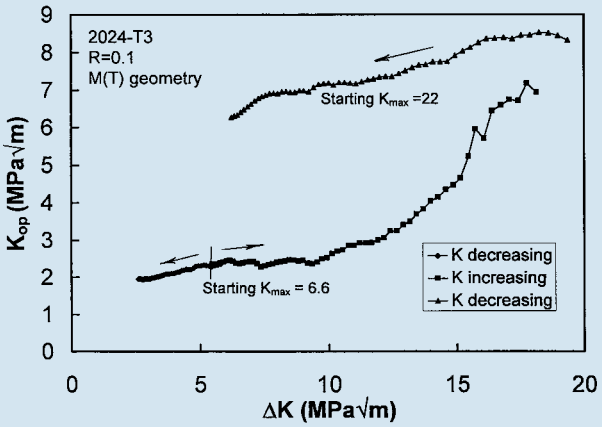

Fig. 1 - For a standard fatigue crack growth rate test in 2024-T3 aluminum alloy, the K_{op} is fairly constant at low K_{max} levels. At higher K_{max} levels, the contribution of plasticity-induced closure significantly elevates the K_{op} level. The K_{op} level remains high for decreasing K from a high starting K_{max} level.

Although the data are not shown in Fig. 1, the test that generated the upper curve of data was continued until crack growth rates near threshold were achieved. The opening load at threshold was found to be about 50% higher than the cyclic maximum load at threshold. Using the traditional definition of ΔK_{eff} (i.e., the calculation shown in Eq. (2)) would not be meaningful, because K_{max} is less than K_{op}; under these conditions, Eq. (2) would yield a negative value for ΔK_{eff}. Therefore, the results of this test are clearly strong evidence for the occurrence of cyclic crack-tip strain at values of stress intensity below K_{op}.

Figure 2 shows that the influence of the starting K_{max} level on the near-threshold behavior in 2024-T3 aluminum alloy occurs above a starting K_{max} of

15 MPa√m. However, if a decreasing K test is initiated at a K_{max} level that produces predominantly plane strain conditions, neither the K-gradient nor the starting K_{max} level appears to have any impact on the resulting value of ΔK_{th}. Figure 3 shows seven decreasing K tests using different K-gradients and crack lengths on three separate test samples. The variation in ΔK_{th} for these seven tests is only about 3%. Although the ΔK_{th} determined from these tests would still be considered a "long crack" threshold, the crack closure effects observed appear to be related to the presence of roughness and oxide, not plasticity.

The influence of near crack-tip vs. crack wake influence on crack closure: Perhaps the biggest controversy surrounding closure is the relative importance of crack surface contact near the crack tip versus contact over the entire crack wake. The notion that small cracks and long cracks behave differently because of wake effects also suggests that the forces exerted over the entire crack wake may be important. The magnitude and distribution of these forces depend on the location, height and distribution of asperities or other interference mechanisms. However, solving for crack wake forces is not straightforward, and therefore closure measurement has traditionally relied on contact to estimate ΔK_{eff}.

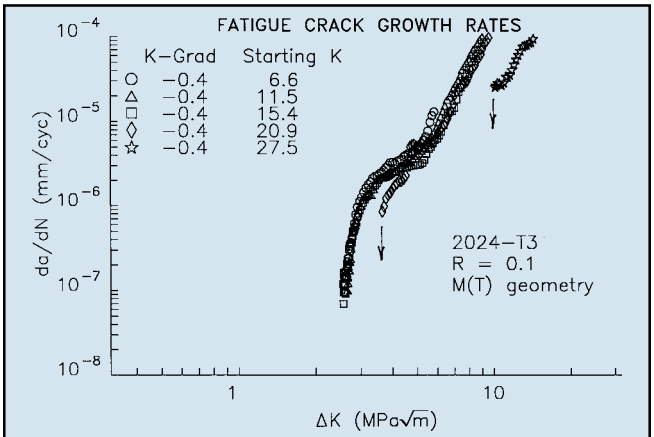

Fig. 2 – Fatigue crack growth rate plot that shows the effects of different values for starting K_{max}

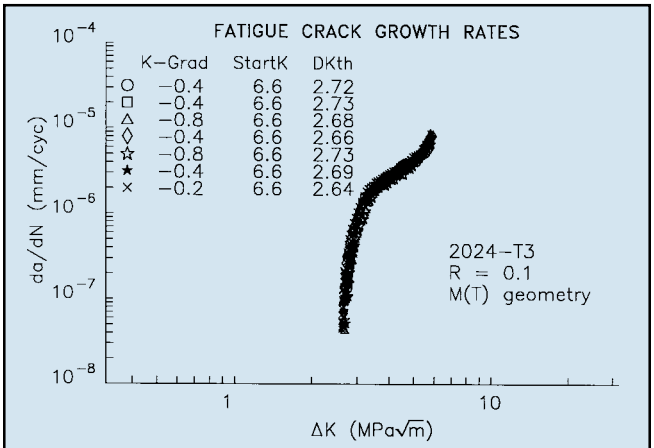

Fig. 3 - Fatigue crack growth rate plot that shows the effects of decreasing K-gradient

There is strong evidence to support additional crack tip cyclic strain below the contact or opening load (i.e., even after contact between the crack surfaces occurs), although in such cases the effective change in stress intensity (ΔK_{eff}) would no longer be directly proportional to the applied change in stress intensity (ΔK_{app}). It is this evidence that supports the partial crack closure and crack wake force distribution models (discussed below) as alternatives to traditional opening load concepts.

Alternative Procedures for Estimating ΔK_{eff}

Several methods of estimating ΔK_{eff} have been attempted [12] and will be briefly summarized here. Each of these methods analyzes the same raw load/displacement data; the difference in the various methods lies in the interpretation of that data. Four of these alternative methods are briefly summarized below, and then analytical results using each of the techniques is presented.

The 2/π correction to the opening load method: The partial crack closure model proposes to account for the crack-tip strain that occurs at values of applied load below the opening load. This "partial closure" interference is modeled as a thin rigid wedge of uniform height with a small gap at the crack tip [13]; the effective change in stress intensity factor (ΔK_{eff}) is calculated as follows:

$$(\Delta K_{2/\pi}\ \text{method}) \qquad \Delta K_{eff} = \Delta K_{op} + (\Delta K_{app} - \Delta K_{op}) \cdot \left(1 - \frac{2}{\pi}\right), \quad (3)$$

where ΔK_{app} is the change in stress intensity between the maximum and the minimum values of stress intensity for the loads applied to the test specimen, and ΔK_{op} is the stress intensity value calculated for the crack opening load.

The adjusted compliance ratio method: Another means of calculating ΔK_{eff} is based on interpreting measurements of strain near the crack tip [14]. This technique, which is called the compliance ratio method, assumes that the crack driving force should be proportional to the magnitude of the elastic strain field near the tip of the crack. Therefore, ΔK_{eff} is based on the ratio of the measured strain magnitude (which is proportional to the secant compliance, C_s) to that which would have occurred in the absence of closure (which is proportional to the fully open compliance C). (Figure 4 graphically depicts each of these parameters.)

An alternate form of this technique, which is referred to as the adjusted compliance ratio (ACR) method, has been developed to estimate ΔK_{eff} by using remote measurements of compliance (i.e., those taken at locations far from the crack surface or crack tip). This technique estimates ΔK_{eff} by subtracting the initial compliance (C_i, measured prior to the initiation of a crack), from the compliance ratio as follows [15,16]:

$$(\Delta K_{ACR} \text{ method}) \qquad \Delta K_{eff} = \frac{C_s - C_i}{C - C_i} \cdot \Delta K_{app}, \qquad (4)$$

where ΔK_{app} is the change in stress intensity between the maximum and the minimum values of stress intensity for the loads applied to the test specimen. The compliance parameters shown in Eq. (4) are defined as shown in Fig. 4.

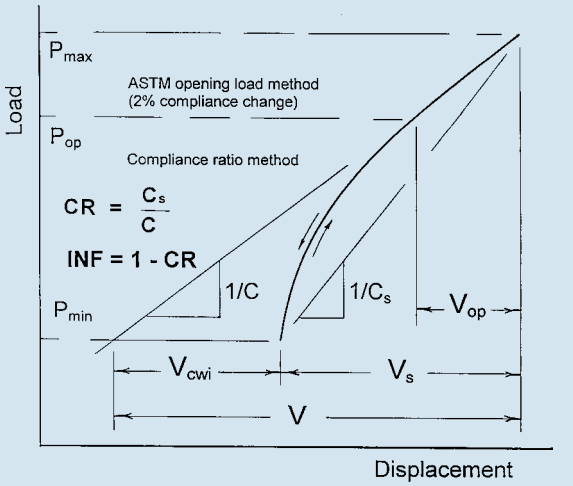

Fig. 4 - Load-displacement trace that shows the influence of opening load, compliance ratio and crack wake

The crack wake influence method: The previously discussed methods of estimating ΔK_{eff} are based primarily on the direct analysis of experimental data. The crack wake influence (CWI) method, however, attempts to mathematically describe the effect of interference in the wake of the crack (i.e., crack closure) on measurements of crack surface displacement and on the stress intensity at the crack tip [17].

Solving the complex mathematical equations that describe the stress and strain fields surrounding a crack provides a method of relating measurements of compliance far from the crack tip to the reduction in elastic strain at the crack tip, which has a direct impact on the magnitude of the cyclic plastic crack tip strains that cause fatigue damage.

The CWI method calculates ΔK_{eff} as follows:

$$(\Delta K_{CWI} \text{ method}) \qquad \Delta K_{eff} = \Delta K_{app} \cdot \left(1 - \frac{V_{cwi}}{V \cdot IFR}\right) \qquad (5)$$

where ΔK_{app} is the change in applied stress intensity, V_{cwi} and V are displacement measurements that are obtained from load/displacement curves (these parameters are shown and defined in Fig. 4), and IFR are non-dimensional (i.e., solely numerical) functions that depend only upon the position of the crack wake interference in relation to the crack tip [17].

When the amount of crack growth is small compared to the overall length of the crack, the ACR method is equivalent to the CWI method for a distributed force that tapers linearly from some value at the point of crack initiation to a value of zero at the crack tip. This equivalence allows us to use the mathematical results from the CWI method to improve the empirically determined estimates obtained from the ACR method of estimating ΔK_{eff}.

The modified adjusted compliance ratio method (n2): The equivalence of the mathematical CWI method and the empirical ACR method for certain crack growth conditions allows the development of an improved ACR method for estimating ΔK_{eff}. A slight modification of the ACR formula (Eq. (4)) replaces the initial compliance (C_i) with the compliance of the load displacement curve at minimum load, C_{n2}, as follows:

(ΔK_{ACRn2} method) $$\Delta K_{eff} = \frac{C_s - C_{n2}}{C - C_{n2}} \cdot \Delta K_{app} \qquad (6)$$

Experimental results: To evaluate these various methods of estimating ΔK_{eff}, fatigue crack growth was measured in laboratory tests of center crack tension samples (also known as M(T) geometry specimens) fabricated from 2024-T3 aluminum alloy. The crack growth data were generated at stress ratios of 0.1 and 0.7 using decreasing K (below 1 x 10^{-5} mm/cycle) and increasing K (above 1 x 10^{-5} mm/cycle) test procedures.

Figure 5 shows crack growth data obtained at a stress ratio of 0.1 for the 2024-T3 alloy as a function of ΔK_{app} (small open circle symbol) and of the ΔK_{eff} calculated from the five estimation procedures (including the traditional opening load concept, which is shown as a large circle symbol). For comparative purposes, a second sample of 2024-T3 aluminum alloy was used to generate crack growth rate data at a stress ratio of 0.7. Analysis of the load-displacement data obtained at a stress ratio of 0.7 revealed no evidence of non-linearity associated with crack closure. Therefore, the data at this stress ratio could serve as a baseline for evaluating the various methods of estimating ΔK_{eff}. Note that at near-threshold growth rates, the opening load (OP) method gives a distinctly lower value for ΔK_{eff} than is obtained from the other methods. Also note that all of the estimation methods that account for crack tip cyclic strain below the opening load are in good agreement with the data obtained at high stress ratio (R = 0.7). Finally, note that for crack growth rates above 5 x 10^{-6} mm per cycle of stress, the ΔK_{eff} data using the opening load method agrees very well with the crack growth data obtained at high stress ratio.

The Role of K_{max}

The observations noted above do not account for second-order effects that are due to differences in K_{max} at a stress ratio of 0.1 and 0.7. Previous work has shown that properly correlating stress ratio effects requires the correct closure methodology as well as an evaluation of the K_{max} contribution to stress ratio effects [12,15,16,18]. Research has shown that this K_{max} dependence can be fitted by a power-law function, with the magnitude of the exponent being a measure of K_{max} sensitivity. The combined effects of ΔK_{eff} and K_{max} can be normalized using the following relationship [18]:

$$\Delta K_{norm} = \Delta K_{eff}^{(1-n)} \cdot K_{max}^{n} \qquad (7)$$

where n is a normalized K_{max} sensitivity exponent determined from experimental data.

To investigate the sensitivity of the 2024-T3 alloy to changes in K_{max} , specimens were tested at a constant K_{max} of 6.6, 9.9, 14.8, 22.0, 33.0, and 49.5 MPa√m and a decreasing ΔK. Figure 6 shows the data obtained from these tests. At near-threshold crack growth rates, the value of stress ratio for the constant K_{max} test varies from 0.78 to 0.98; therefore, none of these data should be affected by crack closure. These results suggest that

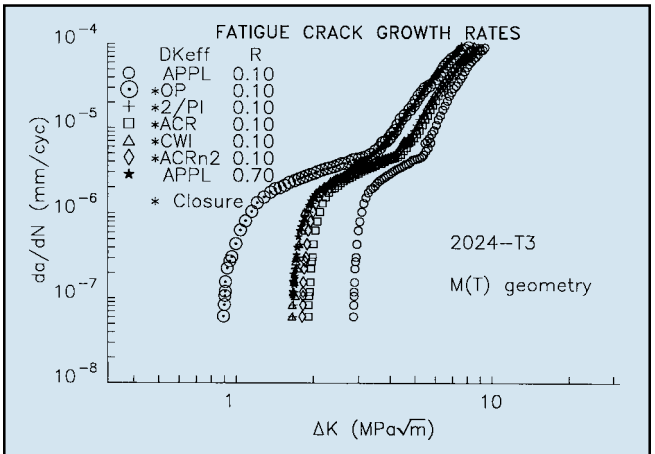

Fig. 5 - Fatigue crack growth rate plot that shows data collected at stress ratios R = 0.1 and R = 0.7 as a function of ΔK_{app} and five estimation methods for ΔK_{eff}

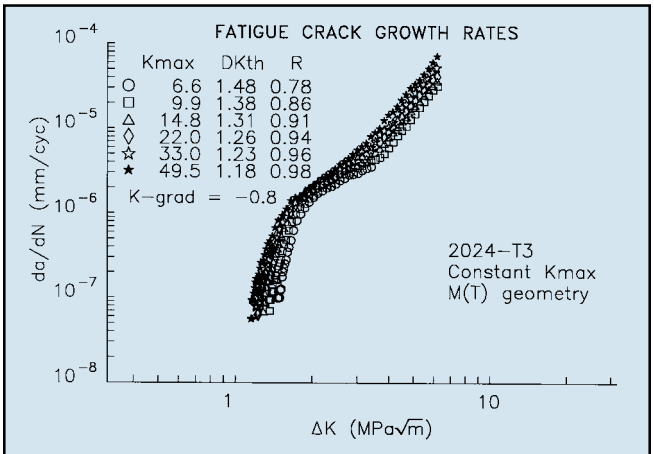

Fig. 6 - Fatigue crack growth rate plot that shows the effect of K_{max} at a stress ratio above the influence of crack closure

the difference between the curves in Fig. 6 is real and is actually related to differences in K_{max}. To test this hypothesis, the data are replotted in Fig. 7 using a K_{max} sensitivity exponent (n) of 0.100 in Eq. (7). As can be seen in Fig. 7, the separate crack growth data curves from Fig. 6 collapse into a single curve that provides a unique crack growth rate curve that is intrinsic to that material. Although unproven, it is reasonable to assume that K_{max} sensitivity may play a role at low stress ratios as well. If so, then the K_{max} sensitivity exponent may be universal over a wide range of K_{max} and ΔK, although crack closure is expected to play a more dominant role at low stress ratios.

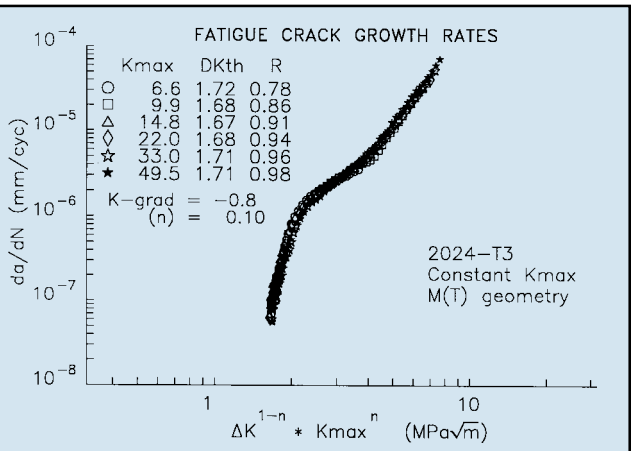

Fig. 7 - Fatigue crack growth rate plot that shows a unique intrinsic curve obtained by plotting the crack growth rate as a function of $\Delta K^{0.9} * K_{max}^{0.1}$

Figure 8, which is a plot of ΔK versus K_{max} at threshold, shows how the data obtained from the constant K_{max} tests (shown in Fig. 6) converge with the data obtained at low stress ratio for all ΔK_{eff} estimation methods (ΔK_{other}) except opening load (ΔK_{op}). As noted in Fig. 8, when the experimental crack growth data and the empirically determined K_{max} sensitivity exponent (n) of 0.100 are plugged into Eq. (7), ΔK_{norm} for 2024-T3 aluminum is determined to be 1.69. Figure 8 also shows a sharp rise in ΔK_{app} at low stress ratio due to crack closure, as well as a drop in ΔK_{op} due to the ignored elastic crack-tip cyclic strain below the opening load.

Summary and Conclusions

The experimental determination of ΔK_{eff} using the opening load concept is sensitive to the location where

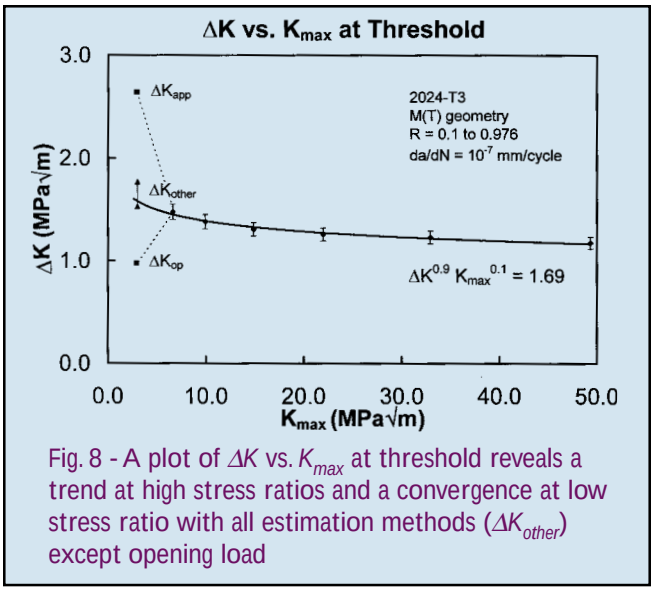

Fig. 8 - A plot of ΔK vs. K_{max} at threshold reveals a trend at high stress ratios and a convergence at low stress ratio with all estimation methods (ΔK_{other}) except opening load

the displacement of the material is measured (whether close to or far from the crack surface), the arbitrary nature of the percent offset, and the variability associated with selecting a specific percent offset due to noise and non-linearity. However, it appears that an opening load method may be appropriate under the right circumstances. At growth rates above 10^{-5} mm/cycle, the ASTM opening load method appears to provide satisfactory results.

The $2/\pi$ method of making a correction to the opening load has a physical model and is simple to apply. Although the model may only approximate typical mechanisms of crack closure, it does provide a means by which cyclic crack tip strain that occurs below the opening load may be accounted for. One disadvantage, however, is that the opening load must be either measured or predicted to utilize this method.

The adjusted compliance ratio (ACR) method is also simple to apply and appears less sensitive to variability than the opening load method. Experiments that measure displacement of the material at multiple locations have shown the ACR results to be insensitive to the measurement location. The measurements are also unique (i.e., no arbitrary percent offset is required) and repeatable, because full range load and displacement (rather than the deviation in linearity between load and displacement/strain) are measured. However, results of the comparison of the crack wake influence and the ACR methods suggest that the ACR method only partially accounts for crack-tip interference due to closure.

The modified adjusted compliance ratio (ACRn2) method attempts to account for limitations in the ACR method through refinements in the initial assumptions about the initial compliance. At present, however, these refined assumptions lack a solid theoretical basis and warrant further investigation.

The crack wake influence (CWI) method is mathematically complex and requires knowledge of the crack wake force distribution, which limits its usefulness. Like the ACR method, however, the CWI method is based on the change in crack surface displacement at minimum load due to closure, rather than the load at which contact in the crack wake first occurs.

The overwhelming difficulty associated with experimental estimations of ΔK_{eff} arises both from the challenges of obtaining quality experimental data and from the broad range of assumptions required to interpret the measurements. By nature, estimating ΔK_{eff} from a single load-displacement curve is indeterminant. Furthermore, the estimation of ΔK_{eff} is complicated by evidence that K_{max} also influences stress ratio effects. Because the procedures used to estimate ΔK_{eff} are not exact, it is difficult to separate the precise roles or effects of crack closure and K_{max}. Additional research should provide a better understanding of these phenomena and should lead to improvements in fatigue life prediction methodology.

Acknowledgments

The author wishes to acknowledge the support of Fracture Technology Associates, Alcoa Technical Center (Alcoa Center, Pennsylvania), and the Office of Naval Research in the above endeavors. Many thanks for the contributions of Paul C. Paris and Hiroshi Tada as well.

References

1. W. Elber, "Fatigue Crack Closure Under Cyclic Tension," *Engineering Fracture Mechanics*, Vol. 2, 1970, pp. 37-45.

2. W. Elber, "The Significance of Fatigue Crack Closure," *Damage Tolerance in Aircraft Structures, ASTM Special Technical Publication (STP) 486* (American Society for Testing and Materials, Philadelphia, PA, 1971), pp. 230-242.

3. R.W. Hertzberg, C.H. Newton, and R. Jaccard, "Crack Closure: Correlation and Confusion," *Mechanics of Fatigue Crack Closure, ASTM STP 982* (American Society for Testing and Materials, Philadelphia, PA, 1988), pp. 139-148.

4. E.P. Phillips, "Results of the Round Robin on Opening-Load Measurement," *NASA Technical Memorandum 101601*, NASA Langley Research Center, Hampton, VA, 1989.

5. E.P. Phillips, "Results of the Second Round Robin on Opening-Load Measurement," *NASA Technical Memorandum 109032*, NASA Langley Research Center, Hampton, VA, 1993.

6. K. Sadananda and A.K. Vasudevan, "Analysis of Fatigue Crack Closure and Thresholds," *Fracture Mechanics: 25th Volume, ASTM STP 1220*, edited by Erdogan and Hartranft (American Society for Testing and Materials, Philadelphia, PA, 1995).

7. K. Sadananda and A.K. Vasudevan, "Short Crack Growth Behavior," *Fatigue and Fracture Mechanics: 27th Volume, ASTM STP 1296*, edited by R. Piascik, N. Dowling, and J. Newman, (American Society for Testing and Materials, West Conshohocken, PA, 1997).

8. D.L. Chen, B. Weiss, and R. Stickler, "Contribution of the Cyclic Loading Portion Below the Opening Load to Fatigue Crack Growth," *Materials Science and Engineering*, A208, 1996, pp. 181-187.

9. D.E. Macha, D.M. Corbly, and J.W. Jones, "On the Variation of Fatigue-Crack-Opening Load with Measurement Location," *Experimental Mechanics*, June 1979, pp. 207-213.

10. J.E. Allison, and C.P. You, "Problems Associated with the Quantification of Fatigue Crack Closure," in *Fatigue '90, The Proceedings of the 4th International Conference of Fatigue and Fatigue Thresholds*, edited by H. Kitigawa and T. Tanaka (Materials and Components Engineering Publications, Ltd., United Kingdom, 1990), pp. 1249-1255.

11. J.K. Donald, "A Procedure for Standardizing Crack Closure Levels," *Mechanics of Fatigue Crack Closure, ASTM STP 982*, edited by J.C. Newman, Jr. and W. Elber (American Society for Testing and Materials, Philadelphia, PA, 1988), pp. 222-229.

12. J.K. Donald, and P.C. Paris, "An Evaluation of ΔK_{eff} Estimation Procedures on 6061-T6 and 2024-T3 Aluminum Alloys," *Fatigue Damage of Structural Materials II*, Engineering Foundation Conference, September 7-11, 1998, Hyannis, MA. *To be published in International Journal of Fatigue, Elsevier Science Ltd.*

13. P.C. Paris, H. Tada, and J.K. Donald, "Service Load Fatigue Damage — A Historical Perspective," *Fatigue Damage of Structural Materials II*, Engineering Foundation Conference, September 7-11, 1998, Hyannis, MA. *To be published in International Journal of Fatigue.*

14. J.K. Donald, "Introducing the Compliance Ratio Concept for Determining Effective Stress Intensity," *International Journal of Fatigue*, Vol. 19, Supp. No. 1, 1997, pp. 191-195.

15. J.K. Donald, G.H. Bray, and R.W. Bush, "An Evaluation of the Adjusted Compliance Ratio Technique for Determining the Effective Stress Intensity Factor," *29th National Sympo-*

sium on Fatigue and Fracture Mechanics, ASTM STP 1332, edited by T.L. Panontin, and S.D. Sheppard (American Society for Testing and Materials, West Conshohocken, PA, 1998).

16. G.H. Bray and J.K. Donald, "Separating the Influence of K_{max} from Closure-Related Stress Ratio Effects Using the Adjusted Compliance Ratio Technique," *Advances in Fatigue Crack Closure Measurement and Analysis: Second Volume, ASTM STP 1343,* edited by R.C. McClung and J.C. Newman, Jr. (American Society for Testing and Materials, West Conshohocken, PA, 1998).

17. J.K. Donald, G.M. Connelly, P.C. Paris, and H. Tada, "Crack Wake Influence Theory and Crack Closure Measurement," *National Symposium on Fatigue and Fracture Mechanics: 30th Volume, ASTM STP 1360,* edited by K.L. Jerina and P.C. Paris (American Society for Testing and Materials, West Conshohocken, PA, 1999).

18. J.K. Donald, G.H. Bray, and R.W. Bush, "Introducing the K_{max} Sensitivity Concept for Correlating Fatigue Crack Growth Data," *High Cycle Fatigue of Structural Materials (Professor Paul C. Paris Symposium),* edited by W. Soboyejo and T.S. Srivatsan (The Minerals, Metals & Materials Society, West Conshohocken, PA, 1997), pp. 123-141.

The Author

Mr. J. Keith Donald received his B.S. degree in Mechanical Engineering from Lehigh University in 1972 and is currently the director of Fracture Technology Associates. FTA was formed in 1984 to provide software and testing services for fatigue crack growth and fracture toughness testing. Mr. Donald has been active in developing automated test techniques for fatigue crack growth rate testing since the 1970s and has authored numerous papers on the subject. His past activities within the American Society for Testing and Materials (ASTM) have included chairing the organization's task group on Near-Threshold Fatigue Crack Growth and co-chairing the task group on Non-Visual Methods of Crack Length Determination. Mr. Donald was co-editor for ASTM Special Technical Publication (STP) 1251 on "Special Applications and Advanced Techniques for Crack Size Determination." He is currently co-chairman of ASTM task group E08.06.03 on Crack Closure Measurement and Analysis.

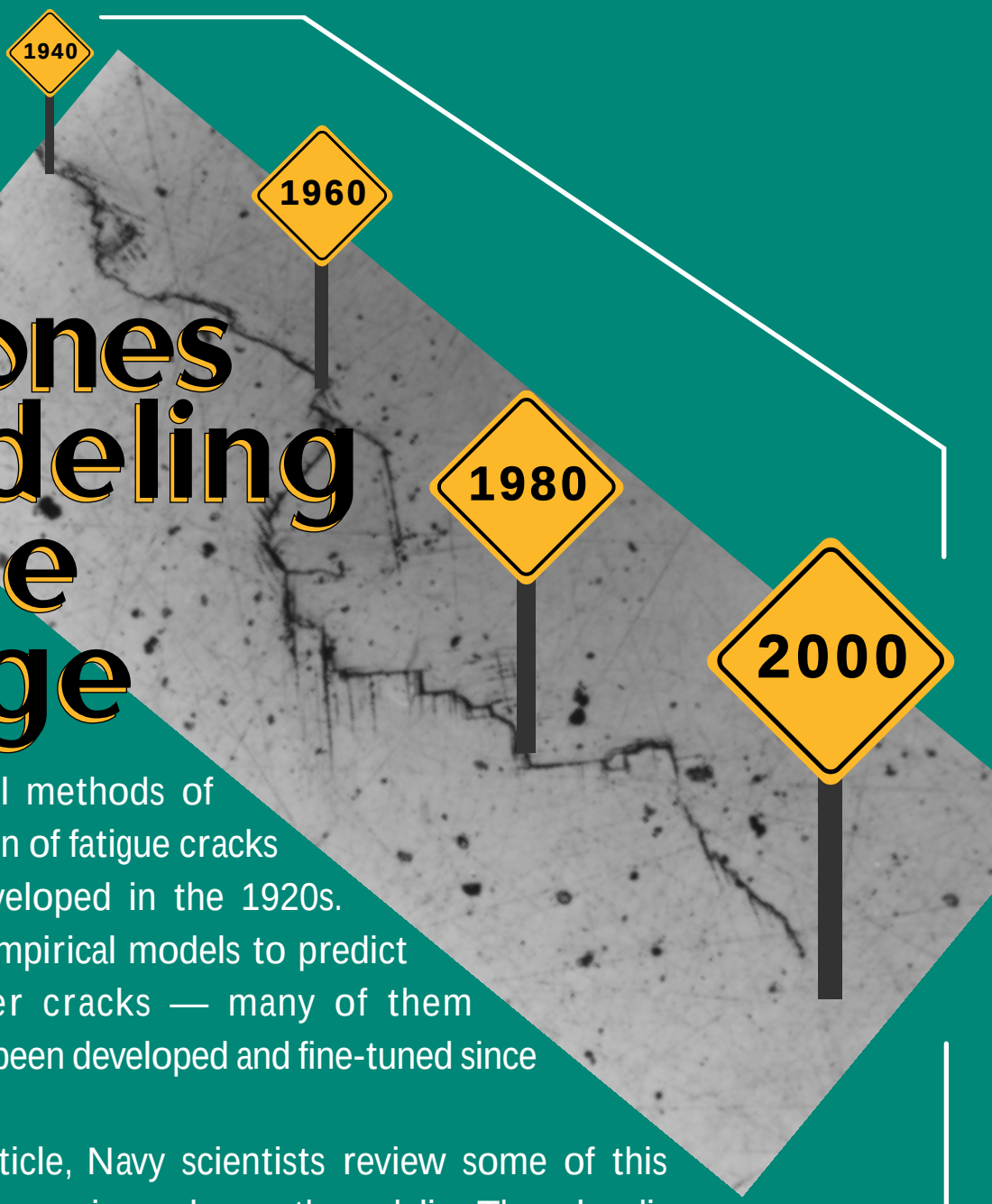

Milestones in Modeling Fatigue Damage

The first successful methods of modeling the nucleation of fatigue cracks in materials were developed in the 1920s. Today's multitude of empirical models to predict the growth of longer cracks — many of them computerized — have been developed and fine-tuned since the 1960s.

In the following article, Navy scientists review some of this century's significant advances in crack growth modeling.They also discuss a new unified model that incorporates two main crack driving forces for long fatigue cracks. In this model, the presence of internal stresses helps to explain deviations from long crack behavior, such as the significant differences between the crack growth rates for short cracks and long cracks.

This comprehensive new model may, for the first time, allow researchers to model fatigue damage behavior from the point of crack nucleation at small material defects to a component's final failure.

– S.P.

A Unified Framework for Fatigue Damage Analysis

K. Sadananda

Naval Research Laboratory – Materials Science and Technology Division
Washington, DC

A.K. Vasudevan

Office of Naval Research – Materials Science Division
Arlington, VA

Background

Fatigue damage can be divided into several stages: crack nucleation, short crack growth, long crack growth, and final failure. The rate of damage accumulation in each of these four stages depends upon a variety of factors: loads, environment, alloy chemistry, the presence of stress concentrations, specimen geometry, etc. In the past several decades, empirical approaches have been used to predict the life at each stage of fatigue damage.

Early methods to predict fatigue life included determining the relationship between stress or strain and the number of load cycles to needed to produce component failure. One of the most common life prediction calculations used for components subjected to variable loads was based on the Palmgren-Miner linear damage law [1,2]. This law proposes that damage sustained by the component at different stress levels is linearly additive; in such a case, the component's total life can be estimated by summing the incremental damage n/N_f, where n is the number of cycles of stress experienced at a certain level of stress, and N_f is the number of cycles needed to produce a component failure at that stress level. (This number is usually obtained from laboratory tests of specially prepared specimens.) When $\Sigma\,[n/N_f] = 1$, the component is considered to have failed.

The Palmgren-Miner model of fatigue damage accumulation has undergone several modifications [3,4]. The most important drawback of these linear damage models is that they do not account for the effects of prior loading history. In other words, the damage caused by each cycle is not affected by the size or the sequence of the previous cycles of stress. Another important consideration: if an unknown defect or flaw were present, the total life of the component would be significantly less than that predicted by the Palmgren-Miner model. Finally, these models are specifically suited to address predictions of total component life when the crack propagation stage of fatigue damage is significantly small compared to the crack nucleation.

In the strain-life approach, the material in the component is assumed to be highly strained near areas of stress concentration (such as notches), and this ligament of material is assumed to behave the same as virgin material (without the stress concentration) having the same stress-strain history. Therefore, for such fatigue damage models, the only material property data needed to estimate the component life are the cyclic stress-strain and strain-life curves. In comparison to the stress-life model, the strain-life approach accounts for any local plasticity effects at regions of stress concentration. There are over 70 different crack initiation models [3], and these models are described in detail by Dowling [5,6] and Polak [7].

Most of the models that describe the behavior of short cracks are concerned with the prediction of high crack growth rates at lower stress intensities (below the long crack threshold). These approaches encompass semi-

empirical formulations of Hobson [8], subsequent extensions of this model [9,10], and dislocation-based models [11-14] in terms of the effects from material inhomogenities like grain boundaries and local plasticity. These models predict the existence of a threshold for a short crack and its variation from deceleration to acceleration. Recently, Navarro and de los Rios [15] have modified these models to predict the short crack growth lives under constant and variable amplitude loading [16].

There are about 40 empirical models proposed for the prediction of long crack growth [17]. Among these models, a modified Forman equation [18] is considered the best approximation for the engineering application. Newman and co-workers [19,20] have done extensive work in the past 20 years to predict fatigue life of commercial aluminum and titanium alloys. They modified the Dugdale strip yield model to include plasticity-induced closure and introduced a life prediction code called FASTRAN to predict the lives of alloys using small crack theory. The plastic zone and the wake zone are modeled for rigid-perfectly-plastic elemental strips with an average stress between the yield stress and the ultimate stress for the material. A crack tip constraint factor α was assumed to account for the three-dimensional state of stress at the crack tip. This constraint factor α varies from a value of 1 for plane stress (which is usually encountered in thin sheets of material) to a value of 3 for plane strain (usually encountered in thick materials), and it is determined by a trial-and-error method by fitting the crack growth curves at high and low values of stress ratio *R*. Furthermore, α varies from material to material; for instance, for aluminum alloys α is 2 and for steel it is 2.5.

Research shows that the constraint factor α is not very sensitive to constant amplitude loadings. As a result, long crack spike overload data (which is taken from plots of crack length vs. number of cycles) is used to fine tune the α values. For small cracks, a plane strain condition is assumed and therefore the value of α is selected between 2 and 3. The estimated value of α is then used to correlate the long crack growth rates as a function of ΔK_{eff} for constant amplitude loading conditions; for which the analytical functional relations for crack opening stress in terms of crack length (a), stress ratio (R), and applied stress is used. With some modifications of the ΔK_{eff} at near-threshold regions, the model was fit to the small crack data and endurance limits. It was then used to predict the fatigue lives of aluminum alloys and titanium alloys for notched samples under both constant and variable amplitude loadings. An equivalent initial flaw size concept was used to bound the fatigue lives in agreement with test results. Their model does predict the ΔK_{th} decrease with load ratio for constant amplitude loading, which is commonly observed under environment. They are able to predict to a reasonable extent the life of short and long cracks under constant and variable amplitude loading and also under some service loading conditions. The analytical predictions from these models of crack growth have been incorporated into several other computer programs [21].

Lazzeri et al. [22] have compared the life predictions from various such empirical models for an aircraft spectrum under a flight-by-flight load history at a mean flight load of 75 MPa. The results are shown in Fig.1. All of the models underpredicted the flights to failure. The MODGRO (1988) model has been improved recently and renamed AFGROW, which now seems to be comparable to the FASTRAN model [23]. Improvements in these models that will incorporate the effects of material slip behavior and of the environment are in progress. Commonly, inadequacies in the prediction methods are compensated by using several adjustable parameters that are correlated using component test data. In practice, vehicle safety is guarded by the use of safety factors in design, the selected use of component test data, periodic non-destructive inspections, the use of statistics to assign data scatter, material quality control, etc.

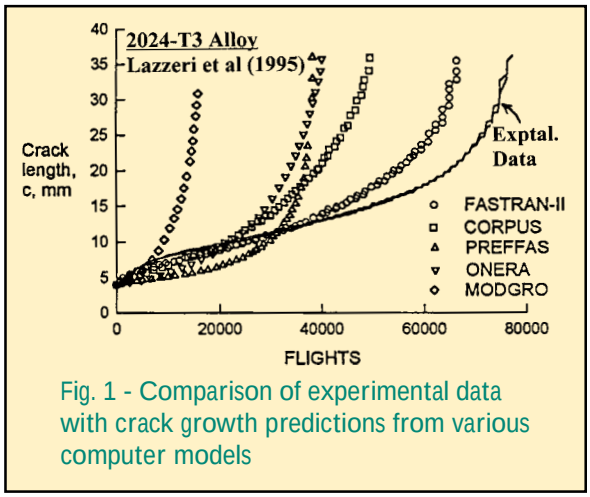

Fig. 1 - Comparison of experimental data with crack growth predictions from various computer models

The drawbacks in the prediction of fatigue life by the abovementioned empirical models stem from several sources, including: (1) the assumption of plasticity induced closure, (2) the lack of terms in the model that address environmental effects and slip behavior, and (3) several adjustable parameters to fit the experimental data. In order to develop a more reliable life prediction model, one must first recognize the correct physics of the problem. We find that a better approach is to treat the overall damage as an intrinsic behavior instead of an extrinsic factor such as crack closure. First, we must recognize that the true material behavior is represented in the long crack growth properties. Second, fatigue damage has to be described by two driving force parameters instead of one; these two driving forces are ΔK and K_{max}. Third, we must recognize that deviations from the long crack growth behavior arise from internal stresses that are present ahead of the crack. For example, these internal stresses are responsible for the accelerated crack growth in the short crack region and the decelerated growth due to overloads. Finally, the overall damage must be described from the initiation stage to final failure.

The following is a brief description of the analysis of damage that bridges the gap between stages of fatigue in a unified manner. Due to the restriction of space, we discuss only damage in the long and short fatigue crack growth regions. The analysis has also been extended to include overloads and underloads.

Long Fatigue Cracks

It has been established that for long fatigue cracks there is a threshold stress intensity [ΔK_{th}] below which crack propagation does not occur. The threshold values have been experimentally observed to depend primarily upon stress ratio [$R = K_{min}/K_{max}$], microstructure of the material, and environment. These stress ratio effects have been rationalized on the basis of premature crack closure in the wake of a crack that reduces the applied crack tip stress intensity [$\Delta K_{app} = K_{max} - K_{min}$] by an amount due to closure [K_{cl}]. Therefore, the effective driving force [$\Delta K_{eff} = K_{max} - K_{cl}$] that is less than the applied force [ΔK_{app}], which tends to retard the crack growth process. All of these parameters are depicted schematically in Fig. 2.

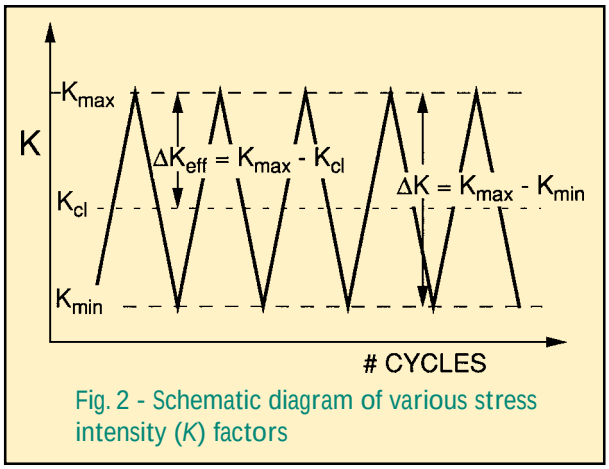

Fig. 2 - Schematic diagram of various stress intensity (K) factors

Premature crack closure is believed to be a result of: (1) plasticity, (2) asperities from oxides or other corrosion products, (3) surface roughness, (4) viscous fluids, and (5) phase-transformed material ahead of the crack tip. While this interpretation has been used for more than two decades, questions have been raised in a number of areas, including experimental uncertainties, interpretation of the closure data and basic physical concepts. For detailed discussions on the topic of crack closure, see Suresh [24] and ASTM proceedings [25]. From recently published articles on crack closure [26-30], however, one can summarize that: (1) plasticity-induced closure is not possible (which complies with the experimentally observed vacuum results where ΔK_{th} is independent of stress ratio), and (2) roughness- and oxide-induced closure are not significant enough in most common aqueous environments (like lab/moist air) to account for the large variations in the dependence of ΔK_{th} on stress ratio (i.e., factors of 3 to 7) that have been experimentally observed.

Fatigue crack growth results are traditionally presented in terms of variation in ΔK with stress ratio. Figure 3 shows such a plot, which compares crack growth data for 7075-T7351 aluminum alloy obtained in a vacuum with that obtained for the alloy in laboratory air. The data in Fig. 3 is taken from different sources [31-33]. Most materials show a linear reduction in ΔK_{th} with increase in stress ratio for lab air conditions; however, Fig. 3 seems to show no such dependence for data obtained in a vacuum. The former condition is interpreted as being due to plasticity-induced crack closure, and the latter due to lack of it. Crack closure is considered to be prevalent only at low stress ratio, with

closure levels decreasing towards higher stress ratios. The relative magnitude of the reduction in ΔK_{th} with stress ratio in air depends on the alloy and the environmental conditions in which the test was conducted. Attempts to correlate the closure values to variations in alloy microstructure and environmental conditions have led to conflicting conclusions [28,29]. Closure interpretations are considered as extrinsic since the effects are due to the effects in the wake of a crack (i.e., behind the crack tip). However, one can interpret the results shown in Fig. 3 without invoking closure explanations. This view accepts the fatigue behavior of the material to be intrinsic to the conditions of the applied loading and environment. The implications of this explanation are interesting and are basic to the behavioral properties of the material.

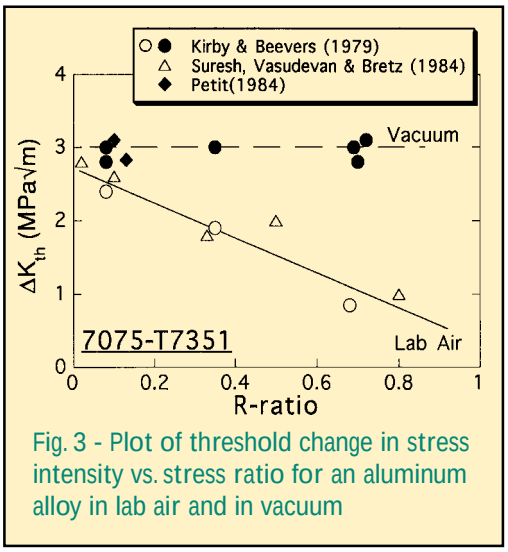

Fig. 3 - Plot of threshold change in stress intensity vs. stress ratio for an aluminum alloy in lab air and in vacuum

This new interpretation can be described using an example from the behavior of a 2024 aluminum alloy, for which larger amounts of data are available. Figures 4a and 4b show data obtained by Kemper et al. [34] in laboratory air conditions for a 2024-T3 alloy over a wide range of stress ratio (from –10 to +0.8). In Fig. 4a, values for both ΔK_{th} and K_{max} are plotted against stress ratio. The data show that ΔK_{th} decreased linearly as R increased until the stress ratio reached approximately 0.4 and then leveled off. We have designated a critical cyclic stress intensity [ΔK^*_{th}] when stress ratio is greater than 0.4, a region where K_{max} increases nonproportionally and ΔK_{th} is constant. This portion of the plot is labeled as a ΔK-controlled region, where K_{max} must increase to maintain the minimum ΔK_{th} for crack growth. As the stress ratio approaches a value of 1, K_{max} would increase to a level that is dictated by the toughness of the material. On the other hand, in the region where stress ratio is less than 0.4, K_{max} approaches a constant critical value [K^*_{max}] with an attendant decrease in ΔK_{th}. This portion of the plot is labeled as a K_{max}-controlled region, which means that ΔK_{th} must be varied to maintain the critical static stress intensity K^*_{max} constant for crack growth. In the entire range of stress ratios (i.e., from -10 to +0.8), while both ΔK^*_{th} and K^*_{max} critical values are being satisfied, either one parameter or the other is controlling the fatigue damage process. Thus, we postulate that the crack advancement will occur if these two critical stress intensities are simultaneously satisfied. These two limiting values are the minimum conditions necessary for crack growth to occur independent of closure. The magnitude of these critical stress intensities for a given alloy can vary, and they also depend on the load history and environmental conditions.

Because stress ratio is not a driving force for crack growth, the data from Fig. 4a can be replotted in terms

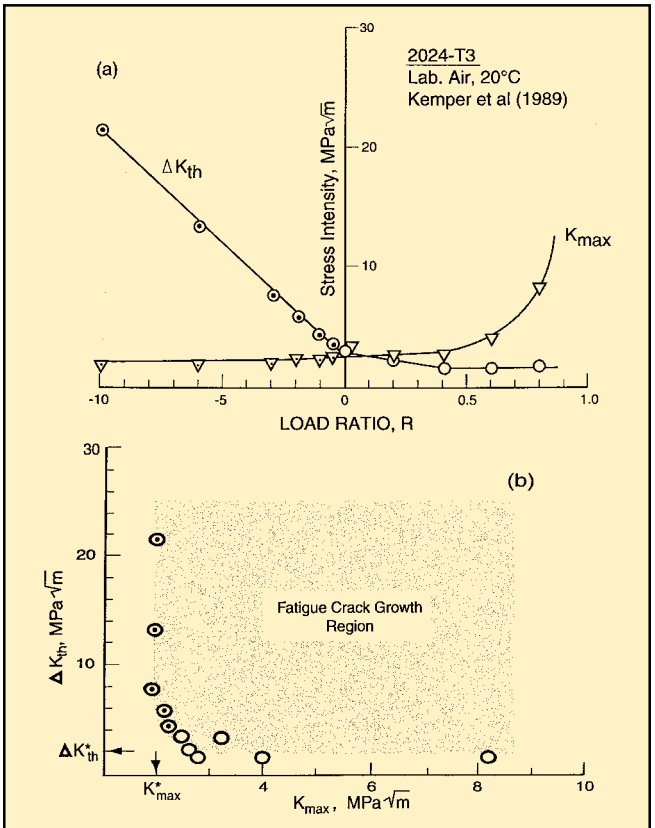

Fig. 4 - [a] A plot of K_{max} and ΔK_{th} vs. stress ratio, and [b] the same data plotted as ΔK_{th} vs. K_{max}

of ΔK_{th} vs K_{max}. The result, Fig. 4b, shows an L-shaped curve that defines the region where crack growth can occur. Critical values of ΔK^*_{th} and K^*_{max} are marked by the two arrows along the axes of the plot. For 2024 alloy, the critical values of ΔK^*_{th} and K^*_{max} are approximately 1 MPa$\sqrt{m}$ and 3 MPa$\sqrt{m}$, respectively, for the given environmental and loading condition. Such an interpretation is independent of testing methods [28,29] and is applicable to many types of materials. Figures 5a and 5b show a well-defined values for both ΔK^*_{th} and K^*_{max} at low and high temperatures for a variety of materials ranging from monolithic alloys to composites. Plots such as these can be developed from any constant crack growth rate data that allow the extraction of ΔK and K_{max} values for the material.

Using these concepts, one can extend the analysis to classify the fatigue crack growth behavior of a variety of materials (including metals, ceramics, and polymers) that fall into five different types, where each is distinguished by the relative contributions from the environment and cyclic plasticity [35,36]. For a given material, the classification scheme applies over the entire crack growth rate and identifies the transitions of the behavior from one class to another [35,36]. The analysis presented above would move the fatigue analysis more towards the intrinsic material behavior which is needed for reliable life prediction analysis.

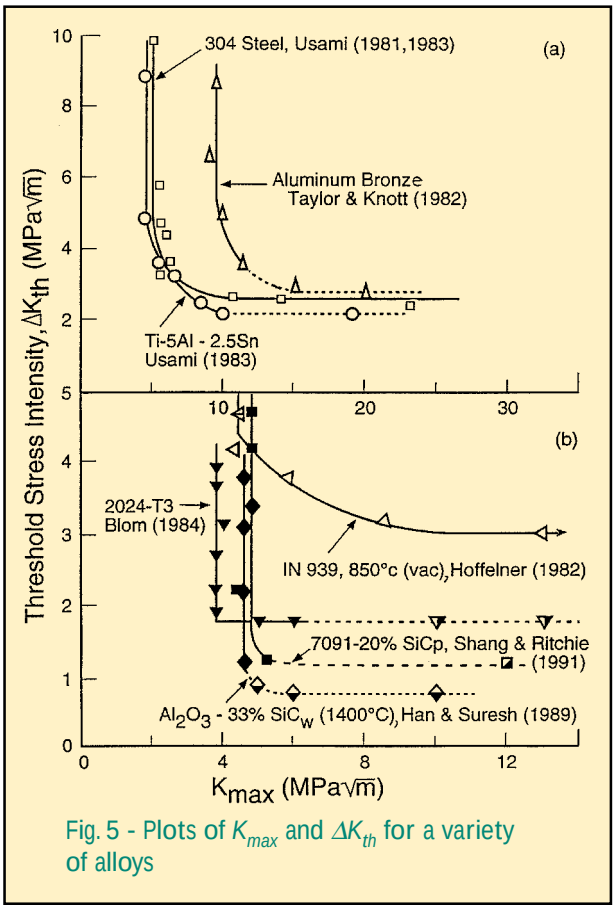

Fig. 5 - Plots of K_{max} and ΔK_{th} for a variety of alloys

A literature survey indicates that several key studies [37-42] have directly or indirectly noted the role of two driving force parameters, ΔK and K_{max}, in fatigue. (See Table 1.) Wilkinson and Roberts [43] were able to predict the ΔK_{th} vs. K_{max} curve for copper using a computer simulation of dislocation motion near a crack tip. This is the first attempted theoretical work that confirms the need for two parameters to model the driving force for crack advance, without invoking crack closure.

We have rationalized these observations of early investigators and proposed the following physical basis for crack growth:

- The two driving forces ΔK and K_{max} are intrinsic to the material behavior and are prerequisites to uniquely defining the cyclic damage, independent of closure
- The critical driving forces ΔK^*_{th} and K^*_{max} are dependent on the alloy microstructure, slip mode and environment
- The two driving forces are independent of testing methods
- The long crack growth behavior represents a material property for a given environment

Short Fatigue Cracks

Research shows that long crack growth behavior does not accurately describe all fatigue damage, including phenomena such as short crack growth, accelerations in crack growth due to underloads, and retardations in crack growth due to overloads. These deviations from long crack growth behavior are caused by internal stresses present at the crack tip. In the following sections we discuss the characteristics and the role of internal stresses that affect the short crack behavior. The ΔK and K_{max} analysis discussed previously can be extended to analyze the growth of short cracks.

Table 1 - Research that has noted that the driving force for fatigue crack growth depends on two parameters (specifically, on ΔK and K_{max})

Year	Authors	Alloy	Remarks
1968	Erdogan	Model	Semi-empirical crack growth model that related the rate of crack propagation to the size of two plastic zones: the alternating plastic zone that depended on ΔK, and the pulsating zone based on K_{max}.
1973	Schmidt and Paris	Aluminum alloy	Explained the experimentally determined ΔK_{th}-stress ratio using closure concept, but plotted ΔK_{th} and K_{max} thresholds vs. stress ratio. Indicated that K_{max} was constant where K_{min} was less than K_{cl} but when K_{min} was greater than K_{cl}, ΔK_{th} was constant. Did not plot ΔK vs. K_{max}.
1981, 1983	Doker and Marci	Aluminum and titanium alloys	First to plot data in the form of ΔK_{th} vs. K_{max}, but explained their experimental results using closure concepts. Implied that there are two critical thresholds.
1981	Priddle	Mild steels	Similar explanation to Schmidt and Paris. Plotted ΔK_{th} vs. K_{max} curves but interpreted the results to be consistent with the concept of oxide-induced closure.
1990	Lal and Namboodhiri	Aluminum and steel	Analyzed fatigue thresholds without invoking crack closure on the basis that for stress ratios greater than 0.6 the crack growth is ΔK-controlled and for stress ratios less than 0.6 it is K_{max}-controlled. Did not plot ΔK vs. K_{max}.
1993	Vasudevan and Sadananda	All materials	Explicit statements that two independent driving forces ΔK and K_{max} are required for crack growth, independent of crack closure. Applicable to the entire crack growth region and to variety of materials. (Details given in the text.)
1996	Wilkinson and Roberts	Copper	First dislocation model using ΔK and K_{max} for threshold fatigue that predicts the need for the two parameters and gives a fundamental reason for their occurrence. Predicted da/dN vs. ΔK and ΔK vs. K_{max} without invoking closure.

There is no clear distinction between the nucleation of a crack and its early growth, primarily due to the lack of a conceptual definition of a nucleation event and the inability to measure such an event. Therefore, the crack nucleation stage can encompass all the growth events of a vanishingly small crack below the limits of experimental detection. For the sake of discussion, one can define a short crack to be one that has a length below the limit detectable by means of non-destructive inspection techniques.

There are several definitions of short cracks [44,45], including *mechanically short* (where the crack is smaller than the plastic zone size), *physically short* (where the crack is shorter than a long crack), and *microstructurally short* (where the crack is shorter than the grain size of the material). These classifications have been given to understand and quantify the behavior of these cracks, which are considered to be representative of the intrinsic characteristic of the material. In comparison, long crack behavior is considered intrinsic only after the closure corrections are made. It has been noted [46,47] that all these types of short cracks are indistinguishable in the experimental data scatter. Furthermore, they all show faster growth rates at stress intensities that are much lower than the long crack growth thresholds commonly represented in terms of ΔK.

Experimental observations have pointed out that short crack behavior is anomalous; the source of this anomaly has been attributed to the lack of plasticity-induced closure in the wake of a crack that has negligible length. Deviations in the short crack growth behavior also have been explained in terms of: (1) intrinsic material behavior, (2) small crack sizes that result in larger contributions from non-singular, second-order crack tip stress fields, which decrease rapidly with increase in crack length contributing to the crack tip driving force (3) plastic zone size that is larger than the crack length resulting in violation of small-scale yield condition (4) crack closure, and (5) microstructural obstacles such as grain boundaries giving rise to data scatter with discrete jumps in

growth rates. Regardless of cause, however, the breakdown of similitude for short cracks (as compared to long cracks) clearly shows that equal crack tip forces do not result in equal crack growth rates. For mechanically short cracks, this breakdown of the *K*-similitude has been interpreted in terms of large-scale yielding and closure. For microstructurally short cracks, it is due to crack tip plasticity influenced by the microstructure.

After some careful analysis of the short crack literature, one can consider the short crack behavior from a different view [46,47]. This can be envisioned by first defining the behavior of long cracks to represent the basic material characteristics and then recognizing some of the salient differences between the long and short crack growth characteristics:

(1) we recall that plasticity originated from a crack tip does not cause crack closure [27-30], thus eliminating this phenomenon as an issue between the short and long cracks,

(2) there is a large experimental scatter in the short crack data compared to the long cracks [45],

(3) short crack growth data for multiple samples taken from the same alloy or from the same alloy with different microstructures (due to heat treatments) tend to fall within the same scatter band when compared to the respective long cracks [44,48] data,

(4) the crack growth rate decreases and then increases or arrests with an increase in ΔK for the short cracks, while there is only a monotonic increase in crack growth with long cracks [44], and

(5) there is a reproducibly unique threshold value for a given *R*-ratio for the long cracks with minimum scatter in the data [45], while there appears to be no unique threshold for short cracks [44,45].

Figure 6 illustrates some examples of crack growth behavior that deviate from the normal growth of a long crack, in terms of a crack growth per cycle (*da/dN*) vs. K_{max}. These examples include short cracks growing from a notch or other region of stress concentration, as well as long cracks that have been subjected to a single underload or overload. These plots clearly show two phenomena:

- Growth rates for short cracks can either accelerate or decelerate; in some cases, the short cracks can cease growing altogether
- Growth rates for short cracks eventually converge with the crack growth rates obtained for long cracks during constant amplitude fatigue tests

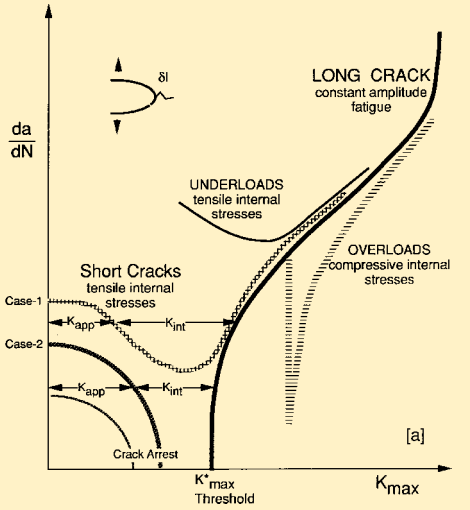

Fig. 6 - Perturbations in long crack behavior due to tensile or compressive internal stresses

Based on the above differences between long and short cracks, we have postulated [46,47] that:

- For a given microstructure and environment, the long crack growth behavior under constant amplitude loading represents the material crack growth curve
- The two long crack growth thresholds ΔK^*_{th} and K^*_{max} represent unique fatigue crack thresholds that are applicable for a combination of material, environment, and microstructure
- Short cracks should also satisfy the same long crack thresholds for their growth
- Pre-existing internal stresses, or those that are generated in-situ during cycling, contribute an additional driving force that helps short cracks satisfy the same long crack thresholds required for crack growth.

Hence, the assumption about the breakdown of similitude between short cracks and long cracks can be rejected. The apparent anomaly in the short crack growth behavior mainly arises from an insufficient description of the total crack tip driving forces (due to the lack of recognition of the internal stresses) and from not considering the second threshold requirement $[K^*_{max}]$ in addition to the normally considered threshold of $[\Delta K^*_{th}]$.

Tanaka et al. [49,50] have systematically studied the crack growth behavior of short cracks nucleated from notches, free surfaces, and specimen corners. Figure 7a shows crack growth data for small and long cracks in a variety of specimen geometries in low carbon steel. Interestingly, one can note that the short crack growth data from free-surface specimens (designated by open figures) fall within the same scatter band of data for the sharp notch specimens (darkened figures). While the internal stress gradients from notches can be readily identifiable, the existence of such high stress gradients is not obvious for free-surface specimens. However, internal stress gradients must be present to induce or sustain short crack growth. Therefore, we postulate that for cases where there are no pre-existing internal stresses, these gradients are generated *in situ* by irreversible plasticity during cycling and are therefore unavoidable. For example, internal stresses can manifest themselves as intrusions and extrusions, slip band intersections, etc., which lead to crack nucleation and then short crack growth.

Figure 7a also shows crack growth data for long cracks in the same material. The amount of internal stress can be computed as the difference between the driving forces for the long and the short cracks; this difference is shown schematically in Fig. 6a as ΔK_{int}. When the values for ΔK_{int} are normalized by the values for ΔK_{Ic} for long cracks taken at the same growth rate, and then plotted against a parameter $(\Delta K_{sc})^2$, which is proportional to the length of the short crack, as in Fig. 6b, then we can see that the functional form of the internal stresses for all specimen geometries are similar.

This suggests that the internal stress gradients also occur in smooth specimens (for example, via the formation of intrusions and extrusions) and that all of the different types of internal stresses decay rapidly with distance from the source and show similar

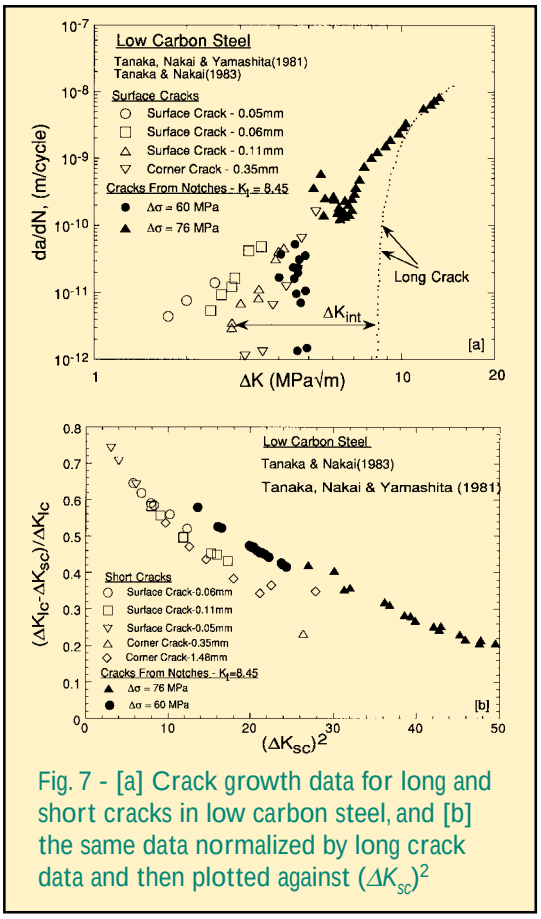

Fig. 7 - [a] Crack growth data for long and short cracks in low carbon steel, and [b] the same data normalized by long crack data and then plotted against $(\Delta K_{sc})^2$

functional forms. Therefore, short cracks grow in the presence of internal stress fields that can accentuate applied stresses to produce the driving force necessary for crack growth to occur. From these analyses, one can reach an important conclusion that there is no violation of the similitude between the long and short cracks. This analysis also can be extended to other types of deviations from the long crack growth, such as those arising from overloads and underloads. We can then restate the similitude concept with a modification:

- *Equal crack tip forces cause equal crack growth rates if all factors that contribute to the crack tip driving forces are considered and if the crack growth mechanism remains the same.*

Type and Nature of Internal Stresses

Internal stress fields [47] can be either short-range or long-range. Short-range stress fields occur in a material near point defects such as vacancies or interstitials but do not significantly affect the growth of short cracks. It is important to consider long-range stresses, however, because they do contribute to the growth of short cracks.

Long-range stresses can arise from a number of sources, including:

- dislocation pile ups at low- and high-angle grain boundaries, with stresses varying with distance as $f[1/r]$,
- microvoids and inclusions, with stresses varying with distance as $f[1/r^3]$,
- cracks-tip stresses, which vary as $f[1/\sqrt{r}]$,
- persistent slip bands,
- notch tip stress fields,
- transformation-induced stresses,
- residual stresses from cold working, shot peening, ion implantation, machining, or other mechanical processes, and
- thermal stresses from quenching, welding, etc.

The generic term "internal stress" encompasses all of these types of stresses, some of which are depicted in Fig. 8. A correct assessment of the crack tip forces must include all of the stresses applicable to the situation, both applied and internal.

Stacey and Webster [51] studied the effect of compressive residual stresses on long crack growth in an autofrettaged thick-walled tube made of a low alloy steel. In addition, measurements of compliance were used to determine the stiffness change in the material due to the autofrettage treatment. The fatigue samples for this research — some with the residual stresses, and some without — were sectioned from the tube; each sample had a crack starting at the inner wall of the tube. Figure 9a shows the long crack growth data for the two conditions. The difference between the two curves gives the magnitude of the internal stresses (ΔK_{int}) that are induced by the autofrettage treatment. Figure 9b shows the contribution of internal stresses to the overall stress intensity as a function of crack length. Figure 9c shows the values of stress intensity due to the residual stresses (calculated from compliance measurements, using a weight function method).

AUTOFRETTAGE. A technique for fabricating thick-walled tubes that uses high pressure inside the tube to induce compressive stresses on the tube's inner wall.

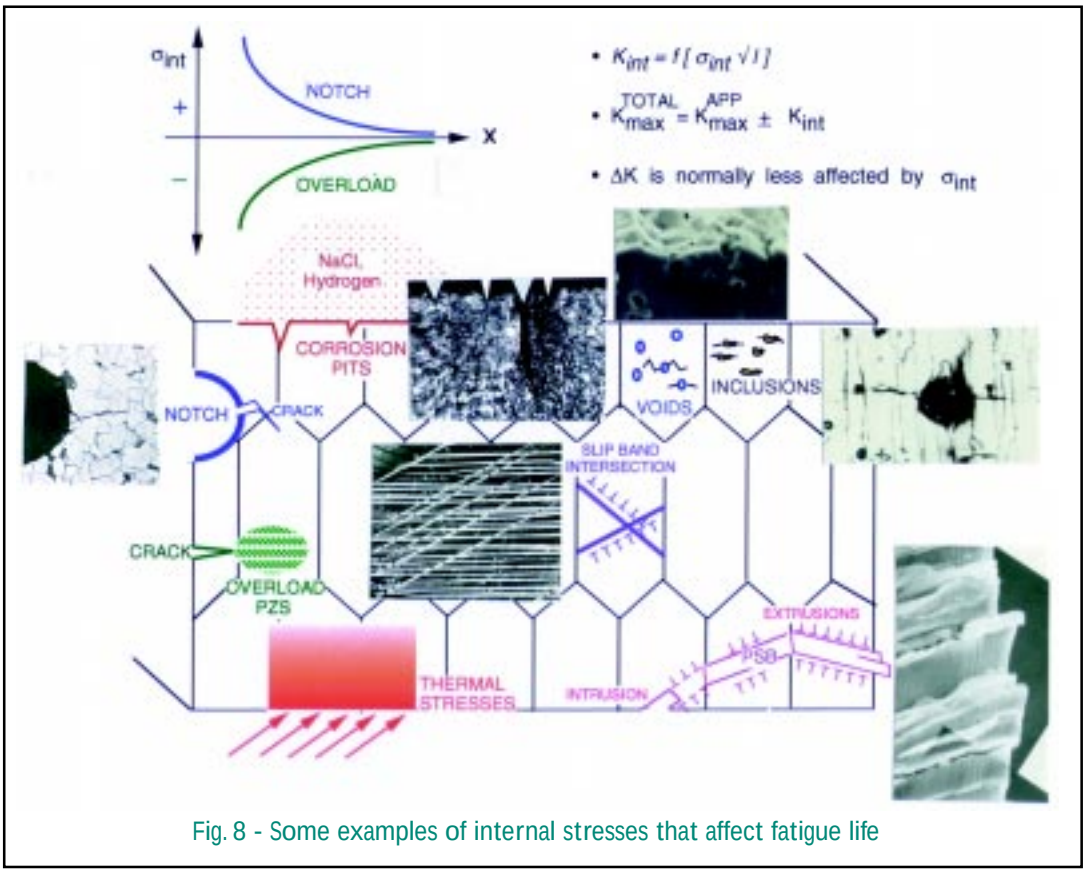

Fig. 8 - Some examples of internal stresses that affect fatigue life

A comparison of Figs. 9b and 9c shows that the internal stresses estimated from the crack growth data are in agreement with the results from calculated internal stresses using the weight function method. This confirms that the compressive stresses created by the autofrettage process generate the internal stress gradients necessary to reduce the crack tip driving forces. Note that the length scales of the internal stress gradients are of the order of a few millimeters. High-precision methods like low angle X-ray and neutron diffraction may be used to measure the internal stress gradients ahead of a crack tip. To date, however, such results are not available.

Linking Crack Nucleation to Short Cracks and Long Cracks

Kitagawa and Takahashi [52] proposed a graphical method to link the data for short and long cracks with the fatigue limit $\Delta\sigma_e$, which was obtained from level of stress vs. cycles to failure data for smooth fatigue specimens. From a Kitagawa-Takahashi diagram (such as the one shown in Fig. 10), one can extract a parameter called critical crack size (a^*).

FATIGUE LIMIT $\Delta\sigma_e$. The level of cyclic stress needed to nucleate a crack. Once nucleated, a crack will grow rapidly to failure unless $\Delta\sigma_e$ is reduced continuously.

Kitagawa and Takahashi found that for cracks that were shorter than the critical crack size a^*, the threshold condition for crack growth could be represented by a critical stress $\Delta\sigma_{th}$ that approaches the smooth tensile fatigue limit $\Delta\sigma_e$ for vanishingly small crack sizes. For such short crack lengths, the fatigue limit is essentially independent of the crack length. On the other hand, for cracks that were longer than a^*, the specimen's crack growth and fatigue life are dictated by the threshold stress at a given stress ratio, $\Delta K_{th}\, f(R)$. The intersection between the long and the extremely short crack region defines the critical crack length a^* for a given stress ratio R. The critical crack length a* marks the point where the growth behavior of short cracks transitions to that of the long cracks. One can infer from their analysis that $a^* f(R) = (1/\pi)\,[\Delta K_{th}/\Delta\sigma_e]$. Other researchers have attempted to link critical crack size with characteristic microstructural scales in a variety of materials [53,54].

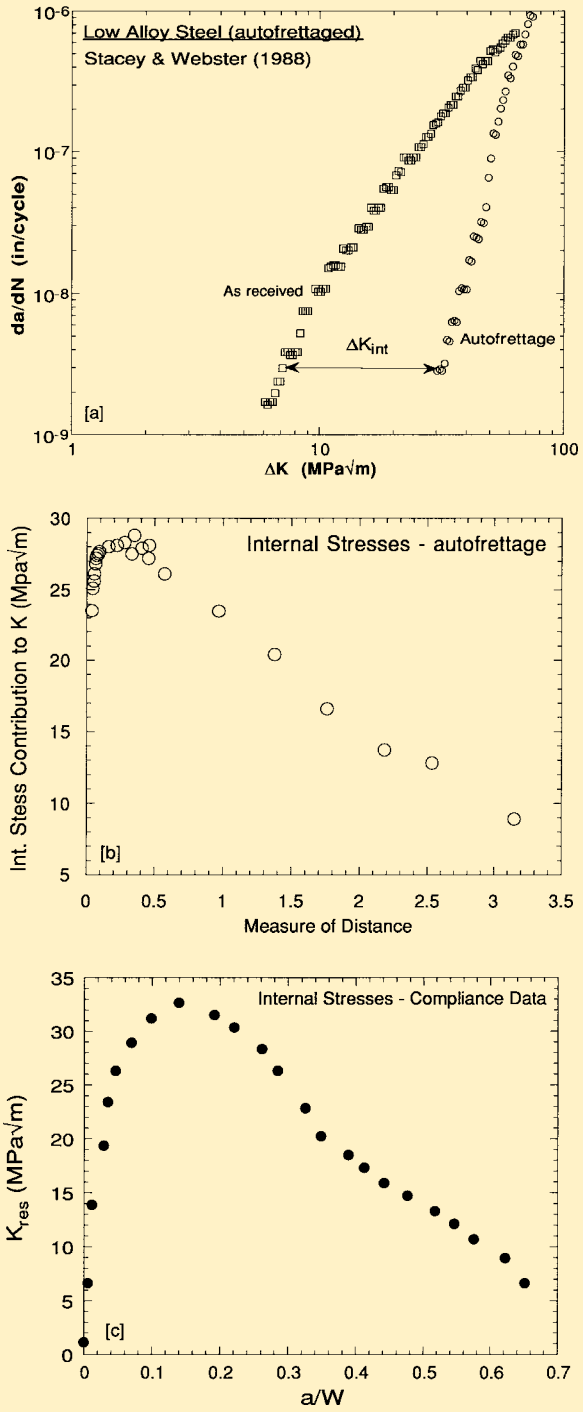

Fig. 9 - [a] Long crack growth data for low alloy steel tubing (with and without autofrettage treatment), [b] the contribution of internal stresses to overall stress intensity as a function of crack length, and [c] the value of stress intensity due to residual stresses

Figure 10 uses this technique [55] to plot Usami's data on 13Cr-steel alloy at different stress ratios [56]. The linear portion of the change in stress ($\Delta\sigma$) vs. crack length (a)

plot at long crack lengths is given by linear elastic fracture mechanics as $\Delta K_{th} = \Delta\sigma_{th}\sqrt{\pi a}$. At smaller crack lengths, the curve approaches the fatigue limit $\Delta\sigma_e$. As can be seen in Fig. 10, the parameters of fatigue limit ($\Delta\sigma_e$), threshold change in stress intensity (ΔK_{th}), and critical crack size (a^*) are all functions of stress ratio R. As stress ratio R increases, the values of a^*, ΔK_{th}, and $\Delta\sigma_e$ decrease.

Each curve in Fig. 10 represents data for a single stress ratio; data for different stress ratios can be collapsed into one curve by normalizing each of the ordinates with the respective $\Delta\sigma_e$ and a^*. This unique curve is characteristic of the material-microstructure-environment linking the region of crack nucleation and short crack growth to the realm where long crack growth occurs. As Usami has shown [56-58], a change in the environment would affect the thresholds and therefore shift the curves in the Kitagawa diagram.

As previously shown in Fig. 4, ΔK_{th} approaches a limiting threshold value ΔK^*_{th} at high stress ratios, and at low values of stress ratio K_{max} approaches K^*_{max}. Similarly, one should expect asymptotic values for $\Delta\sigma_e$. The two parametric requirements under the nucleation (level of stress vs. cycles to failure) curve are complicated by contributions from compressive plastic flow, which have been addressed by Goodman [59]. The question as to how the two parametric requirements for crack growth in terms of ΔK and K_{max} translate into two parametric requirements in level of stress vs. cycles to failure curves needs further investigation. Needless to say, at least for positive values of stress ratio R, the Kitagawa diagram directly links the behavior of the fracture mechanics specimen [crack growth per cycle (da/dN) vs. change in stress intensity (ΔK)] to fatigue limits in smooth samples (obtained from level of stress vs. cycles to failure curves) as a function of stress ratio R.

There are additional physical connections between short and long cracks that can be explained in terms of the contribution from internal stresses. When the long crack portion of the curve is extrapolated to the short crack region (i.e., below the critical crack size a^*); we observe that an extremely short crack should be growing at an enormously high stress level. The Kitagawa diagram, however, indicates that applied stresses approach a plateau, where short cracks nucleate and grow at the stress level of a fatigue limit $\Delta\sigma_e$. We have shown that the same thresholds are valid for both short and long cracks. Hence internal stresses must be generated *in situ* (if they are not pre-existing) to allow the nucleation and growth of short cracks to take place at the fatigue limit. The triangular region defined by arrows in the upper left portion of Fig. 10 defines the minimum internal stress and the gradient required for a short crack to grow at the fatigue limit $\Delta\sigma_e$. For this case, the internal stresses follow a $\sqrt{r}$ dependence to satisfy the thresholds required to produce crack growth. Thus the requirement for the internal stresses follows directly from the Kitagawa diagram; this is also consistent with the arguments presented previously with reference to Fig. 5. Therefore, the two parametric analyses provide a unified framework [55] for fatigue damage evaluation from the stages of early crack nucleation, through the growth of short cracks, to long crack growth.

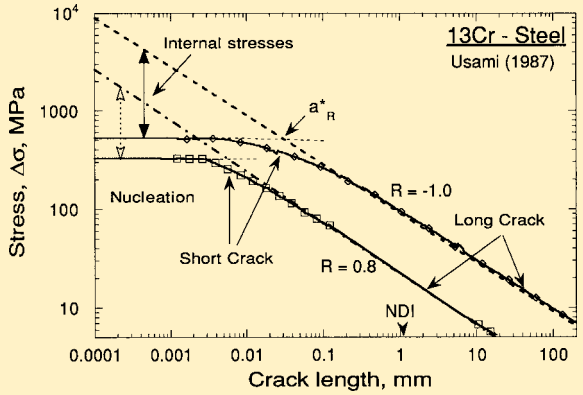

Fig. 10 - Kitagawa-Takahashi diagram (i.e., a plot of crack length vs. the threshold change in stress needed to generate crack growth) for 13Cr-steel alloy

When the length of a crack is greater than the critical crack length a^*, applied stresses are sufficient to sustain the crack growth with the aid of internal stresses. The crack growth behavior then merges with the long crack growth. Physically, a^* defines the critical crack size to which a short crack has to grow before it can be treated as a long crack. It is in this regime that the internal stresses either have to be provided externally via stress concentrations or to be generated internally via slip process. Because (1) both nucleation and growth of short cracks occur in the presence of augmented internal stresses, (2) a^* is well below the NDI limit for crack detection, as noted in

Fig. 10, and (3) the demarcation between nucleation and short crack growth stages is rather arbitrary; we can conveniently define the crack nucleation stage to occur until the crack length a reaches a^*.

Summary

A unified approach to fatigue damage analysis has been developed involving two driving forces for crack growth: the change in stress intensity (ΔK) and the maximum stress intensity (K_{max}). The analysis shows that ΔK vs. K_{max} curves represent the fundamental materials behavior that is applicable to both long and short cracks. Short cracks grow at different rates than long cracks due to the presence of internal stress gradients that primarily affect K_{max} (an intrinsic parameter in the unified framework for fatigue) and not ΔK. Also, despite a wide diversity in the types of internal stresses, their gradients are similar; this indicates that it should be possible to predict the magnitude of internal stresses using analytical methods. Thus, for a more reliable life prediction methodology one requires three main parameters: ΔK, K_{max} and $K_{internal}$. Efforts must be focused to use these parameters to develop such models.

References

1. A. Palmgren, *Zeit. Ver. Deuts. Ing.*, **24**, 339-341 (1924).
2. M.A. Miner, *J. Appl. Mech.*, **12**, 159-164 (1945).
3. G. Halford, *Int. J. Fat.*, **19**, S253-S260 (1998).
4. G. Glinka, *Int. J. Fat.*, **4**, 59-67 (1982).
5. N.E. Dowling, in *Durability in Design*, SAE Publ. # SP-730, Paper # 871966.
6. N.E. Dowling, *Mechanical Behavior of Materials* (Prentice-Hall, Englewood Cliffs, NJ, 1993).
7. J. Polak, *Cyclic Plasticity and Low Cycle Fatigue of Metals* (Elsevier, Amsterdam, 1991).
8. P.D. Hobson, *Fat. Fract. Engg. Mater. Struct.*, **5**, 323-327 (1982).
9. J.R. Yates and L. Grabowsi, in *Fatigue '90, , The Proceedings of the 4th International Conference of Fatigue and Fatigue Thresholds*, edited by H. Kitigawa and T. Tanaka (Materials and Components Engineering Publications, Ltd., United Kingdom, 1990), 2369-2376.
10. L. Grabowski and J.E. King, *Fat. Fract. Engg. Mater. Struct.*, **15**, 595-606 (1992).
11. J. Weertman, *Int. J. Fract.*, **2**, 460-467 (1966).
12. K. Tanaka, Y. Akinawa, and Y. Nakai, *Engg. Fract. Mech.*, **34**, 803-819 (1986).
13. *Small Fatigue Cracks*, edited by R.O. Ritchie and J. Lankford (The Metallurgical Society of AIME, Warrendale, PA, 1986).
14. K. Tanaka, Y. Nakai, and M. Yamashita, *Int. J. Fract.*, **17**, 519-533 (1981).
15. A. Navarro and E.R. de los Rios, *Phil. Mag.*, **10**, 15-36 (1988).
16. M.N. James and E.R. de los Rios, *Fat. Fract. Engg. Mater. Struct.*, **19**, 413-426 (1996).
17. D.W. Hoeppner and W.E. Krupp, *Engg. Fract. Mech.*, **6**, 47-70 (1974).
18. R.G. Forman, V.E. Kearney, and R.M. Engle, *J. Basic Engg.*, **89**, 459-64 (1967).
19. J. C. Newman, Jr, "FASTRAN-II: A Fatigue Crack Growth Structural Analysis Program," *NASA Technical Memorandum 104159*, NASA Langley Research Center, Hampton, VA, 1992.
20. J.C. Newman, Jr, *J. Engg. Mater. Tech*., **117**, 433-439 (1995).
21. K. Walker (Paper presented at *USAF Aircraft Structural Integrity Program Conference*, San Antonio, Texas, 2-4 Dec 1997).
22. L. Lazzeri, A. Pieracci, and A. Salvetti; (Paper delivered at *18th Symposium of Int. Committee on Aeronautical Fatigue*, Melbourne, Australia, May 1995).
23. J. Harter, personal communication (1998).
24. S. Suresh, *Fatigue of Materials* (The University Press, Cambridge, 1998).
25. *Mechanics of Fatigue Crack Closure, ASTM STP 982* (American Society for Testing and Materials, Philadelphia, PA, 1988); and E.P. Phillips, "Results of the Round Robin on Opening -Load Measurement Conducted by ASTM Task Group E24.04.04 on Crack Closure Measurements and Analysis," *NASA Technical Memorandum 101601*, NASA Langley Research Center, Hampton, VA, 1989.
26. A.K. Vasudevan, K. Sadananda, and N. Louat, *Scripta Metall. Et Mater.*, **27**, 1673 (1992).
27. N. Louat, K. Sadananda, A.K. Vasudevan, and M. Duesbery, *Met Trans.*, **24A**, 2225 (1993).
28. A.K. Vasudevan, K. Sadananda, and N. Louat, *Mat. Sci. Engg.*, **A188**, 1 (1994).
29. K. Sadananda and A.K. Vasudevan, "Analysis of Fatigue Crack Closure and Thresholds," *Fracture Mechanics: 25th Volume, ASTM STP 1220*, edited by Erdogan and Hartranft (American Society for Testing and Materials, Philadelphia, PA, 1995), 484-501.
30. J. Weertman, *Phys. Status Solidi B*, **172**, 27-40 (1992).
31. B.R. Kirby and C.J. Beevers, *Fat. of Engg. Matrls. and Structures*, 1979, **1**, 203-215.
32. S. Suresh, A.K. Vasudevan, and P.E. Bretz, *Metall. Trans.*, **15A**, 369-379, (1984).
33. J. Petit, in proceedings of *Symposium on Fatigue Crack Growth Threshold Concepts*, Philadelphia, Pennsylvania, 1984, edited by D.L. Davidson and S. Suresh (The Metallurgical Society of AIME, Warrendale, PA, 1984), 3-24.

34. H. Kemper, B. Weiss, and R. Stickler, *Engg. Fract. Mech.*, **32**, 591 (1989).

35. A.K. Vasudevan and K. Sadananda, *Scripta Metall et Mater.*, **28**, 65-70 (1993).

36. A.K. Vasudevan and K. Sadananda, *Metall. Mater. Trans.*, **26A**, 1221-1234 (1995).

37. F. Erdogan, *Crack Propagation Theories - Fracture-an Advanced Treatise* (Academic Press, New York, 1968).

38. P.C. Paris, M.P. Gomez, and W.P. Anderson, *The Trends in Engg.*, **13**, 9 (1961).

39. R.A. Schmidt and P.C. Paris, *Progress in Fatigue Crack growth and Fracture Testing, ASTM STP 536*, (American Society for Testing and Materials, West Conshohocken, PA, 1973), 79-94.

40. H. Doker and G. Marci, *Int. J. of Fatigue*, **5**, 187 (1983).

41. E.K. Priddle, in proceedings of *Symposium on Fatigue Threshold*, Stockholm, Sweden, 1981, edited by I Backlund, A. Blom, and C.J. Beevers, (EMAS Ltd., Warley), 581-600.

42. D.N. Lal and T.K.G. Namboodhiri, *Mater. Sci. Engg.*, **A130**, 37 (1990).

43. A.J. Wilkinson and S.G. Roberts, *Scripta et Matl.*, **35**, 1365 (1996).

44. J.C. Newman and P.R. Edwards, in proceedings of *Symposium on Short Crack Growth Behavior in Various Aircraft Materials*, AGARD-R732 (Defense Technical Information Center, Alexandria, Virginia).

45. *Small Fatigue Cracks*, edited by R.O. Ritchie and J. Lankford (The Metallurgical Society of AIME, Warrendale, PA, 1986)

46. K. Sadananda and A.K. Vasudevan, *Fatigue and Fracture Mechanics: 27th Volume, ASTM STP -1296*, edited by Robert S. Piascik, (American Society for Testing and Materials, Philadelphia, PA, 1997), 301-316.

47. K. Sadananda and A.K. Vasudevan, *Int. J. Fatigue*, 1998, in press.

48. K.J. Miller, *Fat. Engg. Matls. Struct. Part I and II*, **10**, 1987.

49. K. Tanaka and Y Nakai, *Fat. Eng. Mat. Struc.*, **6**, 315 (1983).

50. K. Tanaka, Y. Nakai, and M. Yamashita, *Int. J. Fract.*, **17**, 519-533 (1981).

51. A. Stacey and G. Webster, *Analytical and experimental Methods for residual Stress Effects in Fatigue, ASTM STP 1004*, (American Society for Testing and Materials, West Conshohocken, PA, 1988), 107-121.

52. H. Kitagawa and S. Takahashi, in proceedings of *Second International Conference on Mechanical Behavior of Materials*, (ASM, Metals Park, Ohio, 1976), 627-631.

53. J. Lankford, *Fat. Enng. Matts. Struct.*, **5**, 233-248 (1982).

54. C.W. Brown and M.A. Hicks, *Fat. Enng. Matts. Struct.*, **6**, 67-76 (1983).

55. K. Sadananda and A.K. Vasudevan, in proceedings of *FATIGUE '96*, Berlin, Germany, 1996, edited by G. Lutjering and N. Nowack (Pergamon Press, New York), 375-380.

56. S. Usami, in proceedings of *Short Crack Fatigue Properties-Current Research on Fatigue Cracks*, edited by T. Tanaka (1987), 119-147.

57. S. Usami and S. Shida, *Fat. Engg. Matls. Struct.*, **1**, 471-481 (1979).

58. S. Usami, in proceedings of *Symposium on Fatigue Threshold*, Stockholm, Sweden, 1981, edited by I Backlund, A. Blom, and C.J. Beevers, (EMAS Ltd., Warley), 205-238.

59. J. Goodman, *Mechanics Applied to Engineering* (Longmans Green, London, 1899).

The Authors

Dr. K. Sadananda is a researcher in the Materials Science and Technology Division at the Naval Research Laboratory in Washington, DC. His broad areas of expertise include the mechanics of dislocations behavior, deformation in high-temperature order alloys and intermetallics, alloy microstructure-load-environmental interactions in gas turbine engine materials, creep-fatigue-environmental interactions, and nanocrystalline coatings for wear and corrosion applications. Dr. Sadananda has published more than 150 articles covering many areas of mechanics and metallurgy, and he has made more than 100 invited presentations in Europe, Asia, and the United States. He has been awarded four NRL research publication awards for papers published in *International Journal of Fracture*, *Metallurgical Transactions*, and *Metal Science Reviews*. Other awards include the Sigma Xi Applied Science award in 1980 and the Burgess Memorial Award from the Washington, DC, Chapter of ASM International in 1998.

Dr. A.K. Vasudevan is a Scientific Officer at the Office of Naval Research (ONR) Materials Science Division in Arlington, Virginia. He has initiated and managed basic and applied technical programs for high temperature engine materials, casting, diamond films, Ospray processing, condition-based maintenance, and nanocrystalline materials for coating applications. Prior to joining ONR in 1988, he was employed at ALCOA Research Labs in Pittsburgh as a scientist developing high strength aluminum alloys for aerospace and automobile applications. These aluminum alloys are currently being used in the Airbus A-333 and MD-11, as well as various military aircraft, helicopters, and racecars. Dr. Vasudevan has been actively involved with committees related to various NATO, U.S. Air Force, and NASA technical programs. He has published extensively and has given talks in Europe and the United States on topics relating to mechanical and physical properties associated with microstructural features.

Profiles in Science

Dr. K. Sadananda
Materials Science and Technology Division
Naval Research Laboratory
Washington, DC

Dr. K. Sadananda has been one of the Naval Research Laboratory's foremost researchers for the past two decades. He has made extensive contributions in several areas of research related to aircraft alloys, including high-temperature creep damage; dislocation theories that describe the deformation of alloys; and fatigue damage in metals, ceramics, and composites. In addition, he has developed specifications for the rejuvenation of turbine blades damaged by creep during service.

Dr. Sadananda's broad areas of expertise include the mechanics of dislocations behavior, deformation in high-temperature order alloys and intermetallics, alloy microstructure-load-environmental interactions in gas turbine engine materials, creep-fatigue-environmental interactions, and nanocrystalline coatings for wear and corrosion applications. He is currently involved in developing a unified theory for fatigue damage that encompasses damage from the crack nucleation stage to final fracture.

Dr. Sadananda has published more than 150 articles covering many areas of mechanics and metallurgy, and he has made more than 100 invited presentations in Europe, Asia, and the United States. He has been awarded four NRL research publication awards for papers published in *International Journal of Fracture*, *Metallurgical Transactions*, and *Metal Science Reviews*. He received the Sigma Xi Applied Science award in 1980 for "his pioneering research on the understanding and development of new concepts on high temperature crack growth in metals." In 1998, he was presented the Burgess Memorial Award from the Washington, DC Chapter of ASM International for his "outstanding research contributions and management of research in the last five years."

NAVAL RESEARCH REVIEWS

Naval Research Reviews, a theme-issue quarterly journal, publishes articles about Department of the Navy Science and Technology programs conducted by academia, government laboratories, for-profit and nonprofit organizations, and industry.

The journal is available on the World Wide Web at

http://www.onr.navy.mil/onr/pubs.htm

800 North Quincy Street
Arlington, VA 22217-5660